UNESP - Universidade Estadual Paulista
"Júlio de Mesquita Filho"
Faculdade de Odontologia de Araraquara

Jonas Bianchi

Osteoartrite na articulação temporomandibular: análise integrativa de marcadores por imagem, clínicos e biomoleculares

Araraquara

2019

UNESP - Universidade Estadual Paulista

"Júlio de Mesquita Filho"

Faculdade de Odontologia de Araraquara

Jonas Bianchi

Osteoartrite na articulação temporomandibular: análise integrativa de marcadores por imagem, clínicos e biomoleculares

Tese apresentada à Universidade Estadual Paulista (Unesp), Faculdade de Odontologia, Araraquara para obtenção do título de Doutor em Ciências Odontológicas, na Área de Ortodontia

Orientador: Prof. Dr. João Roberto Gonçalves

Araraquara

2019

Bianchi, Jonas
Osteoartrite na articulação temporomandibular: análise integrativa de marcadores por imagem, clínicos e biomoleculares/ Jonas Bianchi. -- Araraquara: [s.n.], 2019
86 f.; 30 cm.

Tese (Doutorado em Ciências Odontológicas) – Universidade Estadual Paulista, Faculdade de Odontologia
Orientador: Prof. Dr. João Roberto Gonçalves

1.Osteoartrite 2. Tomografia computadorizada de feixe Cônico 3. Biomarcadores I. Título

Ficha catalográfica elaborada pela Bibliotecária Marley C. Chiusoli Montagnoli, CRB-8/5646
Universidade Estadual Paulista (Unesp), Faculdade de Odontologia, Araraquara
Serviço Técnico de Biblioteca e Documentação

Jonas Bianchi

Osteoartrite na articulação temporomandibular: análise integrativa de marcadores por imagem, clínicos e biomoleculares

Comissão julgadora

Tese para obtenção do grau de doutor em ciências odontológicas

Presidente e orientador: Prof. Dr. João Roberto Gonçalves

2º Examinador: Prof. Dr. Luiz Gonzaga Gandini Junior

3º Examinador: Prof. Dr. Ary dos Santos Pinto

4º Examinador: Profª. Drª. Lúcia Helena Soares Cevidanes

5º Examinador: Prof. Dr. Antônio Carlos de Oliveira Ruellas

Araraquara, 06 de dezembro de 2019.

DADOS CURRICULARES

Jonas Bianchi

NASCIMENTO: 20 de abril de 1990 – São Carlos – São Paulo

FILIAÇÃO: Sandra Regina de Oliveira
Paulo Roberto Gonçalez Bianchi

2009 - 2014: Curso de Graduação em Odontologia: Faculdade de Odontologia de Araraquara – UNESP

2014 - 2016: Curso de Pós-Graduação: Especialização em Ortodontia. Faculdade Mozarteum de São Paulo - FAMOSP

2014 - 2016: Curso de Pós-Graduação: Mestrado pelo programa de Ciências Odontológicas. Área de concentração em Ortodontia: Faculdade de Odontologia de Araraquara – UNESP

2017 - 2019: Curso de Pós-Graduação: Doutorado pelo programa de Ciências Odontológicas. Área de concentração em Ortodontia: Faculdade de Odontologia de Araraquara – UNESP

Dedico esse trabalho ao pai e mãe de família que acorda e luta todos os dias em busca de uma vida melhor. Dedico esse trabalho aos que não tiveram a oportunidade que eu tive de desenvolver uma carreira acadêmica. Dedico esse trabalho aos filantrópicos(as), que ajudam os mais necessitados. Dedico esse trabalho ao ser humano de bom coração, que enxerga o próximo como seu irmão. Acredito numa sociedade mais justa, menos pobre e com maior igualdade a todos, que nunca falte comida, educação e saúde a ninguém que necessitar.

AGRADECIMENTOS

A Deus, por guiar da sua forma única o meu caminho, minha família e de todos ao meu redor. Sem fé não existe esperança e sem esperança não existe vida. Que os próximos anos continuem sendo de muita saúde e luz, para todos.

À minha esposa Júlia Vieira Pastana Bianchi. Faltam-me palavras para agradecê-la. Essa quase uma década juntos me mostrou que você é a companheira que a vida me deu e que talvez eu nem merecia. Obrigado por ser minha parceira em todos os momentos, obrigado por aceitar os desafios e ir para cima deles ao meu lado. Espero poder recompensar todo seu sacrifico, humildade e amor. Obrigado, eu te amo ontem, hoje e sempre. Aos meus sogros Carlos e Beth, sempre nos apoiando. E ao nosso querido Barthô, um anjinho de 4 patas que nos traz alegrias e nos une sempre ainda mais.

Aos meus pais Paulo e Sandra, as minhas irmãs Sara e Debora e toda minha família. Aprendi com vocês o que é enfrentar a vida. Parece que Deus traçou nossa jornada para ser assim, um início desafiador, batalhas diárias que serviram para ver que a vida é muito mais do que dinheiro ou reconhecimento social. Obrigado por tudo, esse doutorado não é meu, é de vocês, sintam-se doutores, pois merecem muito mais que qualquer um.

Ao meu orientador e amigo Prof. João Roberto Gonçalves, o meu sincero obrigado. O senhor sempre acreditou em mim e essa confiança fez eu alcançar sonhos impossíveis. Jamais serei capaz de demonstrar toda minha gratidão. Palavras nunca serão suficientes para descrever a admiração que tenho. Agradeço também a Prof.ª Daniela Godoi Gonçalves, pois como todos sabemos, junto de um grande homem sempre existe uma grande mulher, e vice-versa.

À Profª. Drª. Lúcia Cevidanes. Muito obrigado por me acolher em Ann Arbor. Sua prontidão em ajudar e espírito bondoso me mostraram que o caminho para o sucesso é baseado na humildade e força de vontade. Sua contribuição em minha vida foi e é essencial, tanto eu quanto a Júlia seremos eternamente agradecidos. Com você pude ver que na verdade o sucesso é a felicidade em fazer o que se ama e estar cercado de boas pessoas.

Ao Prof. Dr. Antônio Ruellas e sua querida esposa Elaine. Obrigado pelo acolhimento e amizade. A sua orientação no desenvolvimento desse trabalho foi primordial, porém mais que isso, seus conselhos e amizade agregaram muito em

minha vida. Sempre serei grato por toda disponibilidade e atenção, jamais poderei retribuir sua confiança e ajuda. Obrigado por tudo.

Um agradecimento especial aos Prof. Luiz e Marcia Gandini. Vocês acreditaram em meu potencial e abriram as portas para a minha vida profissional. Além disso, o acolhimento pessoal e amizade são coisas que jamais poderei retribuiu, espero contar com a amizade de vocês por todo o sempre.

Ao Prof. Pedro Paulo Chaves de Souza. Obrigado meu amigo, por ser meu primeiro orientador e me tornar um pesquisador melhor. Você é um grande exemplo para mim além de um grande amigo. Aos também professores: Roland Koberle e Deusdediti Spavieri, meus coorientadores do mestrado. Obrigado pelo conhecimento transmitido e terem me ajudado a ser um pesquisador melhor.

Aos professores da disciplina de Ortodontia, Ary dos Santos Pinto, Dirceu Barnabé Raveli, Lídia Parsekian Martins e Maurício Sakima. Obrigado por sempre oferecerem ajuda. Um agradecimento especial ao professor Ary, meu muito obrigado por aceitar fazer parte dessa banca de Doutorado. Você é um exemplo de professor a ser seguidos, sempre disposto a ajudar todos em sua volta. Muito obrigado por abrir as portas da sua sala e sempre estar disposto a me ouvir.

À todos meus amigos de pós-graduação e colegas da Faculdade de Odontologia de Araraquara – UNESP. Em especial ao meu colega Juan, grande amigo e as orientadas de mestrado Karina e Julianna que sempre estiverem dispostas a ajudar. Aos alunos e ex-alunos do programa, obrigado, espero que sigam seus sonhos e conquistem-nos com muita perseverança e alegria. Também deixo meu carinho aos colegas da Universidade de Michigan, Karine, Camila, Aron, Serge, Maxime, Reza entre outros que trabalhei e convivi diretamente.

À Marília Yatabe e família, Karine e família, obrigado pela amizade e ajuda sempre que precisei, a presença de amigos é fundamental principalmente no exterior. Vocês nos ajudaram a tornar nossa estadia em Michigan especial.

Aos professores: Fabiana Soki, Erika Benavides, Lawrence Ashman obrigado por ajudarem a construir esse trabalho e pela ajuda profissional e pessoal que sempre me deram. Um obrigado também ao colega Juan Prieto e Beatriz Paniagua, sempre dispostos a ajudar.

Ao programa de Pós-graduação em Ciências Odontológicas da Faculdade de Odontologia de Araraquara – UNESP, representado pela coordenadora Prof. Dr^{a}.Fernanda Lourenção Brighenti.

À Faculdade de Odontologia de Araraquara, da Universidade Estadual Paulista “Júlio de Mesquita Filho” – UNESP, nas pessoas da diretora Prof.ª Dr.ª Elaine Maria Sgavioli Massucato e vice-diretor Prof.º Dr.º Edson Alves de Campos.

À Universidade de Michigan pelo acolhimento pessoal e profissional, aceitando minha condição de aluno sanduiche durante o período de 2018 a 2019.

Aos funcionários da FOAr e da Universidade de Michigan, obrigado pela ajuda e prestação de serviços. Ao amigo Diego, técnico em Ortodontia da UNESP, obrigado pela amizade e conselhos.

À CAPES: O presente trabalho foi realizado com o apoio da Coordenação de Aperfeiçoamento de Pessoal de Nível Superior – Brasil (CAPES) – Código de financiamento 001.

Ao National Institue of Health (NIH): Grants R01DE024450, R01MH116527, R21DE025306.

“We are just an advanced breed of monkeys on a minor planet of a very average star. But we can understand the Universe. That makes us something very special.”
Stephen Hawking*

* Hawking S. Hamburgo, Alemanha: Der Spiegel Magazine; 1988.

Bianchi J. Osteoartrite na articulação temporomandibular: análise integrativa de marcadores por imagem, clínicos e biomoleculares [tese de doutorado]. Araraquara: Faculdade de Odontologia da UNESP; 2019.

RESUMO

A osteoartrite (OA) é a forma mais comum das artrites. Na articulação temporomandibular (ATM) ela se destaca por causar degeneração da cartilagem de forma progressiva, remodelação do tecido ósseo condilar, quadros agudos e crônicos de dor. Atualmente, o diagnóstico da OA na ATM vem se tornando mais preciso, devido ao desenvolvimento de novas tecnologias, exames por imagem como a tomografia computadorizada de feixe cônico (TCFC) de alta resolução, análises computacionais e inteligência artificial. Dessa forma, esse trabalho teve como principal objetivo avaliar possíveis novos biomarcadores para a OA utilizando marcadores clínicos, por imagem e biomoleculares. Os objetivos secundários foram de comparar diferentes softwares para análises dos marcadores por imagem; avaliar o poder de diagnóstico desses marcadores; e por fim, desenvolver um modelo integrativo utilizando inteligência artificial, dados clínicos, biomoleculares e por imagem para o diagnóstico da OA na ATM. Como metodologia, foram desenvolvidos 3 artigos científicos, apresentados em sequência nessa tese. Nossa amostra foi composta por pacientes com diagnóstico clínico de OA na ATM e pacientes controles, sendo que foram coletados exames de TCFC, sangue, saliva e dados clínicos. Nossos resultados mostraram que o software desenvolvido pelo nosso grupo para análises das imagens é confiável e que os novos marcadores por imagens são capazes de diferenciar pacientes controles e com OA. Também demonstramos que nosso modelo estatístico integrativo de marcadores clínicos, biomoleculares, por imagem e inteligência artificial é capaz de diagnosticar a doença com acurácia de 0.837 ([0.761,0.902]). Por fim, nossos resultados sugerem que diferentes biomarcadores e uma integração estatística e computacional dos dados podem diagnosticar a doença e que estudos futuros devem ser realizados a fim de avaliar o comportamento das variáveis em relação a predição da AO na ATM.

Palavras chave: Osteoartrite. Tomografia Computadorizada de Feixe Cônico. Biomarcadores.

Bianchi J. Temporomandibular joint osteoarthritis: integrative analysis of clinical, biomolecular and imaging markers [tese de doutorado]. Araraquara: Faculdade de Odontologia da UNESP; 2019.

ABSTRACT

Osteoarthritis (OA) is the most common form of arthritis. In the temporomandibular joint (TMJ) it stands out for causing progressive cartilage degeneration, condylar bone tissue remodeling, acute and chronic pain. Nowadays, the TMJ OA diagnosis is improved by the development of new technologies and imaging exams such as high-resolution cone beam computed tomography (CBCT), advanced computational analysis and artificial intelligence. Thus, this study aimed to evaluate possible new biomarkers for OA using clinical, imaging and biomolecular markers. The secondary objectives were to compare different software for image marker analysis; evaluate the diagnostic power of these markers; and finally, to develop an integrative model using artificial intelligence, clinical, biomolecular and imaging markers for the diagnosis of TMJ OA. As methodology, 3 papers were developed, presented in sequence in this thesis. The sample consisted of patients with clinical diagnosis of TMJ OA and control patients. CBCT, blood, saliva and clinical data were collected. Our results showed that the software developed by our group for image analysis is reliable and that the new imaging markers can differentiate controls and OA patients. We also demonstrate that our integrative statistical model of clinical, biomolecular, imaging markers and artificial intelligence can diagnose the disease with an accuracy of 0.837 ([0.761.0.902]). Finally, our results suggest that different biomarkers and a statistical and computational integration of the data can diagnose the disease and future studies should be performed in order to evaluate the behavior of the variables regarding the prediction of OA in the TMJ.

Keywords: Osteoarthritis. Cone-Beam Computed Tomography. Biomarkers.

SUMÁRIO

1 INTRODUÇÃO

A osteoartrite (OA) é a forma mais comum das artrites. Seu ciclo natural de desenvolvimento leva à degeneração dos tecidos musculoesqueléticos e é considerada um problema de saúde mundial[1]. Acomete grande parte da população, sendo que na Europa uma prótese substitui uma articulação a cada 1.5 minutos e nos Estados Unidos a cada 1 minuto[2]. Dentre os diferentes sítios de acometimento da doença, a osteoartrite na articulação temporomandibular (ATM) se destaca por causar degeneração da cartilagem de forma progressiva, remodelação do tecido ósseo condilar, quadros agudos e crônicos de dor além de representar 42.6% dos desarranjos internos da ATM[3–5].

Esse processo se desenvolve quando há um desequilíbrio na fisiologia funcional da ATM, sendo o resultado da diminuição na capacidade adaptativa devido a diferentes formas de estresses, como as sobrecargas funcionais, deslocamento do disco articular, mediadores inflamatórios e aumento da fricção mecânica, podendo agir juntos na progressão das degenerações teciduais na OA[6,7]. Também ocorre uma interação dos mediadores bioquímicos, que induzem localmente e sistematicamente a liberação de moléculas como fatores de crescimento, radicais livres, metaloproteinases, citocinas pró inflamatórias e interleucinas. A etiologia é multifatorial, complexa e não totalmente elucidada na literatura, considerando que a idade, genética, fatores hormonais, gênero e traumas podem estar envolvidos[5,8,9]. Além disso, os sinais e sintomas para diagnóstico não são detectados precocemente, sendo que geralmente a doença se encontra em um estágio tardio de desenvolvimento, prejudicando a possibilidade de tratamentos conservadores.

A OA não possui um único biomarcador para diagnóstico e diferentes protocolos/exames são necessários para avaliar as condições dos tecidos. Dentre esses, a ressonância magnética (MRI) auxilia no diagnóstico da condição dos tecidos moles, permite a caracterização da morfologia e atividade metabólica, sendo utilizada até mesmo para acompanhamento da evolução natural da doença[3,10]. Porém, nesse exame, não é possível avaliar com qualidade as características do tecido ósseo, como os côndilos. Preenchendo essa lacuna, existe o exame de tomografia computadorizada de feixe cônico (TCFC). Este, em comparação com a tomografia médica emite menor radiação, e mesmo tendo uma resolução de

contraste inferior é um dos exames de escolha quando existe a necessidade do diagnóstico complementar da ATM[11,12].

Dessa forma, o diagnóstico precoce da OA é grande desafio clínico e científico, tornando-se o foco de pesquisadores no mundo todo. Cevidanes e colabores desenvolveram uma forma padronizada para avaliação computacional da morfologia condilar em pacientes com osteoartrite na ATM, por meio da correspondência de forma (SPHARM-PDM) no software 3D-Slicer[13,14]. Recentemente, esses pesquisadores avaliaram e caracterizaram as diferenças morfológicas dos côndilos com osteoartrite e saudáveis, em busca de um novo conjunto de biomarcadores por imagens ósseas e biomoleculares com base no sistema BIPED[15]. Foram observadas correlações em diferentes regiões de remodelação óssea na superfície condilar com o envolvimento de alguns mediadores moleculares no diagnóstico inicial da OA. O grupo também desenvolveu um índice de osteoartrite para o diagnóstico preliminar com base na morfologia da superfície condilar.

Mesmo com esses resultados promissores, ainda é necessário investigar detalhadamente os processos dinâmicos que ocorrem nos tecidos da ATM com osteoartrite. Dessa forma, além das caracterizações das mudanças morfológicas superficiais, as análises do tecido ósseo subcondral têm um papel importante no diagnóstico, desenvolvimento e progressão da OA[16]. Estudos tem demonstrado que esse tecido possui uma íntima relação com a articulação, sendo considerado uma estrutura dinâmica que responde biomecânicamente e molecularmente aos estímulos sofridos por meio da remodelação da microarquitetura óssea e liberação de mediadores bioquímicos[16–18]. Trabalhos recentes têm avaliado o tecido ósseo subcondral bidimensionalmente e tridimensionalmente por meio de tomografia computadorizada (TC)[19,20], entretanto esses estudos não precisam com exatidão a microarquitetura óssea, pois geralmente avaliam aspectos como a densidade e volume ósseo.

Atualmente, com o surgimento do tomógrafo computadorizado de feixe cônico de alta resolução (HR-TCFC) e a aplicação de metodologias avançadas computacionais no campo médico, é possível atingir novos desafios clínicos no campo do diagnóstico precoce. A possibilidade de coordenar e investigar os eventos que precedem as degenerações severas musculoesqueléticas na ATM potencializam as chances de identificar pacientes de risco a esse quadro. Sendo

assim, a hipótese principal desse estudo é de que as características ósseas tridimensionais condilares diferem entre os pacientes saudáveis e portadores de osteoartrite e que essas alterações precedem as alterações degenerativas da história natural da doença. Diante do fluxo intenso de informações[21], aquisição de dados de pacientes e constante evolução de algoritmos computacionais[22], existe uma necessidade de trabalho conjunto com profissionais de diferentes áreas, incluindo engenharia, matemática, saúde e outros. Nessa necessidade o termo data science[23] refere-se a um conjunto de procedimentos, voltados para a aquisição, gerenciamento, manutenção e análise de informações. Nos campos de aquisição, geralmente os profissionais de saúde são responsáveis por adquirir as informações, enquanto etapas mais avançadas, requerem pesquisas e desenvolvimento de web-systems, algoritmos de machine-learning (inteligência artificial), voltados um diagnóstico e tratamento específico para cada paciente[24].

Nesse trabalho, utilizamos informações clínicas[25], de imagens[3,26] e biomoleculares de sujeitos controle e pacientes com TMJ OA para a análise e desenvolvimento de metodologias computacionais voltadas para o diagnóstico da OA. Foram avaliadas as características ósseas da microarquitetura textural subcondral, proteínas por meio de protocolos padronizados em sangue e saliva, sinais e sintomas clínicos, a fim de obter-se novos modelos computacionais e estatísticos para auxiliar na criação de ferramentas e diagnóstico da osteoartrite na ATM.

2 OBJETIVO

Investigar novos biomarcadores e desenvolver modelos estatísticos para o diagnóstico da Osteoartrite na Articulação Temporomandibular baseado na integração de informações clínicas, por imagem e biomoleculares.

2.1 Objetivos Específicos

Avaliar diferentes softwares para análise da textura óssea subcondral em imagens de tomografia computadorizada de alta resolução.

Avaliar a performance de diagnóstico de novos marcadores por imagem em côndilos com AO na ATM e saudáveis, em diferentes regiões subcondrais.

Desenvolver utilizando inteligência artificial modelos para o diagnóstico da OA na ATM com base na correlação e integração entre os dados clínicos, marcadores ósseos texturais subcondrais, e proteínas em sangue e saliva.

3 PUBLICAÇÕES

Essa tese é apresentada no formato de 3 artigos, sendo eles:

1) Software comparison to analyze bone radiomics from high resolution CBCT scans of mandibular condyles – Publicado na revista Dentomaxillofacial Radiology.

2) Quantitative Bone Imaging Biomarkers to Diagnose Temporomandibular Joint Osteoarthritis – Em revisão na revista Dentomaxillofacial Radiology

3) Osteoarthritis of the Temporomandibular Joint can be diagnosed earlier using biomarkers and machine learning – Em submissão para a revista Nature Communications.

3.1 Publicação 1*

Title of the papel: Software comparison to analyze bone radiomics from high resolution CBCT scans of mandibular condyles.

Shortened version of the title: Software comparison to analyze bone radiomics from hr- CBCT.

Type of Manuscript: Research Article

Author names: Jonas Bianchi[1, 2]

João Roberto Gonçalves[2]

Antonio Carlos de Oliveira Ruellas[1]

Jean-Baptiste Vimort[1,3]

Marilia Yatabe[1]

Beatriz Paniagua[3]

Pablo Hernandez3 Erika Benavides[4]

Fabiana Naomi Soki[4]

Lucia Helena Soares Cevidanes[1]

1- Department of Orthodontics and Pediatric Dentistry, School of Dentistry, University of Michigan, Ann Arbor, MI, USA.

2- Department of Pediatric Dentistry, São Paulo State University (Unesp), School of Dentistry, SP, Brazil.

3- Kitware, Inc., Carrboro, NC, USA

4- Department of Periodontics and Oral Medicine, School of Dentistry, University of Michigan, Ann Arbor, MI, USA.

* Artigo publicado e de acordo com as normas de formatação da revista Dentomaxillofacial Radiology.

Software Comparison to Analyze Bone Radiomics from high resolution CBCT scans of mandibular condyles.

ABSTRACT

Objectives: Radiomics refers to the extraction and analysis of advanced quantitative imaging from medical images to diagnose and/or predict diseases. In the dentistry field, the bone data from mandibular condyles could be computationally analyzed using the voxel information provided by high-resolution CBCT scans to increase the diagnostic power of temporomandibular joint (TMJ) conditions. However, such quantitative information demands innovative computational software, algorithm implementation, and validation. Our study aim was to compare a newly developed BoneTexture application to two-consolidated software with previous applications in the medical field, Ibex and BoneJ, to extract bone morphometric and textural features from mandibular condyles.

Methods: We used an imaging database of hr-CBCT TMJs scans with an isotropic voxel size of 0.08 mm3. A single group with sixty-six distinct mandibular condyles composed the final sample. We calculated eighteen variables for bone textural features and five for bone morphometric measurements using the Ibex, BoneJ and Bone Texture applications. Spearman correlation and Bland-Altman plot analyses were done to compare the agreement among software.

Results: The results showed a high Spearman correlation among the software applications (r= 0.7 to 1), with statistical significance for all variables, except Grey Level Non Uniformity and Short Run Emphasis. The Bland-Altman vertical axis showed, in general, good agreement between the software applications and the horizontal axis showed a narrow average distribution for Correlation, Long Run Emphasis and Long Run High Grey Level Emphasis.

Conclusions: Our data showed consistency among the three applications to analyze bone radiomics in high-resolution CBCT. Further studies are necessary to evaluate the applicability of those variables as new bone imaging biomarkers to diagnose bone diseases affecting TMJs.

Keywords: Cone-Beam Computed Tomography; Temporomandibular Joint Disorders; Software Validation; Tomography, X-Ray Computed;

INTRODUCTION

Quantitative imaging of mandibular condyles using Cone-beam Computed Tomography (CBCT) is being developed in Oral and Maxillofacial Radiology research.[1,2] Widespread incorporation of radiomics, that means, extracting quantitative information from medical images by converting them into minable high-dimensional data, will provide more accurate biological and clinical correlations as well as prognostic value.[3] The data provided has the potential to change clinical practice from a qualitative analysis of imaging features to a more dynamic, spatial, and phenotypical characterization of suspected lesions. There is a need for studies of diagnostic methodologies to better classify the imaging findings and the discovery of new biomarkers, that were discussed in different imaging sources such as MR, PET and CT.[4–8]

The High Resolution CBCT (hr-CBCT) is a new modality that provides more information and better spatial resolution. Increasing the amount of acquired voxels provides flexibility for the selection of smaller field of views with higher spatial resolution while following the ALARA/ALADA principle.[9,10] Hr-CBCT also facilitates the analysis of different bone parameters such as bone morphometry and textural features that were only possible using micro-CT, being a promising tool for the analysis of new bone-imaging biomarkers and its applications are promising.[11,12] The applicability of these new biomarkers may directly impact health and disease diagnosis in future studies; however, the computational data extraction depends on precise software and biomarkers validation. Cancer studies have pointed out the role of radiomics in early disease prediction, and bone conditions, such as osteoarthritis, demand an early diagnose in order to reduce the chronic musculoskeletal damage that is usually detected just in late stages.[3,13–15]

For imaging data extraction, different software applications have been developed to improve the radiomics approaches and selection of significant imaging features. Ibex16 (open-source software) and BoneJ[17] (application of Fiji software18) are examples of open-source methods; however, the software user interfaces are still complex and the applications are not specific to CBCT image. To simplify those approaches, Vimort et al.,[19] implemented a new application in the software 3D-Slicer (https://www.slicer.org) called BoneTexture.[20] The software has a user-friendly

interface and validation of ex-vivo computed tomography imaging has been performed.[1,2,12]

Due to the software applications complexity, algorithms implementation and data interpretation, a comparison of the available computational sources is needed before applying such tools for clinical decision-making. Thus, the aim of this study was to compare three software applications: BoneTexture, Ibex and BoneJ for analysis of eighteen bone texture features and five bone morphometric variables from sixty-six condyles. We hypothesized that there are no differences among the variables using the three software applications.

MATERIALS AND METHODS

Study Sample

This study was a secondary data analysis approved by the Institutional Review Board. One group composed our sample, obtained from a database with 34 patients, totalizing 68 hr- CBCT mandibular condyles scans. After outlier analysis, 2 condyles were excluded, (the values differed in three S.D from the 95% C.I), resulting in a single group with 66 condyles.

Sample Characteristics

We aimed to test the agreement and performance of different software to extract bone textural features in a single group with a sample containing real clinical data. Towards this aim, 17 of our subjects had clinical diagnosis of TMJ- OA (RDC/TMD clinical criteria)[13] and 17 were healthy. The goal was not to compare different conditions (disease x healthy) but to have both situations represented in our sample.

Imaging Acquisition

The hr-CBCT scans contained in the database were acquired in a 3D Accuitomo (J. Morita MFG. CORP Tokyo, Japan), according to the following TMJ acquisition protocol: FOV 40x40 mm; 90 kV, 5 mA and 30.8 s and a voxel size of 0.08 mm^3 at the University of Michigan – School of Dentistry.

Image Pre-processing

For image and variable standardization each hr-CBCT DICOM volume was cropped into a small RoI grayscale sample of 50x50x50 slices (voxel size of 0.08 mm3) using the module “Crop-Volume” of the 3D-Slicer Software and saved as a single image volume (.dcm). Additionally, the RoI spatial position was kept to contain the trabecular/cortical condyle bone without extrapolated the condyle boundaries (Figure 1). Others image-processing steps were necessary in order to comply with specific software input file needs as explained in the next sub-sections.

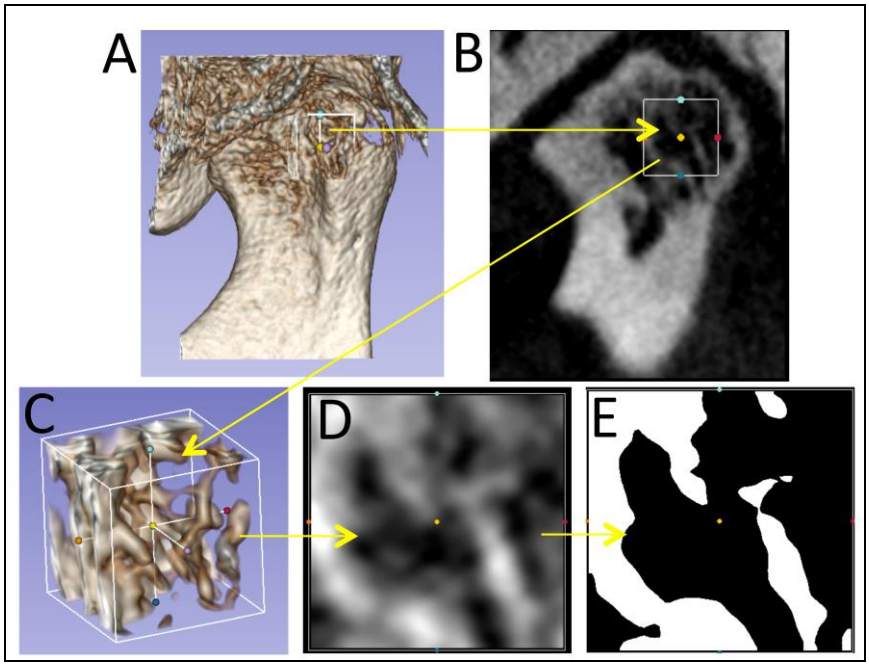

Figure 1 – Computational Image processing and sample preparation. A) 3D condyle rendering and its RoI in the center; B) Original grayscale hr-CBCT in the sagittal slice showing the limits of the RoI; C) RoI - 3D Rendering; D) RoI grayscale volume used to compute GLCM and GLRLM variables (50x50x50 slices); E) RoI after binary transformation using the median thresholding algorithm available in BoneJ. This binary image was used to compute bone morphometry.

Image Processing for Bone Textural Features

The Ibex[16] software requires a Region of Interest (RoI) segmentation in addition to the 50x50x50 slices grayscale samples. The itk-SNAP[21] software was used to create, select and export an annotation RoI (segmentation) as a single image volume, with the same volume and size for each sample. Then, the grayscale samples and their annotations were converted back into DICOM format using the 3D-Slicer. The files were loaded in the Ibex and BoneTexture applications in order to compute bone texture and bone morphometry features (Figure 2). Eighteen variables were divided in two main subgroups: 1) Grey-level Co-occurrence Matrix (GLCM)[22]

and 2) Grey-level Run Length matrix (GLRLM).[23,24] The first group Grey-level Co-occurrence Matrix (GLCM) gives values for the distribution of co-occurring pixel values and includes: Energy, Entropy, Correlation, Inverse Difference Moment, Inertia, Cluster Shade, Cluster Prominence and Haralick Correlation. The second group, Grey-level Run Length matrix (GLRLM),[23,24] gives the size of homogeneous runs for each grey level and includes: Short Run Emphasis, Long Run Emphasis, Grey Level Non Uniformity, Run Length Non Uniformity, Low Grey Level Run Emphasis, High Grey Level Run Emphasis, Short Run Low Grey Level Emphasis, Short Run High Grey Level Emphasis, Long Run Low Grey Level Emphasis and Long Run High Grey Level Emphasis.

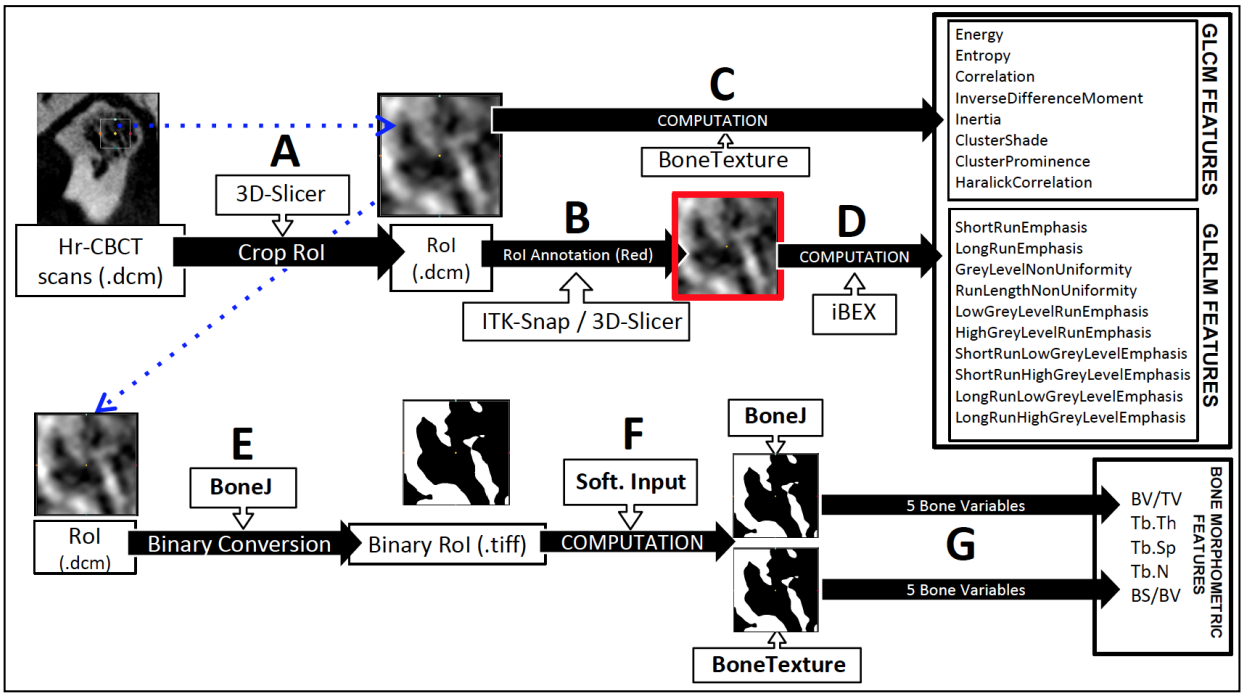

Figure 2 – Computational workflow; A) RoI cropping (50x50x50 slices) from each condyle. B) Annotation (segmentation) process of the RoI using ITK-snap and 3D- Slicer. This additional step was necessary to comply with Ibex requisites; C) BoneTexture computation of the GLCM and GLRLM variables; D) Ibex computation for GLCM and GLRLM variables. This step demands the annotation in addition to the RoI; E) RoI binary conversion using the BoneJ plugin; F) Input of the binary RoIs in the BoneJ and BoneTexture to compute the bone morphometry variables.

Image Processing for Bone Morphometry Variables

Initially the 50x50x50 slices grayscale volume samples were converted into a binary image using the BoneJ Application[18] tool called "median thresholding" and were then exported as Tagged Image File Format (tiff). These images were imported to the BoneJ application and BoneTexture for bone morphometry analysis (Figure 2). The following variables were examined: Trabecular Thickness (Tb.Th), trabecular

separation (Tb.Sp), trabecular number (Tb.N), Bone Volume per Total Volume (BV/TV) and Bone Surface per Bone Volume (BS/BV).[11,25] The values of Tb.N for the BoneJ software were obtained using the formula: Tb.N=(BV/TV)/Tb.Th, since this parameter is not explicitly computed in BoneJ.

Software Parameters

We have based our parameters in an optimized protocol described by BoneTexture developers.[20] The values used in BoneTexture to computed GLRLM variables were: number of bins: 10; Voxel Intensity Range: min -250 /max 4000; Distance range: min 0 / max 1 and Neighborhood Radius: 4. For GLCM: Number of bins: 10; Voxel Intensity Range: min -250 / max 4000 and Neighborhood Radius: 4 For the Ibex software, GLCM values were: direction= 0, 45, 90, 135, 180, 225, 270 and 315; AdaptLimitLevel=0; GrayLimits=-250 / 2100; NumLevels=10; Offset=1; and Symmetric=0. For the GLRLM: Direction = 0, 45, 90, 135, 180, 225, 270, 315; GrayLimits=-250 / 4000; NumLevels=10. Those parameters are sensitive to small changes and different software do not ask for the same inputs. In addition, for Ibex, the average of each direction was computed to have one value per variable and for the BoneTexture one final value is given. No filters were applied to analyze the GLCM and GLRM variables.

Variables Description

An explanation and description of each textural features and bone morphometry are presented in Table 1

Table 1- Description of the variables for bone morphometry and bone textural features.

BONE MORPHOMETRIC FEATURES[11]	DESCRIPTION
BV/TV*	Ratio between bone volume and total volume
Tb.Th*	Trabecular Thickness
Tb.Sp*	Trabecular Separation
Tb.N*	Trabecular Number
BS/BV*	Ratio between bone surface and bone volume (Surface density)
GLRLM FEATURES[18,22,37]	The GLRLM gives the size and length of homogeneous runs/points with the same grey-level value.
ShortRunEmphasis**	Large for fine textures.
LongRunEmphasis**	Large for coarse structural textures.
GreyLevelNonUniformity**	Small if the grey-level values are alike in the image.
RunLengthNonUniformity**	Small if the run lengths are alike through out the image.
LowGreyLevelRunEmphasis**	Large if the image has many low runs grey-value.
HighGreyLevelRunEmphasis**	Large if the image has many high runs grey-value.
ShortRunLowGreyLevelEmphasis**	Large if the image has many short runs of low grey-value.
ShortRunHighGreyLevelEmphasis**	Large if the image has many short runs of high grey-value.
LongRunLowGreyLevelEmphasis**	Large if the image has many long runs of low grey-value.
LongRunHighGreyLevelEmphasis**	Large if the image has many long runs of high grey-value.
GLCM FEATURES[18,32]	The grey-level co-occurrence matrix (GLCM) describes the distribution of co-occurring pixel/voxel values at a given offset/direction.
Energy**	Large if the image has textural uniformity and organization.
Entropy**	Large if the image has a random distribution of grey-level intensities and small for same grey-level distribution.
Correlation**	Indicates the Grey-level linear dependence between the pixels at the specified positions relative to each other.
InverseDifferenceMoment**	Large value for homogeneous images.
Inertia**	Small for image with similar grey-level values. Also known as Contrast.
ClusterShade**	Large for asymmetric images
ClusterProminence**	Large for asymmetric images
HaralickCorrelation**	Linear dependence between pixels relative to each other. **Ibex software gives the Autocorrelation.

*Calculated using BoneJ and BoneTexture applications;**Calculated using Ibex and BoneTexture applications.

Statistical Analysis

A single examiner performed the study and, as the software applications automatically calculated the values, the inter examiner reproducibility was not assessed. The variables presented a non-normal distribution after analysis of the kurtosis and symmetry. Thus, the Spearman correlation test was used to evaluate the correlation among all the variables between the software. Due to the complex algorithms nature, language programming and differences in the scales of the software, normalization of the data was necessary prior to descriptive statistics and

Bland-Altman analysis.[26,27] The normalization formula was: $Xi=(x-\bar{x})/S$ where Xi=new value, x=original value, $\bar{x}$ =average of the values and S= standard deviation.

RESULTS

Table 2 shows the descriptive statistics for the normalized values for each variable and software compared. As expected, the average is close to 0 and the standard deviation close to 1 for all variables with different variation of the confidence interval ranges.

Table 2- Descriptive statistics for each variable and respective software.

	BONETEXTURE APPLICATION				BONEJ APPLICATION			
Variables (n=66)		95% C.I				95% C.I		
	Mean	Min	Max	SD	Mean	Min	Max	SD
BV/TV (%)	-0.01	-3.15	3.22	1.01	-0.01	-3.15	3.21	1.01
Tb.Th (mm)	-0.03	-1.62	4	0.98	-0.01	-1.4	3.04	1.01
Tb.Sp (mm)	-0.01	-1.75	3.58	1.01	-0.02	-2.04	2.74	0.99
Tb.N (mm^{-1})	0.02	-2.44	3.08	0.99	0	-2.22	2.02	1.01
BS/BV (mm^{-1})	0.03	-3.19	2.41	0.98	0.03	-3.05	3.56	0.98
	BONETEXTURE APPLICATION				IBEX APPLICATION			
GLRLM_ShortRunEmphasis	-0.07	-2.66	1.53	0.93	0.06	-1.48	2.53	0.87
GLRLM_LongRunEmphasis	0.07	-1.53	2.66	0.93	-0.11	-0.9	2.38	0.61
GLRLM_GreyLevelNonUniformity	0.04	-1.58	2.45	0.86	0.06	-2.88	1.86	0.93
GLRLM_RunLengthNonUniformity	0.07	-1.63	3.13	0.92	0.07	-2.07	2.93	0.93
GLRLM_LowGreyLevelRunEmphasis	-0.02	-2.75	1.72	1.01	-0.03	-2.47	2.72	0.97
GLRLM_HighGreyLevelRunEmphasis	0.03	-1.43	3.56	1	0.03	-2.02	3.66	0.98
GLRLM_ShortRunLowGreyLevelEmphasis	-0.02	-2.74	1.68	1.01	-0.01	-1.6	2.36	0.91
GLRLM_ShortRunHighGreyLevelEmphasis	0.03	-1.45	3.56	1	0.06	-1.49	2.92	0.96
GLRLM_LongRunLowGreyLevelEmphasis	-0.01	-2.79	1.92	1.01	-0.11	-1.05	2.34	0.64
GLRLM_LongRunHighGreyLevelEmphasis	0.03	-1.36	3.54	0.99	-0.12	-0.85	2.38	0.57
GLCM_Energy	-0.08	-1.61	2.17	0.87	-0.06	-1.75	2.3	0.91
GLCM_Entropy	0.07	-1.6	1.95	0.92	0.06	-1.89	2.02	0.93
GLCM_Correlation	-0.11	-1.25	1.56	0.69	0.02	-1.83	1.86	0.99
GLCM_InverseDifferenceMoment	-0.09	-2.28	1.9	0.84	-0.09	-2.12	2.34	0.87
GLCM_Inertia	0.09	-1.9	2.28	0.84	0.09	-2.34	2.12	0.87
GLCM_ClusterShade	0.02	-1.7	4.16	1.01	0.02	-2.83	4.01	1.01
GLCM_ClusterProminence	0.02	-0.81	4.5	1.01	0.02	-0.8	4.2	1.01
GLCM_HaralickCorrelation	0.02	-0.79	5.15	1.01	0.02	-1.53	4.05	1.00

C.I: Confidence Interval; SD: Standard Deviation;

High Spearman correlations (r= 0.7 to 1) among the different software applications are shown in Table 3. The only variables that did not show a significant correlation were ShortRunEmphasis and GreyLevelNonUniformity. The variables: Correlation, Long Run Emphasis and Long Run High Grey Level Emphasis showed statistically significance but negative correlation, suggesting that the applications used different mathematical approach's to obtain these values.

Table 3- Spearman correlation among the BoneTexture, Ibex and BoneJ applications.

Variables (n=66)	r value	p value
BV/TV*	1	<0.001
Tb.Th*	0.620	<0.001
Tb.Sp*	0.853	<0.001
BS/BV*	0.974	<0.001
Tb.N*	0.891	<0.001
GLCM_Energy**	0.603	<0.001
GLCM_Entropy**	0.857	<0.001
GLCM_Correlation**	-0.835	<0.001
GLCM_InverseDifferenceMoment**	0.755	<0.001
GLCM_Inertia**	0.747	<0.001
GLCM_ClusterShade**	0.747	<0.001
GLCM_ClusterProminence**	0.796	<0.001
GLCM_HaralickCorrelation**	0.896	<0.001
GLRLM_ShortRunEmphasis**	-0.230	0.060
GLRLM_LongRunEmphasis**	-0.882	<0.001
GLRLM_GreyLevelNonUniformity**	-0.061	0.627
GLRLM_RunLengthNonUniformity**	0.855	<0.001
GLRLM_LowGreyLevelRunEmphasis**	0.734	<0.001
GLRLM_HighGreyLevelRunEmphasis**	0.925	<0.001
GLRLM_ShortRunLowGreyLevelEmphasis**	0.482	<0.001
GLRLM_ShortRunHighGreyLevelEmphasis**	0.770	<0.001
GLRLM_LongRunLowGreyLevelEmphasis**	0.762	<0.001
GLRLM_LongRunHighGreyLevelEmphasis**	-0.499	<0.001

$\alpha = 95\%$ and 2-tailed p value; $p<0.001$ statistically significant
*Comparison between BoneTexture and Ibex
**Comparison between BoneTexture and BoneJ

The Bland-Altman plots for comparison among software applications show a good agreement (vertical axis) between each software applications for all of the features as shown in the Figures 3, 4 and 5 with most values within the confidence interval. The horizontal dots distribution (horizontal axis) represent the average for each sample computed by the software applications. A larger distribution is seen for BV/TV, Tb.Th, Tb.Sp, Tb.N (Fig. 3: A to E); GLCM: Energy, Entropy, InverseDifferenceMoment, Inertia, ClusterShade, ClusterProminence, HaralickCorrelation (Figure 4: A, B, D, E, F, G and H) and GLRLM: ShortRunEmphasis, GreylevelNonUniformity, RunLenghtNonUniformity, LowGreyLevelRunEmphasis, HighGreyLevelRunEmphasis, ShortRunLowGreyLevelEmphasis, ShortRunHighGreyLevelEmphasis and LongRunLowGreyLevelEmphasis (Figure 5: A, C, D, E, F, G, H and I). On the other hand, the variables that did not presented such distinction between the sample averages (horizontal axis) were: Correlation for GLCM (Figure 4 - C) and for GLRLM: LongRunEmphasis and LongRunHighGreyLevelEmphasis (Figure 5: B and J).

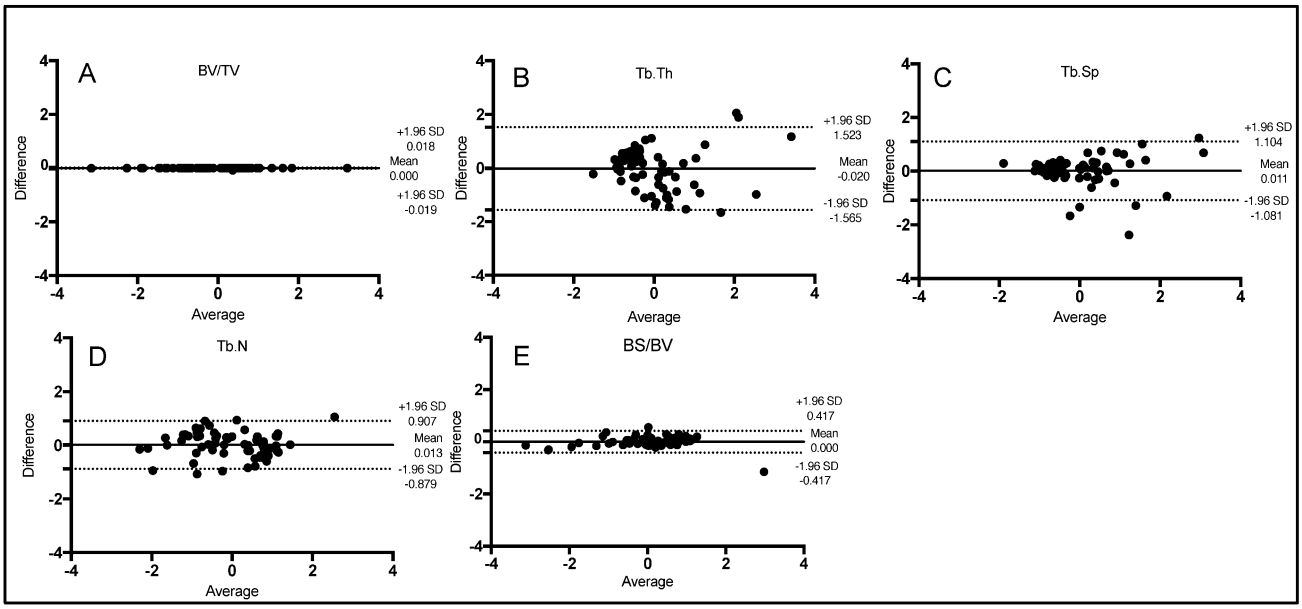

Figure 3 – Bland-Altman analysis of bone features between BoneTexture and BoneJ applications. The normalized values were used to compare.

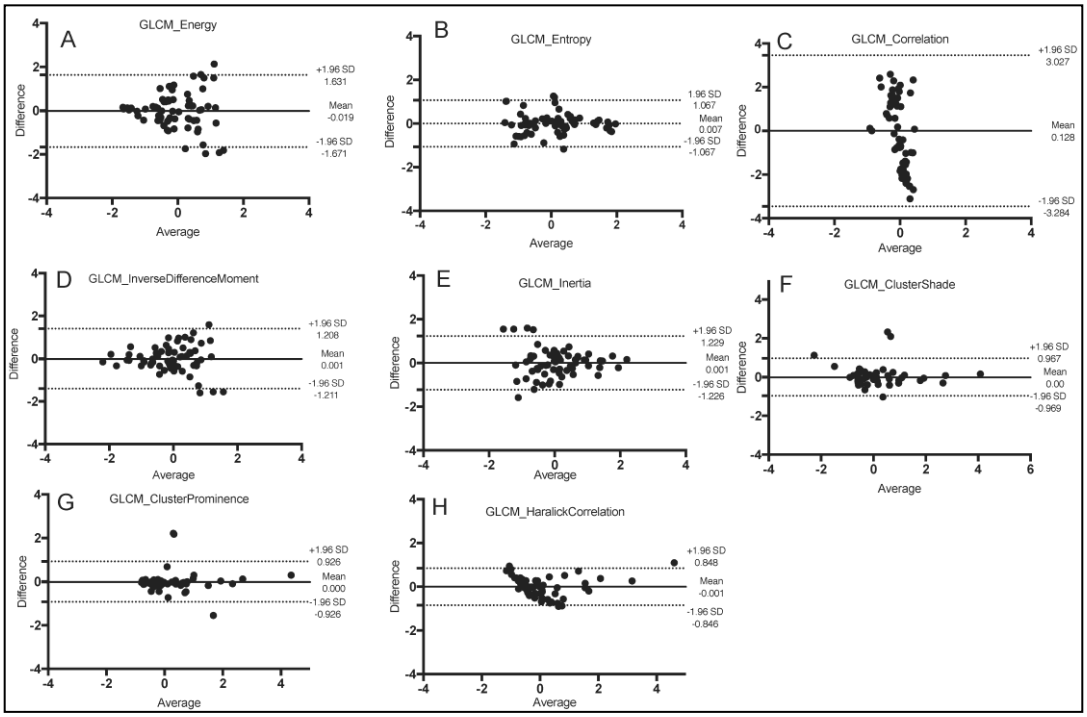

Figure 4 – Bland-Altman analysis of GLCM features between BoneTexture and Ibex applications. The normalized values were used to compare.

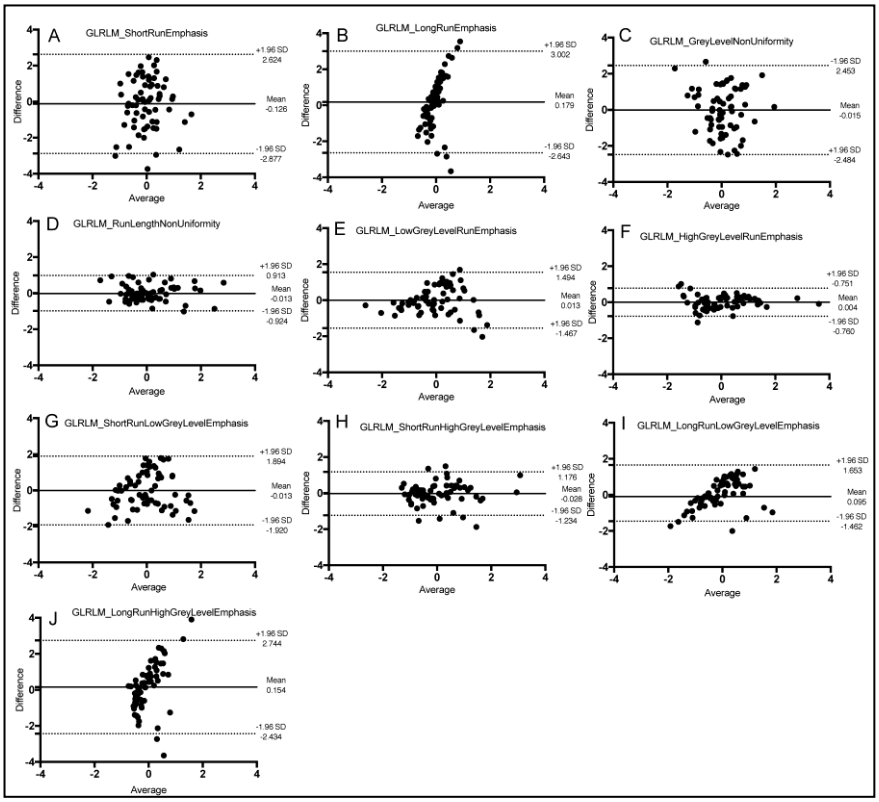

Figure 5 – Bland-Altman analysis of GLRLM features between BoneTexture and Ibex applications. The normalized values were used to compare.

DISCUSSION

The textural features described in this paper have been widely investigated in computed-medical research. Quantitative information extracted from volumetric images (CT and MRI) in cancer research have improved the integration of imaging, clinical and genomic features.[16,28,29] In bone research, the big challenge is to discover specific imaging biomarkers that identify earlier stages and/or predict progression of bone diseases. Caramella et al.,[30] demonstrated that caution should be taken when analyzing grey-level textures in CT images, mainly due to the differences in image acquisition protocols and reconstruction algorithms. The present study has standardized these variables and tested only the effects and differences among the three software applications. We focused on previously published textural features such as GLRLM and GLCM, due to their nature in identifying grey-level patterns[22,23,26,31–33] and morphometric bone features.[11,25] Our results aid the choice of a precise software to assess bone imaging markers, the selection of the best imaging bone biomarkers and evaluate the software parameters, demonstrating the potential applicability of the evaluated software as a method for future bone studies.

Recent studies by Paniagua et al.,[12] and Vimort et al.,[19] showed that GLCM and GLRLM textural features are potential diagnostic markers of TMJ OA. However, those studies focused on methodological developments of a novel software application called BoneTexture. This software is based on the implementation of ITK features, such as fast neighborhood operators, re-use of intermediate computations, and minimization of memory use. These feature computations are n-dimensional.[20] Our study showed the correlation and agreement of BoneTexture with two other software applications previously applied in the medical field: Ibex and BoneJ.[16] The spearman correlation (Table 3) showed a high and significant correlation for Bone Morphometry and all the GLCM features, except for two GLRLM variables: GreyLevelNonUniformity (p=0.627) and ShortRunEmphasis (p=0.06). However,

the negative correlation between BoneTexture and Ibex values for Correlation, Long Run Emphasis and Long Run High Grey Level Emphasis suggests that the applications might use different mathematical approach's to obtain these values. For this reason, further studies should have caution when evaluating these biomarkers using BoneTexture or Ibex. Since the algorithms` implementation demands different computational mathematical libraries and language programming, the results obtained within software differed in terms of scale. For this reason, the results were normalized before the Bland-Altman and descriptive analyses. For the Bland-Altman plots (Fig. 3 to 5), the closer the distribution to the horizontal median line, the better the agreement between the software. The distribution in the horizontal axis shows the variability in the sample average.[26,27] This variability is expected since the sample included 66 different RoIs from human mandibular condyles. In addition, to better understand the confidence interval for Bland-Altman, a direct comparison with the individual confidence interval values (Table 2) makes necessary. As observed, the limits of agreement in Bland-Altman (Fig. 3) for Bone morphometric features were larger than each software's 95% confidence interval (C.I) as shown in Table 2. For GLCM features (Fig. 4), the 95% CIs in Table 2 were larger than the limits of agreement in the Bland-Altman for almost all the variables tested, except for the variable Correlation. On the other hand, the limits of agreement for GLRLM features (Fig. 5) presented wider deviation in comparison to the 95% confidence intervals shown in Table 2. The 6 variables, with narrower confidence intervals were: RunLengthNonUniformity, LowGreyLevelRunEmphasis, HighGreyLevelRunEmphasis, ShortRunLowGreyLevelEmphasis,

ShortRunHighGreyLevelEmphasis and LongRunLowGreyLevelEmphasis. Those results suggest that the GLRLM features are more affected by the software choice. The variables, Short Run Emphasis, Long Run Emphasis, Grey Level Non Uniformity and Long Run High Grey Level Emphasis, presented a wider C.I and should be further investigated in next studies, focusing on how much the software settings and parameters could affect the results.

Additionally, Ebrahim et al.,[1] showed that the measurements of Bone morphometry are suitable bone imaging biomarker. They compared the histological findings with biomarkers from CBCT condyles and found that the GLRLM and GLCM features not present a strong correlation with osteoclast number. This suggests that these biomarkers are mainly involved with other bone characteristics, such as: 3D morphology and grayscale organization, instead of a direct bone resorption response. Figure 6 displays a qualitative description of how complex the interpretation of GLCM and GLRM features could be in clinical research. The BoneTexture application was used to compute and display the 3 selected extreme cases from our sample. The observed results allow us to see how much each biomarker depends on the greylevel organization. A general good ability to differentiate the grayscale patterns is observed among the variables.

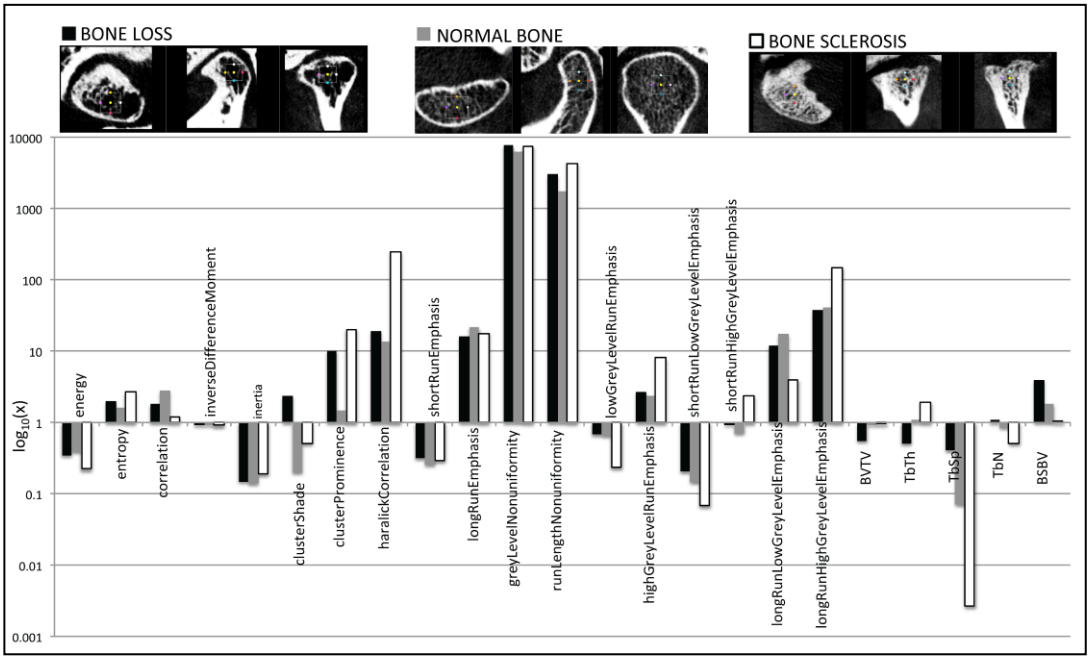

Figure 6 – Computation of 3 selected extreme cases from our sample and the quantitative results for our proposed biomarkers using the BoneTexture application with the parameters described in this paper.

Future studies, with larger samples for adequate power of statistical analysis, are needed to determine the applicability of these biomarkers to diagnose and/or predict progression of bone diseases in longitudinal assessments. Prior to testing the sensitivity and specificity of these surrogate biomarkers to diagnose condylar health and disease, future investigations will require radiology experts and clinical interpretation as gold standard references, as well as standardization of other image processing procedures not tested in the present study, such as segmentation and selection of the same region of interest among the subjects, avoiding bias due to the RoI selection. In summary, we showed the applicability and agreement among 3 different software applications to assess bone textural features and morphometry; additional studies are necessary to elucidate the clinical significance of these variables

CONCLUSION

The BoneTexture application computed textural features and bone morphometry measurements with good agreement and high correlations compared to the BoneJ and Ibex applications. Further studies using hr-CBCT must be conducted to describe the applicability of these textural features to diagnose health and disease in mandibular condyles.

ACKNOWLEDGMENTS

This study was partially funded by the Coordenação de Aperfeiçoamento de Pessoal de Nível Superior - Brasil (CAPES) - Finance Code 001 and supported by NIH grants DE R01DE024450 and R21DE025306.

REFERENCES

[1] Ebrahim FH, Ruellas ACO, Paniagua B, Benavides E, Jepsen K, Wolford L, et al. Accuracy of biomarkers obtained from cone beam computed tomography in assessing the internal trabecular structure of the mandibular condyle. Oral Surg Oral Med Oral Pathol Oral Radiol 2017;124:588–99. doi:10.1016/j.oooo.2017.08.013.

[2] Vimort J-B, Ruellas A, Prothero J, Marron JS, McCormick M, Cevidanes L, et al. Detection of bone loss via subchondral bone analysis. Proc SPIE--the Int Soc Opt Eng 2018;10578:25. doi:10.1117/12.2293654.

[3] Hochhegger B, Zanon M, Altmayer S, Pacini GS, Balbinot F, Francisco MZ, et al. Advances in Imaging and Automated Quantification of Malignant Pulmonary

Diseases: A State-of-the-Art Review. Lung 2018;196:633–42. doi:10.1007/s00408-018-0156-0.

[4] Johnson VL, App B, Ex S, Sc S, Hunter DJ. Osteoarthritis : What Does Imaging Tell Us about Its Etiology ? Semin Musculoskelet Radiol 2012;16:410–9.

[5] Brandi ML. Microarchitecture, the key to bone quality. Rheumatology (Oxford) 2009;48 Suppl 4:iv3-8. doi:10.1093/rheumatology/kep273.

[6] Lewis EL, Dolwick MF, Abramowicz S, Reeder SL. Contemporary Imaging of the Temporomandibular Joint. Dent Clin North Am 2008;52:875–90. doi:10.1016/j.cden.2008.06.001.

[7] Neogi T, Felson DT. Osteoarthritis: Bone as an imaging biomarker and treatment target in OA. Nat Rev Rheumatol 2016;12:503–4. doi:10.1038/nrrheum.2016.113.

[8] Starkov P, Aguilera TA, Golden DI, Shultz DB, Trakul N, Maxim PG, et al. The use of texture-based radiomics CT analysis to predict outcomes in early-stage non-small cell lung cancer treated with stereotactic ablative radiotherapy. Br J Radiol 2019;92:20180228. doi:10.1259/bjr.20180228.

[9] Editorial. ALARA still applies. Oral Surg Oral Med Oral Pathol Oral Radiol Endod 2005;100:395–7.

[10] ICRP, Rehani MM, Gupta R, Bartling S, Sharp GC, Pauwels R, et al. Radiological Protection in Cone Beam Computed Tomography (CBCT). ICRP Publication 129. Ann ICRP 2015;44:9–127. doi:10.1177/0146645315575485.

[11] Dempster DW, Compston JE, Drezner MK, Glorieux FH, Kanis JA, Malluche H, et al. Standardized nomenclature, symbols, and units for bone histomorphometry: A 2012 update of the report of the ASBMR Histomorphometry Nomenclature Committee. J Bone Miner Res 2013;28:2–17. doi:10.1002/jbmr.1805.

[12] Paniagua B, Ruellas AC, Benavides E, Marron S, Wolford L, Cevidanes L. Validation of CBCT for the computation of textural biomarkers. SPIE Med Imaging 2015;9417:1–15. doi:10.1117/12.2081859.

[13] Schiffman EL, Ohrbach R, Truelove EL, Look J, Anderson G, Goulet J, et al. Diagnostic Criteria for Temporomandibular Disorders (DC/TMD) for Clinical and Research Applications: Recommendations of the International RDC/TMD Consortium Network* and Orofacial Pain Special Interest Group. J Oral Facial Pain Headache 2014;28:6–27. doi:10.1002/aur.1474.Replication.

[14] Murphy MK, Macbarb RF, Wong ME, Athanasiou KA. Temporomandibular Joint Disorders: A Review of Etiology, Clinical Management, and Tissue Engineering Strategies HHS Public Access. Int J Oral Maxillofac Implant 2013;28:393–414. doi:10.1126/science.aaa3380.

[15] Castellano G, Bonilha L, Li LM, Cendes F. Texture analysis of medical images. Clin Radiol 2004;59:1061–9. doi:10.1016/J.CRAD.2004.07.008.

[16] Zhang L, Fried D V., Fave XJ, Hunter LA, Yang J, Court LE. Ibex: An open infrastructure software platform to facilitate collaborative work in radiomics. Med Phys 2015;42:1341–53. doi:10.1118/1.4908210.

[17] Doube M, Kłosowski MM, Arganda-Carreras I, Cordelières FP, Dougherty RP, Jackson JS, et al. BoneJ: Free and extensible bone image analysis in ImageJ. Bone 2010;47:1076–9. doi:10.1016/j.bone.2010.08.023.

[18] Paniagua B, Ruellas AC, Benavides E, Marron S, Wolford L, Cevidanes L, et al. Validation of CBCT for the computation of textural biomarkers. Proc SPIE--the Int Soc Opt Eng 2015;9417:94171B. doi:10.1117/12.2081859.

[19] Vimort J-B, McCormick M, Budin F, Paniagua B. Computing Textural Feature Maps for N-Dimensional images. Insight J 2017. http://hdl.handle.net/10380/3574 (accessed January 2, 2019).

[20] Documentation/Nightly/Extensions/BoneTextureExtension - SlicerWiki n.d. https://www.slicer.org/wiki/Documentation/Nightly/Extensions/BoneTexture Extension (accessed April 2, 2019).

[21] Yushkevich PA, Piven J, Hazlett HC, Smith RG, Ho S, Gee JC, et al. User-guided 3D active contour segmentation of anatomical structures: Significantly improved efficiency and reliability. Neuroimage 2006;31:1116– 28. doi:10.1016/j.neuroimage.2006.01.015.

[22] Galloway MM. Texture analysis using gray level run lengths. Comput Graph Image Process 1975;4:172–9. doi:http://dx.doi.org/10.1016/S0146- 664X(75)80008-6.

[23] Haralick R, Shanmugan K, Dinstein I. Textural features for image classification. IEEE Trans Syst Man Cybern 1973;3:610–21. doi:10.1109/TSMC.1973.4309314.

[24] Haralick, R.M. and Shapiro LG. (1992) Computer and Robot Vision. Addison-Wesley Longman Publishing Co., Inc., Boston. Comput. Robot Vis. Vol. 1, Boston, MA: Addison-Wesley Longman Publishing Co., Inc.; 1992, p. 459.

[25] Bouxsein ML, Boyd SK, Christiansen BA, Guldberg RE, Jepsen KJ, Müller R. Guidelines for assessment of bone microstructure in rodents using micro-computed tomography. J Bone Miner Res 2010;25:1468–86. doi:10.1002/jbmr.141.

[26] Bland JM, Altman DG. Statistical methods for assessing agreement between two methods of clinical measurement. Lancet (London, England) 1986;1:307–10.

[27] Giavarina D. Understanding Bland Altman analysis. Biochem Medica 2015;25:141–51. doi:10.11613/BM.2015.015.

[28] Gillies RJ, Kinahan PE, Hricak H. Radiomics: Images Are More than Pictures, They Are Data. Radiology 2016;278:563–77. doi:10.1148/radiol.2015151169.

[29] Nioche C, Orlhac F, Boughdad S, Reuzé S, Goya-Outi J, Robert C, et al. LIFEx: A Freeware for Radiomic Feature Calculation in Multimodality Imaging to Accelerate Advances in the Characterization of Tumor Heterogeneity. Cancer Res 2018;78:4786–9. doi:10.1158/0008-5472.CAN- 18-0125.

[30] Caramella C, Allorant A, Orlhac F, Bidault F, Asselain B, Ammari S, et al. Can we trust the calculation of texture indices of CT images? A phantom study. Med Phys 2018;45:1529–36. doi:10.1002/mp.12809.

[31] Amadasun M, King R. Textural features corresponding to textural properties. IEEE Trans Syst Man Cybern 1989;19:1264–74. doi:10.1109/21.44046.

[32] Dasarathy B V., Holder EB. Image characterizations based on joint gray level-run length distributions. Pattern Recognit Lett 1991;12:497–502. doi:10.1016/0167-8655(91)80014-2.

[33] Tang X. Texture information in run-length matrices. IEEE Trans Image Process 1998;7:1602–9. doi:10.1109/83.725367.

3.2 Publicação 2*

Title of the paper: Quantitative Bone Imaging Biomarkers to Diagnose Temporomandibular Joint Osteoarthritis.

Shortened version of the title: Imaging Biomarkers to Diagnose TMJ Osteoarthritis.

Type of Manuscript: Research Article

Author names

Jonas Bianchi[1,2] - bianchij@umich.edu

João Roberto Gonçalves[2] – joaogonc2002@yahoo.com.br

Antônio Carlos de Oliveira Ruellas[1] - aruellas@umich.edu

Lawrence M Ashman[3] - ashmanl@umich.edu

Jean-Baptiste Vimort[1,4] - jb.vimort@gmail.com

Marilia Yatabe[1] - msyatabe@umich.edu

Beatriz Paniagua[4] - beatriz.paniagua@kitware.com

Pablo Hernandez[4] - pablo.hernandez@kitware.com

Erika Benavides[5] - benavid@umich.edu

Fabiana Naomi Soki[5] - fabisoki@umich.edu

Marcos Ioshida[1] - mioshida@umich.edu

Lucia Helena Soares Cevidanes[1] - luciacev@umich.edu

1. Department of Orthodontics and Pediatric Dentistry, School of Dentistry, University of Michigan, Ann Arbor, MI, USA.

2. Department of Pediatric Dentistry, São Paulo State University (Unesp), School of Dentistry, Araraquara, SP, Brazil.

3. Oral & Maxillofacial Surgery, Hospital Dentistry, University of Michigan, Ann Arbor, MI, USA.

4. Kitware, Inc., Carrboro, NC, USA

5. Department of Periodontics and Oral Medicine, School of Dentistry, University of Michigan, Ann Arbor, MI, USA.

* Artigo submetido e em revisão, de acordo com as normas de formatação da revista Dentomaxillofacial Radiology.

Quantitative Bone Imaging Biomarkers to Diagnose Temporomandibular Joint Osteoarthritis.

ABSTRACT

Objectives: To determine the diagnostic performance of quantitative bone texture imaging biomarkers for diagnosis of temporomandibular joint (TMJ) osteoarthritis (OA).

Methods: This study prospectively collected high-resolution TMJ CBCT images (0.08 mm3 voxel size). The sample consisted of two groups prospectively enrolled, Group TMJ OA: consisted of 51 patients with a clinical diagnosis of TMJ OA and Control Group: 43 asymptomatic subjects. Six regions of each mandibular condyle scan were extracted (lateral, medial, central, posterior, anterior and superior) for computation of five bone morphometric and eighteen grey level texture-based variables. The groups were compared using Mann-Whitney U test. To determine the diagnostic performance, we calculated the receiver operating characteristic (ROC) curve for each variable and for a predictive variable.

Results: Thirteen variables in the lateral and ten variables in the central condylar regions showed statistically significant differences ($p < 0.05$) between the TMJ OA and Control groups. Those variables showed a ROC curve with the area under the curve (AUC) between 0.58 to 0.63 ($p < 0.05$) and the combined predictive variable showed an AUC of 0.74 (CI: 0.67 to 0.81; $p < 0.01$).

Conclusions: Our results showed statistically significant difference between Control and TMJ OA groups in the subchondral bone microstructure in the lateral and central condylar regions. Thirteen imaging bone biomarkers presented good diagnostic performance for diagnosis of TMJ OA indicating that the texture and geometry of the subchondral bone microarchitecture can be useful for quantitative grading of the disease

Keywords: Cone-Beam Computed Tomography; Temporomandibular Joint Disorders; Osteoarthritis; Diagnostic Imaging; Biomarkers

INTRODUCTION

The most common joint disease is osteoarthritis (OA), affecting approximately 10% of women and 18% of men over 60 years old around the world[1]. OA is a degenerative musculoskeletal disease and its natural cycle occurs mainly in three inflammatory stages: enzymatic, cartilaginous and bony changes. In temporomandibular joint (TMJ) osteoarthritis, the signs and symptoms include pain, continuous inflammatory process with articular cartilage degradation, cortical and trabecular bone resorption, sclerotic bone formation and synovial proliferation. Clinically, TMJ OA patients often present deficiency in the TMJ functions and facial asymmetry[2,3].

The clinical assessment is a non-invasive method indicated prior to imaging exams to diagnose TMJ conditions, as part of the standardized diagnostic criteria for temporomandibular disorders (TMD)[4]. Signs and symptoms may; however, manifest only at more advanced stages of the disease in which bone, cartilage, and articular disc alterations have irreversibly progressed. Complementary diagnostic exams, such as radiography and MRI[5–7], continue to be extensively used, while advanced quantitative texture analysis of imaging data is becoming more popular.[8] Machine learning methods have recently been applied to automatically segment joint structures and automatize quantitative imaging grading[9,10]. In light of these technological advances, image analysis workflows are needed for predictive models harnessing multi-modality, multiparametric and demographic data available.

As a progressive degenerative joint disorder, OA has long been viewed as a primary disorder of articular cartilage. However, the microarchitecture of the subchondral bone has recently been reported to play a vital role in the pathogenesis of OA, as evidenced by initial changes in the subchondral bone organization[11]. Such diagnosis has been compromised by the absence of quantitative methodologies to analyze and extract bone texture information[6,12]. A relatively new high resolution low radiation cone beam computed tomography (hr-CBCT) facilitates the analysis of the bone morphometry microstructure and textural features that were previously only possible using micro-CT[2,8,13–18]. Selection of the most informative textural and morphometric subchondral bone features has the potential to change clinical practice from qualitative analysis to a more dynamic and phenotypical characterization of suspected lesions, using integrated textural biomarkers that combine subsets of collected patient data[19,20]. New software applications, with a friendly interface, can

now easily extract large amounts of quantitative features from hr-CBCT grayscale images[21–24]. Towards these promising methodologies, a paradigm shift in diagnosis is necessary, from the traditional radiologic assessments to integrative statistical models. Thus, diseases that have a silent onset, such as TMJ OA, may potentially be detected using non-invasive exams[12,25–27].

For these reasons, this study evaluated the diagnostic performance of quantitative bone texture and morphometry imaging biomarkers extracted from hr-CBCT scans for the diagnosis of OA of the temporomandibular joint. The main objective was to investigate the ability of those biomarkers to differentiate control and TMJ OA patients. We hypothesized that there were significant differences between Control and TMJ OA groups in the condylar subchondral bone microstructure. The null hypothesis was that there were no differences between the tested imaging biomarkers in Control and OA Groups.

MATERIALS AND METHODS

This study followed the STROBE guidelines for observational studies28.

Study Design and Participants

This cross-sectional study was conducted at the University of Michigan, Ann Arbor – MI at the United States of the America, from January 2016 to December 2018, and approved by the Institutional Review Board (HUM00105204 and HUM00113199). All the patients signed informed consent and agreed to participate in this study. The inclusion criteria for prospective data collection were: age between 21 – 70 years old, no history of systemic diseases; no history of jaw joint trauma, surgery or recent jaw joint injections; no currency pregnancy and no congenital bone or cartilage disease. The patients were recruited by advertisement or personal interviews during the first appointment with a single temporomandibular disorders (TMD) specialist from the University of Michigan. A total of 94 patients were recruited, resulting in 188 mandibular condyles hr-CBCT scans. All subjects were clinically evaluated through the clinical symptoms using the Diagnostic Criteria for Temporomandibular Disorders (DC/TMD)[29] and divided into two groups – Control Group (n=43 patients, 86 condyles) and OA Group (n=51 patients, 102 condyles). However, in the control group, two subjects had one condyle excluded (resulting in 84 condyles), and in the TMJ OA group, three patients had one condyle excluded (resulting in 99 condyles). The reasons for exclusion were to reduce possible bias

due to technical problems in the hr-CBCT image acquisition, imaging artifacts, presence of large alterations in the condylar surface and poor image quality. Control subjects should not have any history of clinical signs or symptoms of temporomandibular disorders evaluated using the (DC/TMD)[29]. To be included in the TMJ OA group, patients must present TMJ pain for less than 10 years and clinical symptoms, evaluated using the DC/TMD, including TMJ noise during movement or function in the last 30 days, and crepitus detected during mandible excursive movements[29]. A post-hoc statistical analysis to assess the sample power and effect size was done using the software G-Power (version 3.1.9; Franz Faul Universitat, Kiel, Germany). The sample demographic distribution presented a similar age range, being 39.6 years ± 13.7SD for control and 40.9 years ±12.7SD for TMJ OA. However, both groups showed a higher number of women, corroborating with the literature[30–32].

Imaging Acquisition

All hr-CBCT scans were acquired using the 3D Accuitomo (J. Morita MFG. CORP Tokyo, Japan) scanner. The TMJ acquisition protocol used a field of view 40x40 mm; 90 kVp, 5 mAs, scanning time of 30.8 s and a voxel size of 0.08 mm^3 at the University of Michigan, School of Dentistry. The images were exported in *DICOM (.dcm)* format using the i-Dixel software (J. Morita MFG. CORP Tokyo, Japan). The images were de-identified and coded to avoid investigator bias. The limitation of the exposure to the smallest FOV possible is in accordance with the ALARA[15] (As Low As Reasonably Achievable) principle and this radiation reduction to the patient, maintaining or even improving the level of precision and accuracy in the diagnosis, supports the concept “As Low As Diagnostically Acceptable” (ALADA)[33].

The CBCT acquired for research purposes involves radiation risks: The International Commission on Radiological Protection 2007 calculations estimates that effective adult doses from large FOV examinations are 114 µSv (per TMJ/ scan). This is equivalent to about 18 days of naturally occurring background dose. This is significantly less than the effective dose between 500 and 900 micro Sv for a spiral CT scan of the head, and is about the same as the 9 dental periapical x-rays, less than a chest x-ray. The researchers will try to minimize these risks by: the smallest FOV possible 4cm x 4cm and a lead apron will be used for all patients to cover the chest and the body region that contains the stomach, intestines, liver, and other organs.

Image Pre-Processing

In order to standardize the grey level hr-CBCT images, a novel detailed pre-processing protocol shown in Fig. 1 was used. Two imaging software were used: 3D-Slicer[34] (https://www.slicer.org) and the ITK-SNAP[35]. The common orientation of each 3D condyle mesh allowed standardized selection of the volumes of interests (VoIs). As each patient had a hr-CBCT scan taken in a different spatial position, we approximated the mandibular condyles in a common coordinate system for all subjects (Fig. 2).

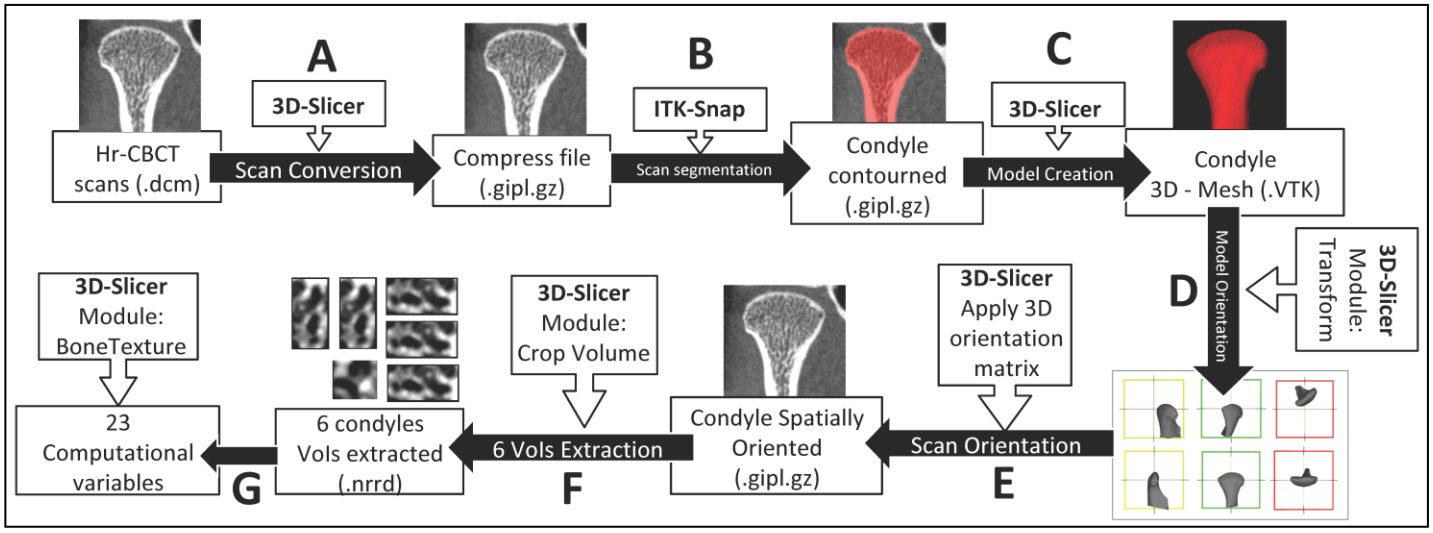

FIGURE 1 – Computational processing workflow. First, all the left hr-CBCT scans were mirrored to the right side using the "Transforms" tool in the 3D-slicer software. The next steps were as follows: A) The 3D-Slicer software was used to convert the original hr-CBCT files to a compressed format; B) The ITK-Snap software was used to segment the entire condyle; C) 3D-Slicer converted the segmented condyle volume to a 3D-Surface; D) Using the "Transform" module in 3D-Slicer a spatial orientation for each condyle 3D model was made; E) The spatial orientation matrix created in the last step was applied to the condyle scan. Each condyle had its proper orientation according to its orientation matrix; F) Using the "Crop-Volume" tool six different regions of the condyle (Anterior, Posterior, Lateral, Medial, Superior and Central) were selected; G) Using the "BoneTexture" module in 3D slicer all the variables studied for each region of the condyle were computed.

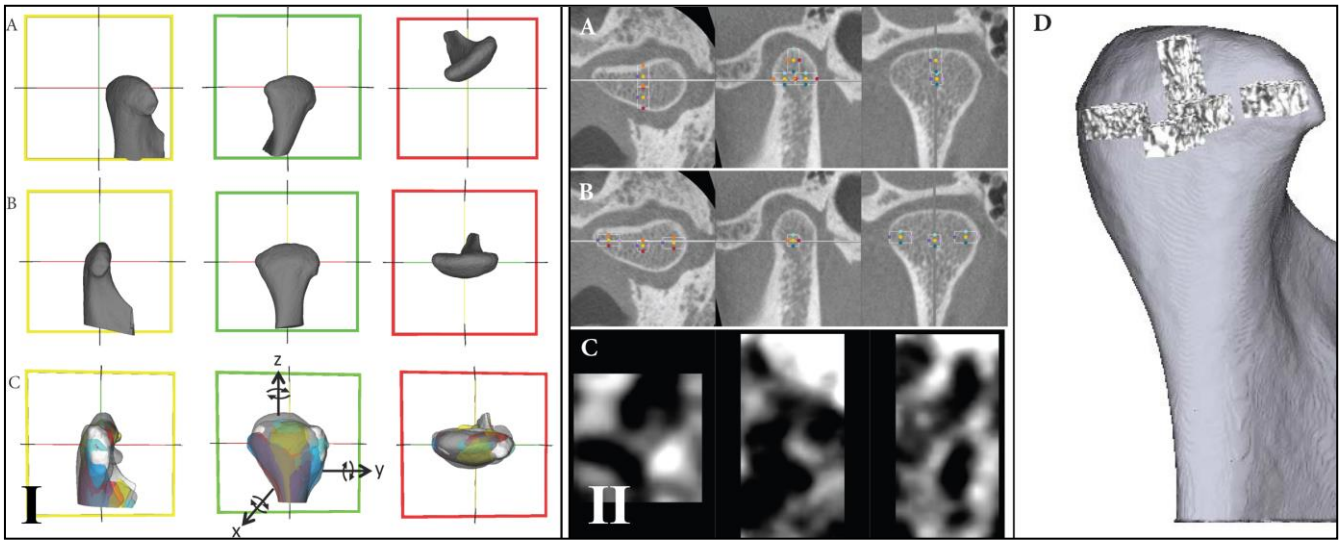

FIGURE 2 – **I)** The "Transforms" tool of the 3D-Slicer software was used to standardize the spatial orientation of the 3D-Condyles. A) The condyle before the orientation; B) The condyle after the orientation. C) Example of 8 condyles oriented. Reference lines (red, green and yellow) were used in the same spatial position for all condyles to allow a common spatial position for all condyles. In a lateral view, the yellow line was parallel to the condylar neck. In the posterior view, the red line connects the lateral and medial poles. In the superior view, the green line also connects the lateral and medial poles. **II)** Volume of Interest (VoI) extractions. After the spatial orientation, the "Crop-Volume" module in 3D-Slicer was used to generate the VoIs. A) Selection of the Anterior, Posterior and Superior VoIs. B) Selection of the Lateral, Medial and Central VoIs; C) Example of the anterior region containing the grayscale information of that volume of interest; D) 3D rendering to illustrate each VoI and the condylar region where its belong. The criteria for the boundaries were: Lateral, Medial, Posterior, Superior and Anterior VoIs – the rectangular prism starts in the most external condylar bone to the direction of the trabecular condyle center; Central: the cube was positioned in the central region of the trabecular bone.

Volumes of Interest (VoI)

Six different volumes of interest (VoIs) regions were selected and extracted using the "Crop-Volume" module of 3D-Slicer software (Fig. 1F). The VoIs were: Lateral, Medial, Posterior, Anterior, Superior and Central (Fig. 2). For the Lateral, Medial, Anterior, Superior and Posterior regions, the VoI had a rectangular prism shape and were cropped with 25 x 25 x 50 slices each and for the Central region had a cube shape with 25 X 25 X 25 slices.

Bone Imaging Biomarkers (Variables)

We evaluated a total of 23 surrogate imaging biomarkers. The five bone morphometry included Trabecular Thickness (Tb.Th), trabecular separation (Tb.Sp), trabecular number (Tb.N), Bone Volume per Total Volume (BV/TV) and Bone Surface per Bone Volume (BS/BV). Eighteen quantitative bone texture features included two main groups of variables: 1) Grey-level Co-occurrence Matrix (GLCM)[36] and 2)

Grey-level Run Length matrix (GLRLM)[37,38]. The GLCM variables quantified the distribution of co-occurring pixel values and include Energy, Entropy, Auto Correlation, Inverse Difference Moment, Inertia, Cluster Shade, Cluster Prominence, and Haralick Correlation. The GLRLM variables quantified the size of homogeneous runs for each grey level and include: Short Run Emphasis, Long Run Emphasis, Grey Level Non Uniformity, Run Length Non Uniformity, Low Grey Level Run Emphasis, High Grey Level Run Emphasis, Short Run Low Grey Level Emphasis, Short Run High Grey Level Emphasis, Long Run Low Grey Level Emphasis and Long Run High Grey Level Emphasis.

Computational Parameters for Bone Imaging Biomarkers Computation

The BoneTexture[39] module of the 3D-Slicer software[34] (https://www.slicer.org) was used to compute the bone imaging biomarkers and obtain the subchondral bone microstructure values. We have chosen the software computation parameters based on the user manual and our pilot calibration studies. The following computational software parameters were selected in the BoneTexture module: for GLCM: *Mask "inside" value*: 1*; number of bins*: 10; *voxel intensity range min*. = -1000, *max*=2500; *neighborhood radius*: 4; for GLRLM: *Mask "inside" value*: 1; number of bins: 10; *voxel intensity range min*. = -1000, *max*=2500; *distance range*: *min*. = 0, *max*=1; neighborhood *radius*: 4. For bone morphometry (BM) the software parameters were: *threshold:* 250 and *neighborhood radius*: 4.

Statistical Analysis

The statistical analysis was performed using the SPSS IBM software (v.25.0). The data distribution between the left and right mandibular condyles showed a non-dependency relation resulting in a number of 2 condyles for each patient (right condyle and left mirrored condyle). The intraclass correlation coefficient (ICC) was assessed with an interval of 2 weeks to evaluate the study repeatability. The Mann-Whitney U test for independent samples compared the two groups and the bone imaging biomarkers rank values were computed due to its non-normal data distribution after analysis of kurtosis and symmetry. We computed a receiver operating characteristic curve (ROC)[40] to determine the biomarkers diagnostic performance to diagnose TMJ OA. In addition, a unique predictive variable was

created using a binary logistic regression with the statistically significant variables and computed in a new ROC curve. We also evaluated the Spearman correlation among the morphometric and texture variables and the patient age.

RESULTS

Participants, Descriptive Data and Method Error

Table 1 shows the patient's demographic distribution, the control group (n=43 subjects) had 6 males and 37 females, and the OA group (n=51 patients) had 7 males and 44 females. The ICC (Table 2) showed high repeatability for all the variables (r ≥ 0.7) except for Cluster Shade (r=0.1), Cluster Prominence (r = 0.1) and Auto Correlation (r=0.6). Due to the poor repeatability, these 3 variables were excluded from the next computational and statistical analysis. The Spearman correlation among the biomarkers and the patients' age did not present statistical significance and for this reason, was not reported.

TABLE 1- Descriptive and demographic distribution of the subjects.

Control Group (n=43 subjects, 84 condyles)				OA Group (n=51 patients, 99 condyles)			
	95% CI				95% CI		
Mean (age years)	Lower	Upper	SD	Mean (age years)	Lower	Upper	SD
39.6	36.6	42.6	13.7	40.9	38.4	43.5	12.7
Male (n)	Female(n)	Total(n)		Male (n)	Female(n)	Total(n)	
6	37	43		7	44	51	

SD: standard deviation; CI: confidence interval.

TABLE 2 – Intraclass correlation for repeated measurements by the same operator in a 2 weeks interval.

Variable (n=20 for each VoI)	ICC Value (r)					
	S	C	P	L	M	A
Energy	0.9	0.9	0.8	0.8	0.9	0.9
Entropy	0.9	0.9	0.8	0.8	0.8	0.9
Auto Correlation	0.9	0.9	0.7	0.7	0.6	0.8
InverseDifferenceMoment	0.9	0.9	0.9	0.9	0.9	0.9
Inertia	0.9	0.9	0.9	0.9	0.9	0.9
ClusterShade	0.8	0.8	0.8	0.8	0.1	0.8
ClusterProminence	0.9	0.9	0.8	0.7	0.1	0.8
HaralickCorrelation	0.9	0.9	0.9	0.8	0.8	0.9
ShortRunEmphasis	0.9	0.9	0.9	0.9	0.8	0.9
LongRunEmphasis	0.9	0.9	0.9	0.9	0.9	0.9
GreyLevelNonUniformity	0.9	0.8	0.9	0.7	0.8	0.9
RunLengthNonUniformity	0.9	0.9	0.9	0.9	0.9	0.9
LowGreyLevelRunEmphasis	0.9	0.9	0.9	0.8	0.9	0.9
HighGreyLevelRunEmphasis	0.9	0.9	0.9	0.8	0.9	0.9
ShortRunLowGreyLevelEmphasis	0.9	0.9	0.9	0.9	0.9	0.8
ShortRunHighGreyLevelEmphasis	0.9	0.9	0.9	0.8	0.8	0.9
LongRunLowGreyLevelEmphasis	0.9	0.9	0.9	0.8	0.9	0.9
LongRunHighGreyLevelEmphasis	0.9	0.9	0.9	0.9	0.9	0.9
BV/TV	0.9	0.9	0.9	0.9	0.9	0.9
Tb.Th	0.9	0.9	0.9	0.8	0.9	0.9
Tb.Sp	0.9	0.9	0.9	0.9	0.9	0.9
Tb.N	0.9	0.9	0.9	0.8	0.9	0.9
BS/BV	0.9	0.9	0.9	0.8	0.9	0.9

$\alpha = 0.05$. All the r-values were statistically significant ($p < 0.05$), except for Auto correlation, Cluster Shade and Cluster Prominence. S: superior, C: central, P: posterior, L: lateral, M: medial and A: anterior VoIs.

Statistical Tests of OA Diagnosis

Table 3 shows the Mann-Whitney U test and the ranked values for each variable. Statistically significant bone changes in texture features were detected in the lateral and central VoI regions of OA patients compared to control subjects ($p < 0.05$). The lateral VoI region of the TMJ OA patients showed significantly decreased values of: Energy, Grey Level Non Uniformity, Low Grey Level Run Emphasis, Short Run Low Grey Level Emphasis, Long Run Low Grey Level Emphasis, and BS/BV; and significantly increased values of: Entropy, Haralick Correlation, High Grey Level Run Emphasis, Short Run High Grey Level Emphasis, Long Run High Grey Level Emphasis BV/TV and Tb.Th. The central VoI region of TMJ OA patients showed significantly decreased values of: Low Grey Level Run Emphasis, Short Run Low Grey Level Emphasis, Long Run Low Grey Level Emphasis, Tb.Sp, and BS/BV; and significantly increased values of: High Grey Level Run Emphasis, Short Run High

Grey Level Emphasis, Long Run High Grey Level Emphasis, BV/TV and Tb.Th. The Fig. 3 summarizes the results obtained using the Mann-Whitney U test. A sample power of 0.80 (β) and effect size of 0.5 was achieve considering the statistically significant biomarkers in the lateral and central regions with α=0.05.

TABLE 3- Man-Whitney U test analysis for two independent samples between Control group and OA group.

VARIABLES	**Lateral**			**Central**			**Medial**		
	Mean Rank			**Mean Rank**			**Mean Rank**		
	C	**OA**	**p**	**C**	**OA**	**p**	**C**	**OA**	**p**
(n)	84	99		84	99		84	99	
Energy	**104.3**	**81.5**	**0.00**	95.1	89.4	0.47	99.2	85.9	0.09
Entropy	**79.8**	**102.3**	**0.00**	89.0	94.5	0.48	85.5	97.6	0.12
InverseDifferenceMoment	99.5	85.7	0.08	92.0	92.0	1.00	94.2	90.2	0.61
Inertia	84.8	98.1	0.09	92.0	92.0	1.00	89.9	93.8	0.61
HaralickCorrelation	**76.8**	**104.9**	**0.00**	83.7	99.1	0.05	84.2	98.7	0.07
ShortRunEmphasis	86.8	96.4	0.22	89.3	94.3	0.53	90.9	92.9	0.80
LongRunEmphasis	99.6	85.6	0.07	92.3	91.7	0.94	91.7	92.2	0.95
GreyLevelNonUniformity	**101.9**	**83.6**	**0.02**	99.8	85.4	0.07	98.0	86.9	0.16
RunLengthNonUniformity	84.7	98.2	0.09	91.5	92.4	0.90	91.1	92.8	0.83
LowGreyLevelRunEmp.	**103.0**	**82.7**	**0.01**	**103.5**	**82.3**	**0.01**	96.6	88.1	0.28
HighGreyLevelRunEmp.	**79.1**	**103.0**	**0.00**	**80.5**	**101.8**	**0.01**	85.2	97.8	0.11
ShortRunLowGreyLevelEmp.	**101.9**	**83.6**	**0.02**	**102.6**	**83.0**	**0.01**	95.6	89.0	0.40
ShortRunHighGreyLevelEmp.	**81.0**	**101.4**	**0.01**	**80.9**	**101.5**	**0.01**	84.9	98.1	0.09
LongRunLowGreyLevelEmp.	**103.2**	**82.5**	**0.01**	**100.8**	**84.6**	**0.04**	95.4	89.1	0.42
LongRunHighGreyLevelEmp.	**81.2**	**101.2**	**0.01**	**81.6**	**100.8**	**0.01**	85.9	97.2	0.15
BV/TV	**82.8**	**99.8**	**0.03**	**82.8**	**99.8**	**0.03**	88.7	94.8	0.44
Tb.Th	**79.2**	**102.9**	**0.00**	**82.6**	**100.0**	**0.03**	85.5	97.6	0.12
Tb.Sp	99.7	85.5	0.07	**101.2**	**84.2**	**0.03**	93.7	90.5	0.69
Tb.N	99.7	85.4	0.07	93.2	91.0	0.78	99.0	86.1	0.10
BS/BV	**105.2**	**80.8**	**0.00**	**101.4**	**84.0**	**0.03**	98.6	86.4	0.12
	Posterior			**Anterior**			**Superior**		
Energy	93.7	90.6	0.70	91.8	92.2	0.96	85.9	97.2	0.15
Entropy	91.4	92.5	0.88	95.2	89.3	0.46	98.9	86.2	0.11
InverseDifferenceMoment	93.1	91.1	0.80	88.3	95.1	0.38	85.6	95.7	0.31
Inertia	91.0	92.9	0.81	95.7	88.8	0.38	96.3	88.4	0.31
HaralickCorrelation	85.4	97.6	0.12	88.6	94.9	0.43	95.3	89.2	0.44
ShortRunEmphasis	89.4	94.2	0.55	94.9	89.6	0.50	89.7	93.9	0.59
LongRunEmphasis	94.7	89.7	0.53	90.4	93.4	0.71	91.3	92.6	0.87
GreyLevelNonUniformity	93.3	90.9	0.76	92.8	91.3	0.85	91.2	92.7	0.86
RunLengthNonUniformity	90.4	93.4	0.70	94.8	89.6	0.51	95.4	89.1	0.42
LowGreyLevelRunEmp.	100.4	84.9	0.05	98.1	86.9	0.15	91.9	92.1	0.98
HighGreyLevelRunEmp.	83.8	99.0	0.05	86.8	96.4	0.22	92.9	91.2	0.83
ShortRunLowGreyLevelEmp.	99.4	85.8	0.08	97.4	87.4	0.21	92.5	91.6	0.92
ShortRunHighGreyLevelEmp.	84.2	98.7	0.07	89.4	94.2	0.53	91.8	92.2	0.96
LongRunLowGreyLevelEmp.	99.5	85.7	0.08	97.4	87.4	0.20	89.8	93.9	0.60
LongRunHighGreyLevelEmp.	84.7	98.2	0.08	86.7	96.5	0.21	92.5	91.6	0.91
BV/TV	85.4	97.6	0.12	86.4	96.8	0.19	92.6	91.5	0.88
Tb.Th	84.5	98.3	0.08	86.0	97.1	0.16	92.8	91.3	0.85
Tb.Sp	98.2	86.7	0.15	97.0	87.8	0.24	92.0	92.0	1.00
Tb.N	96.0	88.6	0.35	94.7	89.7	0.53	88.7	94.8	0.43
BS/BV	99.5	85.7	0.08	98.0	86.9	0.16	91.2	92.7	0.85

$\alpha = 0.05$. The bold values indicate statistical significance ($p < 0.05$).

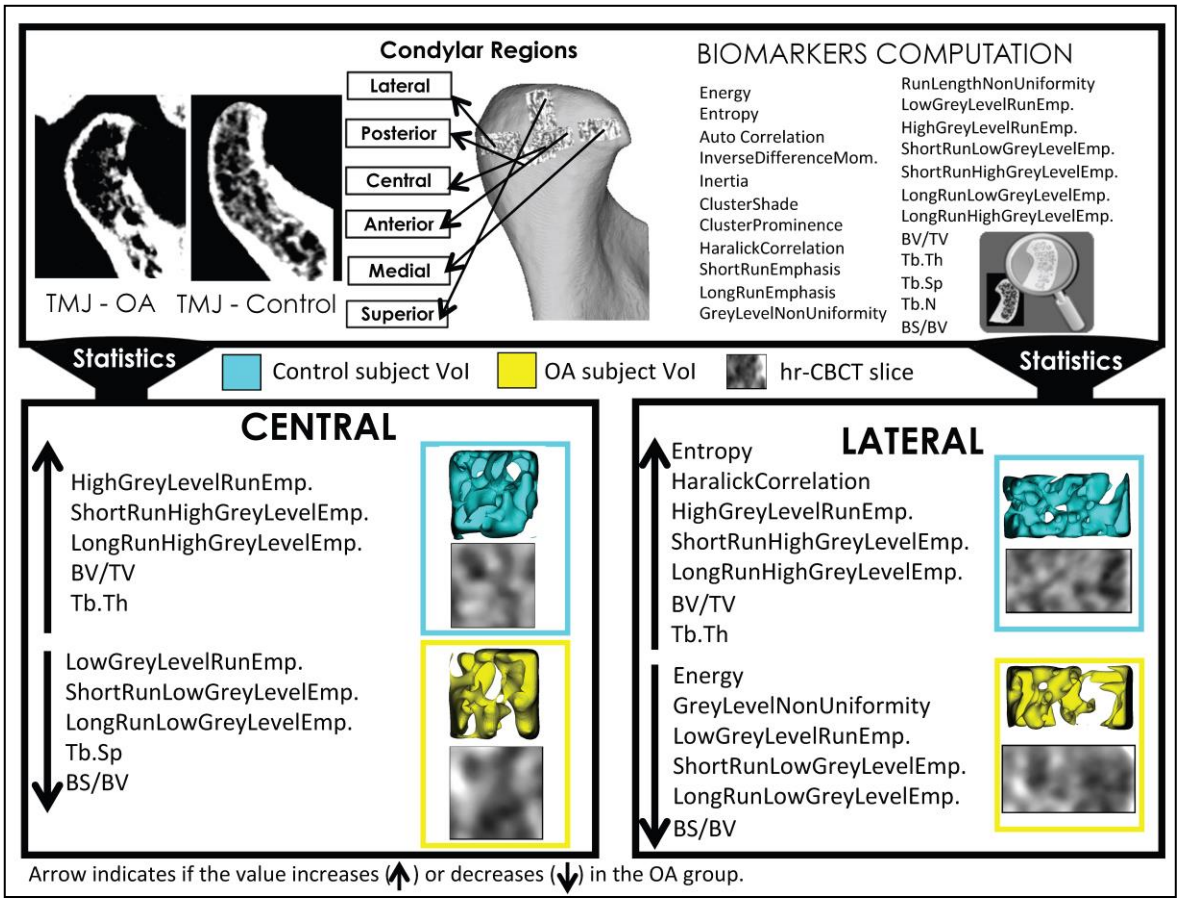

FIGURE 3 – Summary illustration showing the biomarkers that were statistically significant ($p<0.05$) in the Mann-Whitney analysis. Only the Central and Lateral regions showed significant differences between the OA and Control groups. The arrows pointing down are indicating lower expression in comparison with control group.

Figure 4A shows the ROC curve for all the variables that presented statistically significant differences between the OA and Control groups in Table 3. The lines above the diagonal indicate the variables that were significantly increased, and the lines under the diagonal reference lines indicate that the values that were significantly decreased in the OA compared to the control groups. Both the curves above and below the diagonal in Fig. 4A indicate the good diagnostic performance of our proposed biomarkers.

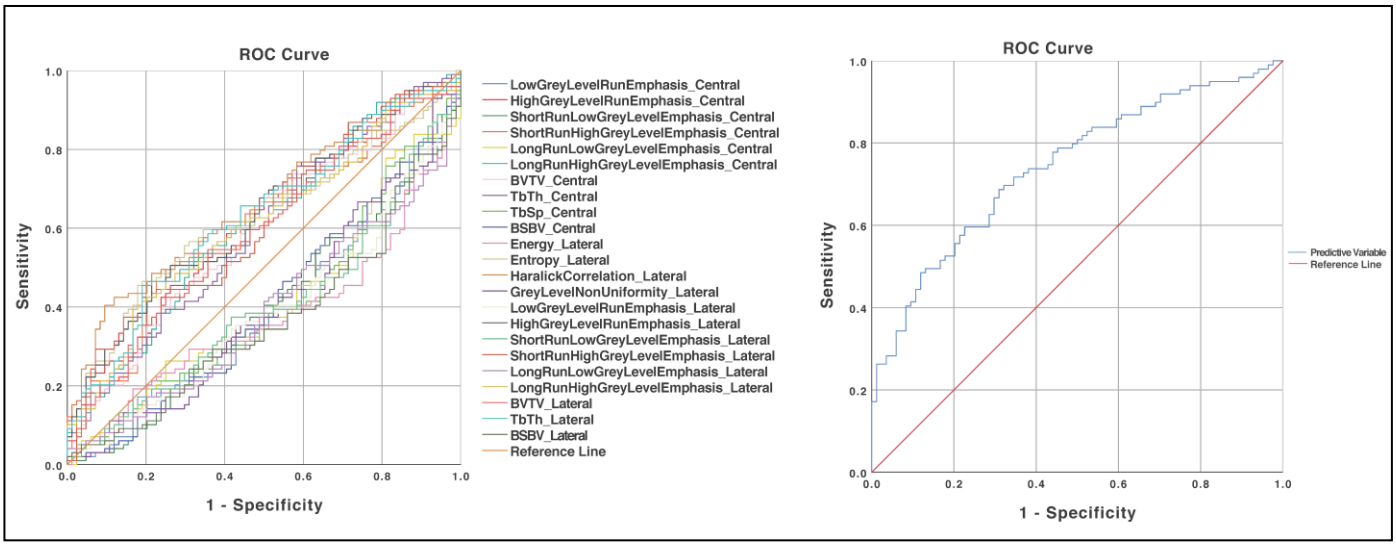

FIGURE 4 – A) Receiver Operating Characteristic (ROC) curves for detecting osteoarthritis using the variables that showed statistical significance in the Mann-Whitney test. The lines above the main diagonal represent that the state value (OA Group) will increase as the test variable decreases and the lines under the main diagonal represent that the state value (OA Group) will decrease as the test variable decreases. B) The ROC curve for the predictive variable created through binary logistic regression combining all the variables shown in figure 3 for detecting osteoarthritis. The Area Under the Curve (AUC) was 0.74 (95% CI were 0.67 to 0.82).

Table 4 details the value of the area under the curve for each variable ranging from 0.58 to 0.63 ($p < 0.05$). Figure 4B shows the ROC curve for the predictive variable created through binary logistic regression combining the biomarkers shown in Fig. 3. The area under the curve was 0.74 (95% CI were 0.67 to 0.82 – Table 4) indicating good diagnostic performance of the combined information provided by these biomarkers.

TABLE 4 - Receiver Operating Characteristics (ROC) curves and their respective Area Under the Curve (AUC) for predicting TMJ-OA.

VARIABLES	Area	SE	p	95% CI	
				Lower	Upper
LowGreyLevelRunEmphasis_Central†	0.61	0.04	0.01	0.53	0.69
HighGreyLevelRunEmphasis_Central	0.62	0.04	0.01	0.54	0.70
ShortRunLowGreyLevelEmphasis_Central†	0.60	0.04	0.01	0.52	0.68
ShortRunHighGreyLevelEmphasis_Central	0.61	0.04	0.01	0.53	0.69
LongRunLowGreyLevelEmphasis_Central†	0.58	0.04	0.04	0.50	0.67
LongRunHighGreyLevelEmphasis_Central	0.61	0.04	0.01	0.52	0.69
BVTV_Central	0.59	0.04	0.03	0.51	0.68
TbTh_Central	0.60	0.04	0.03	0.51	0.68
TbSp_Central†	0.59	0.04	0.03	0.51	0.67
BSBV_Central†	0.59	0.04	0.03	0.51	0.68
Energy_Lateral†	0.62	0.04	0.00	0.54	0.70
Entropy_Lateral	0.62	0.04	0.00	0.54	0.70
HaralickCorrelation_Lateral	0.65	0.04	0.00	0.57	0.73
GreyLevelNonUniformity_Lateral†	0.60	0.04	0.02	0.51	0.68

LowGreyLevelRunEmphasis_Lateral†	0.61	0.04	0.01	0.53	0.69
HighGreyLevelRunEmphasis_Lateral	0.63	0.04	0.00	0.55	0.71
ShortRunLowGreyLevelEmphasis_Lateral†	0.60	0.04	0.02	0.51	0.68
ShortRunHighGreyLevelEmphasis_Lateral	0.61	0.04	0.01	0.53	0.69
LongRunLowGreyLevelEmphasis_Lateral†	0.61	0.04	0.01	0.53	0.69
LongRunHighGreyLevelEmphasis_Lateral	0.61	0.04	0.01	0.53	0.69
BVTV_Lateral	0.59	0.04	0.03	0.51	0.68
TbTh_Lateral	0.63	0.04	0.00	0.55	0.71
BSBV_Lateral†	0.63	0.04	0.00	0.55	0.66

Variable	**Area**	**SE**	**p**	**95% CI**	
				Lower	**Upper**
Predictive Variable††	0.74	0.036	0.00	0.67	0.81

Test under the nonparametric assumption and null hypothesis: true area = 0.5

†AUC value subtracted from 1 (lower variable values were higher in OA patients)

††Created through binary logistic regression combining all the variables included in the first ROC.

DISCUSSION

To our knowledge, this is the first cross-sectional case control study to determine the diagnostic performance of novel imaging bone biomarkers in hr-CBCT scans of TMJ OA patients. This study tested surrogate bone morphometry and textural features and indicate 13 textural imaging biomarkers for diagnosis of subchondral bone changes in TMJ patients. These results are based on 6 VoIs of 183 condyles (control + OA groups), that resulted in 1098 localized hr-CBCT images. The image processing and computation of those large volumetric images led to the novel and open-access methodology presented in this study to mine and extract useful clinical data.

Rapidly progressive OA may involve multiple joints, and severe stages might require joint replacement dependent upon functional limitations [41,42]. TMJ osteoarthritis is successfully managed with conservative therapy that may include nonsteroidal anti-inflammatory, splints, physical therapy, low-energy laser and arthrocentesis[43]. Either surgical or nonsurgical management requires careful follow-up with validated tools to monitor treatment outcome. The greatest challenge in OA treatment is that the disease cannot be diagnosed until it becomes symptomatic, at which point structural alterations are already advanced[40]. Until recently, osteoarthritis frequently referred to as degenerative joint disease, was considered a localized condition that may after only one joint, but recent studies have demonstrated that even though one joint may manifest symptoms before the other,

osteoarthritis is a multijoint disease[44] Furthermore, even with the addition of radiographic criteria to DC/TMD the standardized and widely used protocols for TMJ OA assessment, it still relies on subjective radiological interpretation of pre-existent bone changes and clinical symptoms[29]. Chronic stages of this degenerative disease cannot be conservatively treated, as its natural cycle causes an intermittent inflammation with large bone destruction, pathological remodeling, pain and loss of function[45,46]. It is unlikely that a single marker would drive this complex, and a disease-modifying therapy is still unknown. Therefore, the patients with the diagnosis of TMJ OA in one condyle were classified as TMJ OA patients, even though the clinical manifestation was unilateral. Our proposed imaging biomarkers extract quantitative information using mathematical algorithms (GLCM and GLRLM)[38] to identify the difference in grayscale patterns between images of control subjects and OA patients[7,20,21,23]. Our results exhibited a good diagnostic performance with AUC of 0.74 (Fig. 3B).

Previous studies have shown the role of this tissue in the OA pathogenesis, including sclerosis and hypomineralization due to the abnormal bone remodeling[42,47]. Histopathological findings showed that the changes occur by microdamage, bone marrow edema-like lesions and bone cysts at the subchondral region[11] .In our study, Figure 3 summarizes the statistically significant increase in trabecular thickness and Bone Volume per Total Volume fraction, and well as decreased Bone Surface per Bone Volume fraction suggesting higher porosity in TMJ OA mandibular condyles, and in agreement with the histological findings described in the literature[11,48].

The rationale for selecting volumes of interest in 6 different regions of the condyles in our study is based on previous results[45,49] that indicated that changes occurring in different surface regions, including increased bone formation in the anterior pole, bone resorption in the lateral pole and superior region pole and overall bone surface remodeling. The lateral surface of the condyles has also been highly correlated with specific inflammatory proteins indicating that bone remodeling in this region may play an important role in OA pathogenesis[50]. Thus, a single quantitative value for the entire condyle cannot explain the different inflammatory responses leading to bone apposition and reparation in anterior and medial regions, while bone resorption occurs in other regions particularly the lateral condylar surface. Statistically significant differences were found in this study for 13 imaging biomarkers in the lateral region and 10 in the central region (Table 2 and Fig. 3). Bone resorption in the

lateral VoI region of the condyles of TMJ OA patients may be explained by significantly decreased values of: Energy, Grey Level Non-Uniformity, Low Grey Level Run Emphasis, Short Run Low Grey Level Emphasis, Long Run Low Grey Level Emphasis, and BS/BV. Interestingly, significantly increased values of Entropy, Haralick Correlation, High Grey Level Run Emphasis, Short Run High Grey Level Emphasis, Long Run High Grey Level Emphasis BV/TV and Tb.Th were also observed in the lateral condylar region. The small central VoI region, deeper in the subchondral bone of the condylar head of TMJ OA patients and away from the articular surface, showed significantly decrease in 4 of the same variables (Low Grey Level Run Emphasis, Short Run Low Grey Level Emphasis, Long Run Low Grey Level Emphasis and BS/BV) and increase in 5 of the same variables in the lateral VoI (High Grey Level Run Emphasis, Short Run High Grey Level Emphasis, Long Run High Grey Level Emphasis, BV/TV and Tb.Th). The central condylar region revealed decreased trabecular spacing and no significant differences in Entropy, Haralick Correlation, Energy and Grey Level Non-Uniformity between the OA and control groups. The differences in subchondral bone findings between the lateral and central condylar regions in this study may possibly be related to greater vascularization/innervation and less articular loading in the central condylar region, giving passage to the reparatory response in medial and anterior condylar surfaces.

The clinical diagnosis of degenerative joint disease in this study was performed by a TMD specialist clinical exam using the DC/TMD[29]. A limitation of this study is that the diagnosis by history and clinical examination using DC/TMD has a sensitivity of 0.55 and specificity 0.61 without imaging[29]. The methods proposed in the present manuscript will lead to future investigations on TMJ OA staging based on the absence or severity of the presence of morphological signs of condylar OA.

Recent histology studies by Embree et al.[48], showed that in mice with early-stage TMJ osteoarthritis, the subchondral bone revealed increased osteoclast activity, with gene increase in RANKL/OPG and up expression of 5 genes involved in bone resorption. Ebrahim et al.[51], showed that the some of our proposed imaging biomarkers (Low Grey Level Run Emphasis and Long Run Low Grey Level Emphasis) were statistically correlated with the osteoclast increase in a sample of 26 condyles. Our proposed methodology demonstrated a non-invasive workflow for 3D image analysis that may be applied to further imaging and joints studies with the ultimate goal of assessing bone remodeling using non-invasive imaging rather than

histology. The proposed methods also open opportunities for investigation of correlations between imaging biomarkers for TMJ OA staging and biomolecular findings.

Diagnosis of initial changes in the subchondral bone organization requires quantitative methodologies to analyze and extract bone texture information[6,12,52]. Recent studies have shown the potential and value of the imaging data mining applied in cancer studies to detected early tissue pathologic changes[19,53]. Nieminem et al.[8], from 2017 to 2018, described that radiographic imaging studies were the most commonly performed exams to assess OA. However, spatial and contrast resolution limitations to analyze bone textural imaging features have been reported by Caramella et al.[54]. Such limitations were overcome in the present study by using a standardized image acquisition and processing protocols (Fig. 1) for higher spatial resolution hr-CBCT scans, with a voxel size of 0.08 mm^3. Our novel image processing workflow utilized the 3DSlicer software module called Bonetexture[39] due to its user-friendly interface and fast computational processing.

CONCLUSION

Our results showed statistically significant differences between Control and TMJ OA groups in the subchondral bone microstructure in the lateral and central condylar regions. Thirteen imaging bone biomarkers showed good diagnostic performance for diagnosis of TMJ OA and the ROC curve for the combined predictive variable presented an AUC of 0.74. The workflow for image analysis described in this study can be applied to other imaging modalities and joints and has the potential to further elucidate OA pathogenesis and disease progression in future investigations.

ACKNOWLEDGMENTS

This study was funded in part by the Coordenação de Aperfeiçoamento Pessoal de Nível Superior - Brasil (CAPES) - Finance Code 001 and supported by NIH grants DE R01DE024450 and R21DE025306. We would like to acknowledge the subjects and patients who participated in this study.

REFERENCES

1. Glyn-Jones S, Palmer AJR, Agricola R, Price AJ, Vincent TL, Weinans H, et al. Osteoarthritis. Lancet (London, England) [Internet]. 2015 Jul 25 [cited 2019 Feb 25];386(9991):376–87. Available from: http://dx.doi.org/10.1016/

2. Rando C, Waldron T. TMJ osteoarthritis: A new approach to diagnosis. Am J Phys Anthropol. 2012;148(1):45–53.

3. Abramson SB, Attur M. Developments in the scientific understanding of osteoarthritis. Arthritis Res Ther [Internet]. 2009 Jan [cited 2014 Mar 19];11(3):227. Available from: http://www.pubmedcentral.nih.gov/articlerender.fcgi?artid=2714096&tool=pmcentrez&rendertype=abstract

4. Schiffman E, Ohrbach R, Truelove E, Look J, Anderson G, Goulet J-P, et al. Diagnostic Criteria for Temporomandibular Disorders (DC/TMD) for Clinical and Research Applications: Recommendations of the International RDC/TMD Consortium Network* and Orofacial Pain Special Interest Group† [Internet]. Journal of Oral & Facial Pain and Headache Jan, 2014 p. 6–27. Available from: https://www.ncbi.nlm.nih.gov/pmc/articles/PMC4478082/pdf/nihms-695420.pdf

5. Wenham CYJ, Grainger AJ, Conaghan PG. The role of imaging modalities in the diagnosis, differential diagnosis and clinical assessment of peripheral joint osteoarthritis. Osteoarthr Cartil [Internet]. 2014 Oct 1 [cited 2019 Mar 4];22(10):1692–702. Available from: https://www.sciencedirect.com/science/article/pii/S1063458414011145

6. Neogi T, Felson DT. Osteoarthritis: Bone as an imaging biomarker and treatment target in OA. Nat Rev Rheumatol [Internet]. 2016;12(9):503–4. Available from: http://www.nature.com/doifinder/10.1038/nrrheum.2016.113%5Cnhttp://www.ncbi.nlm.nih.gov/pubmed/27383914

7. Menashe L, Hirko K, Losina E, Kloppenburg M, Zhang W, Li L, et al. The diagnostic performance of MRI in osteoarthritis: a systematic review and meta-analysis. Osteoarthr Cartil [Internet]. 2012 Jan [cited 2019 Mar 5];20(1):13–21. Available from: http://www.ncbi.nlm.nih.gov/pubmed/22044841

8. Nieminen MT, Casula V, Nevalainen MT, Saarakkala S. Osteoarthritis year in review 2018: imaging. Osteoarthr Cartil [Internet]. 2019 Mar;27(3):401–11. Available from: https://doi.org/10.1016/j.joca.2018.12.009

9. Tiulpin A, Thevenot J, Rahtu E, Lehenkari P, Saarakkala S. Automatic Knee Osteoarthritis Diagnosis from Plain Radiographs: A Deep Learning-Based Approach. Sci Rep [Internet]. 2018;8(1):1727. Available from: http://www.ncbi.nlm.nih.gov/pubmed/29379060

10. Norman B, Pedoia V, Majumdar S. Use of 2D U-Net Convolutional Neural Networks for Automated Cartilage and Meniscus Segmentation of Knee MR Imaging Data to Determine Relaxometry and Morphometry. Radiology [Internet]. 2018;288(1):177–85. Available from: http://www.ncbi.nlm.nih.gov/pubmed/29584598

11. Li G, Yin J, Gao J, Cheng TS, Pavlos NJ, Zhang C, et al. Subchondral bone in osteoarthritis: insight into risk factors and microstructural changes. Arthritis Res Ther

[Internet]. 2013 Dec;15(6):223. Available from: http://arthritis-research.biomedcentral.com/articles/10.1186/ar4405

12. Burr DB, Gallant MA. Bone remodelling in osteoarthritis. Nat Publ Gr [Internet]. 2012;8(11):665–73. Available from: http://dx.doi.org/10.1038/nrrheum.2012.130

13. Paniagua B, Pascal L, Prieto J, Vimort JB, Gomes L, Yatabe M, et al. Diagnostic Index: An open-source tool to classify TMJ OA condyles. Proc SPIE--the Int Soc Opt Eng [Internet]. 2017 Feb 11;10137. Available from: http://www.ncbi.nlm.nih.gov/pubmed/28690356

14. Tsiklakis K, Syriopoulos K, Stamatakis HC. Radiographic examination of the temporomandibular joint using cone beam computed tomography. Dentomaxillofacial Radiol. 2004;33(3):196–201.

15. Editorial. ALARA still applies. Oral Surg Oral Med Oral Pathol Oral Radiol Endod. 2005;100(4):395–7.

16. ICRP, Rehani MM, Gupta R, Bartling S, Sharp GC, Pauwels R, et al. Radiological Protection in Cone Beam Computed Tomography (CBCT). ICRP Publication 129. Ann ICRP [Internet]. 2015 Jul;44(1):9–127. Available from: http://www.scopus.com/inward/record.url?eid=2-s2.0-67650484907&partnerID=40&md5=4c9514b22e7bba3b95d181560c25fff6

17. Dempster DW, Compston JE, Drezner MK, Glorieux FH, Kanis JA, Malluche H, et al. Standardized nomenclature, symbols, and units for bone histomorphometry: A 2012 update of the report of the ASBMR Histomorphometry Nomenclature Committee. J Bone Miner Res [Internet]. 2013 Jan [cited 2018 Dec 3];28(1):2–17. Available from: http://www.ncbi.nlm.nih.gov/pubmed/23197339

18. Paniagua B, Ruellas AC, Benavides E, Marron S, Wolford L, Cevidanes L. Validation of CBCT for the computation of textural biomarkers. SPIE Med Imaging [Internet]. 2015;9417:1–15. Available from: http://proceedings.spiedigitallibrary.org/proceeding.aspx?articleid=2209670

19. Gillies RJ, Kinahan PE, Hricak H. Radiomics: Images Are More than Pictures, They Are Data. Radiology. 2016;

20. Lambin P, Rios-Velazquez E, Leijenaar R, Carvalho S, Van Stiphout RGPM, Granton P, et al. Radiomics: Extracting more information from medical images using advanced feature analysis. Eur J Cancer [Internet]. 2012 [cited 2019 Feb 25];48:441–6. Available from: https://ac.els-cdn.com/S0959804911009993/1-s2.0-S0959804911009993-main.pdf?_tid=f494e8af-f638-4ee2-b99a-2283a4caf1ae&acdnat=1551112858_9ad389f387a3ba0a9eea06b0b6a7f549

21. Valentin M, Bom C, Albuquerque M, Albuquerque M, Faria E, Correia M. Texture Classification based on Spectral Analysis and Haralick Features. Notas Técnicas [Internet]. 2016;6(1):28–51. Available from: http://revistas.cbpf.br/index.php/nt/article/view/155/133

22. Paniagua B, Ruellas AC, Benavides E, Marron S, Wolford L, Cevidanes L, et al.

Validation of CBCT for the computation of textural biomarkers. Gimi B, Molthen RC, editors. Proc SPIE--the Int Soc Opt Eng [Internet]. 2015 Mar 17 [cited 2018 Dec 3];9417(March 2015):94171B. Available from: http://proceedings.spiedigitallibrary.org/proceeding.aspx?doi=10.1117/12.2081859

23. Shirvaikar M, Huang N, Dong XN. The Measurement of Bone Quality Using Gray Level Co-Occurrence Matrix Textural Features. J Med Imaging Heal Informatics [Internet]. 2016;6(6):1357–62. Available from: http://www.ingentaconnect.com/content/10.1166/jmihi.2016.1812

24. Vimort J-B, Ruellas A, Prothero J, Marron JS, McCormick M, Cevidanes L, et al. Detection of bone loss via subchondral bone analysis. Gimi B, Krol A, editors. Proc SPIE--the Int Soc Opt Eng [Internet]. 2018 Feb 12 [cited 2018 Dec 3];10578:25. Available from: http://www.ncbi.nlm.nih.gov/pubmed/29769754

25. Jiao K, Niu L-N, Wang M-Q, Dai J, Yu S-B, Liu X-D, et al. Subchondral bone loss following orthodontically induced cartilage degradation in the mandibular condyles of rats. Bone [Internet]. 2011 Feb 1 [cited 2019 Mar 5];48(2):362–71. Available from: https://www.sciencedirect.com/science/article/pii/S8756328210014559

26. Chen J, Sorensen KP, Gupta T, Kilts T, Young M, Wadhwa S. Altered functional loading causes differential effects in the subchondral bone and condylar cartilage in the temporomandibular joint from young mice. Osteoarthr Cartil [Internet]. 2009 Mar 1 [cited 2019 Mar 5];17(3):354–61. Available from: https://www.sciencedirect.com/science/article/pii/S1063458408002653

27. Strimbu K, Tavel JA. What are biomarkers? Curr Opin HIV AIDS [Internet]. 2010 Nov [cited 2019 Feb 18];5(6):463–6. Available from: http://www.ncbi.nlm.nih.gov/pubmed/20978388

28. von Elm E, Altman DG, Egger M, Pocock SJ, Gøtzsche PC, Vandenbroucke JP, et al. The Strengthening the Reporting of Observational Studies in Epidemiology (STROBE) statement: guidelines for reporting observational studies. J Clin Epidemiol [Internet]. 2008 Apr 1 [cited 2019 Feb 18];61(4):344–9. Available from: https://www.sciencedirect.com/science/article/pii/S174391911400212X

29. Schiffman EL, Ohrbach R, Truelove EL, Look J, Anderson G, Goulet J, et al. Diagnostic Criteria for Temporomandibular Disorders (DC/TMD) for Clinical and Research Applications: Recommendations of the International RDC/TMD Consortium Network* and Orofacial Pain Special Interest Group. J Oral Facial Pain Headache. 2014;28(1):6–27.

30. Rando C, Waldron T. TMJ osteoarthritis: A new approach to diagnosis. Am J Phys Anthropol. 2012;148(1):45–53.

31. Hunter DJ, Bierma-Zeinstra S. Osteoarthritis. Lancet. 2019;393(10182):1745–59.

32. Zhao YP, Zhang ZY, Wu YT, Zhang WL, Ma XC. Investigation of the clinical and radiographic features of osteoarthrosis of the temporomandibular joints in adolescents and young adults. Oral Surgery, Oral Med Oral Pathol Oral Radiol Endodontology. 2011;111(2):27–34.

33. Jaju PP, Jaju SP. Cone-beam computed tomography: Time to move from ALARA to ALADA. Imaging Sci Dent [Internet]. 2015 Dec;45(4):263–5. Available from: http://www.ncbi.nlm.nih.gov/pubmed/26730375

34. Kikinis R, Pieper SD, Vosburgh KG. 3D Slicer: A Platform for Subject-Specific Image Analysis, Visualization, and Clinical Support. In: Intraoperative Imaging and Image-Guided Therapy [Internet]. New York, NY: Springer New York; 2014 [cited 2018 Dec 3]. p. 277–89. Available from: http://link.springer.com/10.1007/978-1-4614-7657-3_19

35. Yushkevich PA, Piven J, Hazlett HC, Smith RG, Ho S, Gee JC, et al. User-guided 3D active contour segmentation of anatomical structures: Significantly improved efficiency and reliability. Neuroimage [Internet]. 2006 Jul 1 [cited 2018 Dec 5];31(3):1116–28. Available from: http://www.ncbi.nlm.nih.gov/pubmed/16545965

36. Galloway MM. Texture analysis using gray level run lengths. Comput Graph Image Process [Internet]. 1975;4(2):172–9. Available from: http://www.sciencedirect.com/science/article/pii/S0146664X75800086

37. Haralick R, Shanmugan K, Dinstein I. Textural features for image classification [Internet]. Vol. 3, IEEE Transactions on Systems, Man and Cybernetics. 1973. p. 610–21. Available from: http://dceanalysis.bigr.nl/Haralick73-Textural features for image classification.pdf

38. Haralick, R.M. and Shapiro LG. (1992) Computer and Robot Vision. Addison-Wesley Longman Publishing Co., Inc., Boston. In: Computer and Robot Vision: Vol 1. Boston, MA: Addison-Wesley Longman Publishing Co., Inc.; 1992. p. 459.

39. Documentation/Nightly/Extensions/BoneTextureExtension - SlicerWiki [Internet]. [cited 2019 Apr 2]. Available from: https://www.slicer.org/wiki/Documentation/Nightly/Extensions/BoneTextureExtension

40. Hanley JA, McNeil BJ. The meaning and use of the area under a receiver operating characteristic (ROC) curve. Radiology [Internet]. 1982 Apr [cited 2019 Mar 5];143(1):29–36. Available from: http://pubs.rsna.org/doi/10.1148/radiology.143.1.7063747

41. Abrahamsson AK, Kristensen M, Arvidsson LZ, Kvien TK, Larheim TA, Haugen IK. Frequency of temporomandibular joint osteoarthritis and related symptoms in a hand osteoarthritis cohort. Osteoarthr Cartil [Internet]. 2017;25(5):654–7. Available from: http://www.ncbi.nlm.nih.gov/pubmed/28064031

42. O'Connor RC, Fawthrop F, Salha R, Sidebottom AJ. Management of the temporomandibular joint in inflammatory arthritis: Involvement of surgical procedures. Eur J Rheumatol [Internet]. 2017 Jun;4(2):151–6. Available from: http://www.ncbi.nlm.nih.gov/pubmed/28638693

43. Wang XD, Zhang JN, Gan YH, Zhou YH. Current understanding of pathogenesis and treatment of TMJ osteoarthritis. J Dent Res [Internet]. 2015 May;94(5):666–73. Available from: http://www.ncbi.nlm.nih.gov/pubmed/25744069

44. Nelson AE, Golightly YM, Renner JB, Schwartz TA, Kraus VB, Helmick CG, et al.

Brief report: differences in multijoint symptomatic osteoarthritis phenotypes by race and sex: the Johnston County Osteoarthritis Project. Arthritis Rheum [Internet]. 2013 Feb;65(2):373–7. Available from: http://www.ncbi.nlm.nih.gov/pubmed/23359309

45. Ryan P, Lie SA, Havelin LI, Gillam MH, Salter A, Furnes O, et al. The progression of end-stage osteoarthritis: analysis of data from the Australian and Norwegian joint replacement registries using a multi-state model. Osteoarthr Cartil [Internet]. 2012 Mar 1 [cited 2019 Mar 6];21(3):405–12. Available from: https://www.sciencedirect.com/science/article/pii/S1063458412010539

46. Schaible H-G. Mechanisms of Chronic Pain in Osteoarthritis. Curr Rheumatol Rep [Internet]. 2012 Dec 15 [cited 2019 Mar 6];14(6):549–56. Available from: http://link.springer.com/10.1007/s11926-012-0279-x

47. Embree M, Ono M, Kilts T, Walker D, Langguth J, Mao J, et al. Role of Subchondral Bone during Early-stage Experimental TMJ Osteoarthritis. J Dent Res [Internet]. 2011 Nov 13 [cited 2019 Mar 5];90(11):1331–8. Available from: http://journals.sagepub.com/doi/10.1177/0022034511421930

48. Embree M, Ono M, Kilts T, Walker D, Langguth J, Mao J, et al. Role of subchondral bone during early-stage experimental TMJ osteoarthritis. J Dent Res. 2011;

49. de Dumast P, Mirabel C, Cevidanes L, Ruellas A, Yatabe M, Ioshida M, et al. A web-based system for neural network based classification in temporomandibular joint osteoarthritis. Comput Med Imaging Graph [Internet]. 2018 Jul [cited 2019 Jan 21];67:45–54. Available from: http://www.ncbi.nlm.nih.gov/pubmed/29753964

50. Cevidanes LHS, Walker D, Schilling J, Sugai J, Giannobile W, Paniagua B, et al. 3D osteoarthritic changes in TMJ condylar morphology correlates with specific systemic and local biomarkers of disease. Osteoarthr Cartil [Internet]. 2014 Oct [cited 2019 Mar 7];22(10):1657–67. Available from: http://www.ncbi.nlm.nih.gov/pubmed/25278075

51. Ebrahim FH, Ruellas ACO, Paniagua B, Benavides E, Jepsen K, Wolford L, et al. Accuracy of biomarkers obtained from cone beam computed tomography in assessing the internal trabecular structure of the mandibular condyle. Oral Surg Oral Med Oral Pathol Oral Radiol [Internet]. 2017 Dec;124(6):588–99. Available from: http://dx.doi.org/10.1016/j.oooo.2017.08.013

52. Bousson V, Lowitz T, Laouisset L, Engelke K, Laredo JD. CT imaging for the investigation of subchondral bone in knee osteoarthritis. Osteoporos Int. 2012;23(8 SUPPL):861–5.

53. Starkov P, Aguilera TA, Golden DI, Shultz DB, Trakul N, Maxim PG, et al. The use of texture-based radiomics CT analysis to predict outcomes in early-stage non-small cell lung cancer treated with stereotactic ablative radiotherapy. Br J Radiol [Internet]. 2019 Feb 20 [cited 2019 Jan 7];92(1094):20180228. Available from: http://www.ncbi.nlm.nih.gov/pubmed/30457885

54. Caramella C, Allorant A, Orlhac F, Bidault F, Asselain B, Ammari S, et al. Can we trust the calculation of texture indices of CT images? A phantom study. Med Phys [Internet]. 2018 Apr 1 [cited 2018 Dec 6];45(4):1529–36

3.2 Publicação 3*

Osteoarthritis of the Temporomandibular Joint can be diagnosed earlier using biomarkers and machine learning.

Jonas Bianchi*[1,2] Antônio Carlos de Oliveira Ruellas[1], João Roberto Gonçalves[2], Beatriz Paniagua[3], Juan Carlos Prieto[4], Martin Styner[4], Tengfei Li[5], Hongtu Zhu[5], James Sugai[6], William Giannobile[6], Erika Benavides[6], Fabiana Soki[6], Marilia Yatabe[1], Lawrence Ashman[7], David Walker[8], Reza Soroushmehr[9], Kayvan Najarian[9], and Lucia Helena Soares Cevidanes[1].

[1] University of Michigan, Department of Orthodontics and Pediatric Dentistry, School of Dentistry, Ann Arbor, MI, 48109, USA.

[2] São Paulo State University, Department of Pediatric Dentistry, School of Dentistry, Araraquara, SP, 14801-385, Brazil.

[3] Kitware, Inc., Carrboro, NC, 27510, USA

[4] University of North Carolina, Department of Psychiatry and Computer Science, Chapel Hill, NC, 27516, USA.

[5] University of North Carolina, Department of Biostatistics, Chapel Hill, NC, 27516, USA.

[6] University of Michigan, Department of Periodontics and Oral Medicine, School of Dentistry, Ann Arbor, MI, 48109, USA.

[7] University of Michigan, Department of Oral and Maxillofacial Surgery and Hospital Dentistry, School of Dentistry, Department of Biomedical Engineering, and the Biointerfaces Institute Ann Arbor, MI, 48109, USA.

[8] Private practice, Jacksonville, NC, 28546

[9] University of Michigan, Center for Integrative Research in Critical Care and Michigan Institute for Data Science, Department of Computational Medicine and Bioinformatics, Ann Arbor, MI, 48109, USA.

*bianchij@umich.edu

* Artigo a ser enviado à revista: Nature Communications seguindo suas normas de formatação.

ABSTRACT

After chronic low back pain, Temporomandibular Joint (TMJ) disorders are the second most common musculoskeletal condition affecting 5 to 12% of the population, with an annual health cost estimated at $4 billion. Chronic disability in temporomandibular osteoarthritis (OA) increases with aging, and the greatest clinical challenge is to diagnose the disease before the morphological degeneration occurs. Here, advanced data science to capture, process and analyze 52 clinical, biological and imaging data address the challenges in early diagnosis of TMJ OA. Headaches, Energy, and interactions of VE-cadherin in Serum and Angiogenin in Saliva, Gender and Muscle Soreness, Headaches and TGF-β1 in Saliva, PA1 in Saliva and Range of mouth opening accurately diagnose early stages of this clinical condition, using machine learning approaches. We expect that diagnosis of early stages will boost future studies into osteoarthritis patient specific therapeutic interventions, and thereby improve the health of articular joints.

Introduction

Osteoarthritis (OA) affects millions of people worldwide, causing them many years with pain and disability[1]. Trends in global burden of the disease from 1990 to 2016 show that OA is the second most rapidly rising condition associated with disability, with a 46 percent increase in years lived with disability, just behind diabetes at 52 percent[2].With the aging population and higher rates of obesity, this burden is expected to rise. The rapid increase in prevalence of OA will lead to a growing impact and major challenges for health care and public health systems. OA can occur in different joints in the musculoskeletal system, such as the knee, hips, back, hand, and temporomandibular joint (TMJ), having a multifactorial etiology that includes: excessive mechanical stress, hormonal changes, genetics, aging and others[3–5]. The TMJ is a unique model to study early bone changes in OA, as the bone articular surface is covered only by a thin layer of fibrocartilage in the TMJ condyle. Osteoarthritis of the TMJ (TMJ OA) is a multi-system disease, involving numerous pathophysiological processes, and requiring comprehensive assessments to characterize progressive cartilage degradation, subchondral bone remodeling, and chronic pain[4,6–8].

Studies using in vivo OA disease models now benefit from high-resolution cone-beam tomography imaging (HR-CBCT)[9]. HR-CBCT scans allow diagnosis of the bone environment with sub-millimeter resolution comparable to micro-CT, but with a much lower radiation dose,[10] and have been widely used by clinicians and researchers[11–14]. As treatments to reverse the chronic damage of TMJ OA are unavailable, early diagnosis may provide the best opportunity to prevent extensive and permanent joint damage. However, current diagnosis is based on pre-existent clinical/imaging signs and symptoms markers using standard protocols recommended for Diagnostic Criteria for Temporomandibular Disorders (DC/TMD), meaning to diagnose TMJ OA degradation of the joint must have already occurred[15-16]. The DC/TMD criteria are based on pre-existent condylar damage, such as subcortical cysts, surface erosions, osteophytes, or generalized sclerosis that are present mainly in the later stages of the disease. Towards an early diagnosis that is predictive of disease status, animal studies indicate that the

bone microarchitecture[6,8,17,18] is an important factor in the OA pathogenesis initiation, preceding articular cartilage changes[17,19], and should be investigated in human studies. The estimated increase in OA prevalence in high-income countries over the next decades[20] parallels advances in computational machine learning and data management[21,22]. With the increase in the volume of information acquired from high resolution images, precise data mining algorithms are needed to standardize data from multiple centers and provide personalized treatment[15,20,22–25].

Here, we propose novel standardized data representation/processing, statistical learning, and interactive visualization to fully explore biomarker interactions in relation with disease and health. Our data-driven approaches integrate information patterns to provide new insights into the complex etiology of TMJ OA[25]. Data management includes standardized imaging[26], clinical[15] and biomolecular[27] acquisition, and control of patient information from multiple data sources, with standardized demographic for matching OA patients and healthy controls. We have evaluated fifty-five variables to determine the most relevant integrative feature pools using machine-learning algorithms to detect TMJ OA status (Fig. 1). We hypothesize that by combining standardized patient features from multiple sources using statistical machine-learning approaches, we can accurately diagnose TMJ OA status.

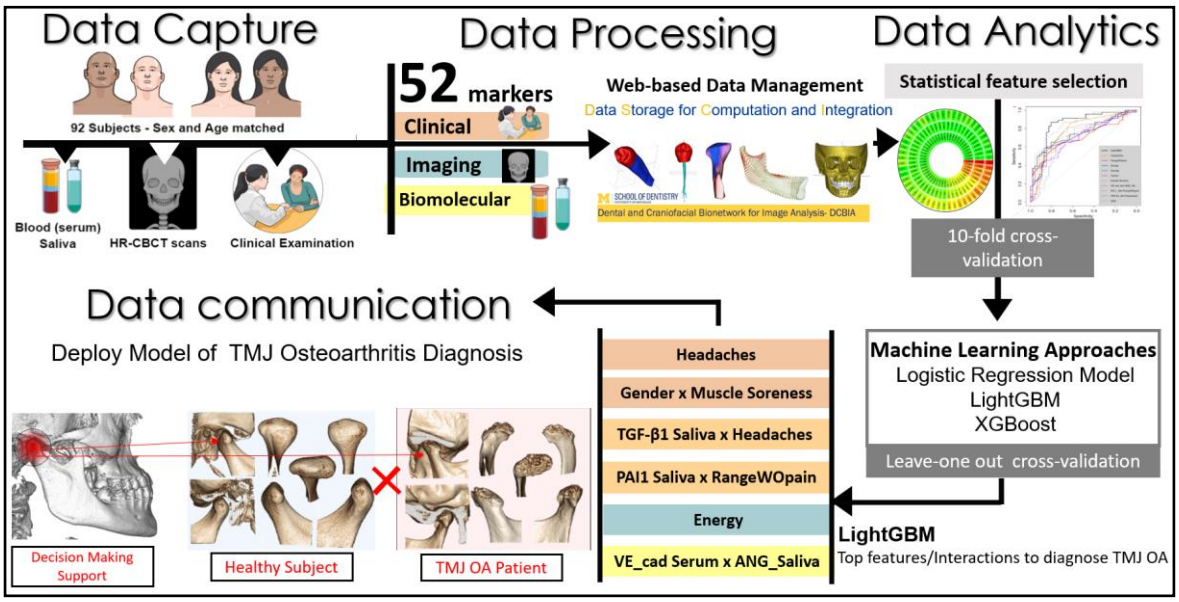

Fig. 1- The spectrum of Data Science to advance TMJ OA diagnosis includes Data capture and acquisition, Data processing with a web-based data management, Data Analytics involving in-depth statistical analysis, machine learning approaches and Data communication to help the decision making support in TMJ OA diagnosis.

Results

Web-based platform to store and compute data analytics of clinical, radiomics and biomolecular markers. Our Data Storage for Computation and Integration (DSCI)[29] web-based system was used for data management with storage and integration of patient information from multiple sources. The DCSI communicates with 3D Slicer[30] platform through the Data Base Interactor[31] plugin that allows the user to upload the clinical, imaging and biological markers. The data was exported in a csv file and we show in Tables 1-3, the descriptive statistics for each variable and their respective nomenclature and abbreviations. As most of the variables did not show parametric distribution (after evaluation of the asymmetry and kurtosis), the descriptive statistics display the median, mean, standard deviation and upper/lower limits for the 95% confidence interval.

		Control Group (n=46) Female (39) Male (7)					**TMJ OA Group** (n=46) Female (39) Male (7)				
Variables	**Abbreviation**			**95% CI**					**95% CI**		
Clinical Variables		**Median**	**Mean**	**Lower**	**Upper**	**SD**	**Median**	**Mean**	**Lower**	**Upper**	**SD**
Age	Age	38.50	39.83	35.89	43.76	13.26	38.00	37.65	33.99	41.32	12.34
Years of Pain Onset (years)	PainY	-	-	-	-	-	3.75	4.34	3.35	5.33	3.34
Facial Current Pain (years)	PainCur	-	-	-	-	-	3.00	3.07	2.47	3.66	2.00
Facial last 6 months Worst Pain (0 to 10)	PainWor	-	-	-	-	-	7.00	6.89	6.06	7.73	2.81
Facial last 6 months Average Pain (0 to 10)	PainAve	-	-	-	-	-	4.50	4.52	3.87	5.17	2.20
Last 6 Months Distressed by Headaches (0 to 10)	Headaches	0.00	0.63	0.33	0.93	1.02	2.00	1.65	1.33	1.97	1.08
Last 6 Months Distressed by Muscle Soreness (0 to 10)	MusSor	0.00	0.37	0.16	0.58	0.71	1.00	1.07	0.74	1.39	1.10
Vertical Range Unassisted Without Pain (mm)	RangeWOpain	44.50	44.91	42.42	47.40	8.39	36.35	39.00	32.44	40.26	13.16
Vertical Range Unassisted Max (mm)	RangeUnaMax	47.50	46.83	44.62	49.03	7.41	45.00	44.28	41.41	47.16	9.68
Vertical Range Assisted Max (mm)	RangeAssMax	50.00	49.21	47.15	51.27	6.94	49.00	47.54	44.69	50.40	9.61

CI: Confidence Interval; SD: Standard Deviation.

Table 1 **– Descriptive and demographic values for each clinical variable.**

The following variables were measured only for the TMJ OA group since the control patients did not present facial and/or TMJ pain: years of pain onset (PainY), current facial pain (PainCur), last six months worst facial pain (PainWor) and last six months average facial pain (PainAve). The TMJ OA and control

groups were age and sex matched. We can note that patients with OA present less range of mouth opening, for radiomics and biomolecular variables both present similar values, and in the Supplementary Fig. 1 we present the statistical differences between them. Finally, the MMP3 protein was not described for saliva, since the expression levels were not detected.

Table 2 – Descriptive values for each imaging variable.

		Control Group (n=46) Female (39) Male (7)					**TMJ OA Group** (n=46) Female (39) Male (7)				
Variables	**Abbreviation**			**95% CI**					**95% CI**		
Radiomics Variables		**Median**	**Mean**	**Lower**	**Upper**	**SD**	**Median**	**Mean**	**Lower**	**Upper**	**SD**
Energy	Energy	0.30	0.31	0.28	0.33	0.07	0.25	0.25	0.23	0.27	0.07
Entropy	Entropy	2.29	2.30	2.20	2.40	0.33	2.56	2.62	2.49	2.75	0.42
Inverse Difference Moment	InvDifMom	0.91	0.90	0.90	0.91	0.02	0.89	0.89	0.89	0.90	0.02
Inertia	Inertia	0.19	0.19	0.19	0.20	0.03	0.21	0.21	0.20	0.22	0.03
Haralick Correlation	HarCor	317.48	375.56	303.63	447.49	242.23	410.36	603.40	467.71	739.10	456.94
Short Run Emphasis	ShortRE	0.33	0.34	0.35	0.34	0.03	0.35	0.35	0.34	0.36	0.03
Long Run Emphasis	LongRE	16.58	16.51	16.01	17.01	1.68	15.44	15.64	15.10	16.18	1.81
Grey Level Non Uniformity	GreyLNU	2405.84	2374.26	2272.67	2475.84	342.08	2240.61	2249.65	2158.63	2340.67	306.50
Run Length Non Uniformity	RunLNU	1239.23	1287.96	1209.65	1366.27	263.72	1443.88	1459.22	1367.19	1551.25	309.91
Low Grey Level Run Emphasis	LowGLRE	0.06	0.06	0.06	0.06	0.01	0.06	0.06	0.05	0.06	0.01
High Grey Level Run Emphasis	HighGLRE	19.10	19.98	18.76	21.19	4.09	21.05	22.47	20.95	23.98	5.11
Short Run Low Grey Level Emphasis	ShortRLowGLE	0.02	0.02	0.02	0.02	0.00	0.02	0.02	0.02	0.02	0.00
Short Run High Grey Level Emphasis	ShortRHighGLE	6.96	7.25	6.72	7.77	1.77	8.15	8.56	7.89	9.24	2.27
Long Run Low Grey Level Emphasis	LongRLowGLE	1.05	1.05	0.98	1.11	0.23	0.95	0.95	0.87	1.03	0.28
Long Run High Grey Level Emphasis	LongRHighGLE	299.09	303.82	283.69	323.95	67.80	309.96	317.43	298.88	335.97	62.45
Bone Volume (%)	BV/TV	0.54	0.54	0.48	0.60	0.20	0.60	0.58	0.52	0.64	0.20
Trabecular Thickness (mm)	Tb.Th	0.35	0.38	0.33	0.43	0.16	0.41	0.44	0.38	0.50	0.19
Trabecular Separation (mm)	Tb.Sp	0.28	0.34	0.27	0.40	0.21	0.26	0.35	0.25	0.44	0.31
Trabecular Number (mm^{-1})	Tb.N	1.47	1.44	1.38	1.51	0.23	1.45	1.36	1.28	1.44	0.28
Bone Surface to Bone Volume Ratio (mm^{-1})	BS/BV	5.79	6.08	5.43	6.73	2.18	4.89	5.30	4.65	5.95	2.18

CI: Confidence Interval; SD: Standard Deviation.

Radiomic features differentiate control subjects and TMJ OA patients. We used a non-invasive protocol validated by our group to detect the initial morphological changes in the mandibular condyle trabecular bone based on radiomics information[10]. We extracted 20 imaging features (GLCM, GLRLM and bone morphometry described in Table 2)[26,32]. These radiomic features were tested using the Mann-Whitney U test (Fig. 2 B and Supplementary Fig. 1 – B) for group comparisons. From the 20 variables, 13 showed differences between the disease and control groups. These findings suggest, and corroborate the literature, that the trabecular bone has an important role in the TMJ OA pathogenesis[6,17,33].

Control and TMJ OA patients present similar expression levels of selected serum and saliva protein biomarkers. We selected proteins that have previously been detected in the TMJ synovial fluid of OA patients[27]. We collected saliva and serum using less invasive procedures and promising screening diagnostic tools[34] to evaluate the diagnostic performance of each protein and their interactions with radiomics and clinical markers. To analyze each protein's expression level, we used a customized human protein micro-array kit (RayBiotech; Norcross, GA) with duplicate samples for each patient, controlling the standard curve and limiting expression as can be seen in supplementary Fig. 2. In both the saliva and serum samples, the levels of proteins did not differ, and large data distribution variability was observed as described in Table 3. We show in Fig. 2 – A, the Mann-Whitney U-test results for comparison between the TMJ OA and control groups. Even though our results at this point showed no differences between our groups, the next sections detail the contribution and diagnostic performance of those proteins to diagnose TMJ OA status.

Table 3 - **Descriptive values for each biomolecular variable.**

		Control Group (n=46) Female (39) Male (7)					**TMJ OA Group** (n=46) Female (39) Male (7)				
Variables	**Abbreviation**			**95% CI**					**95% CI**		
Biomolecular Variables (pg/ml)		**Median**	**Mean**	**Lower**	**Upper**	**SD**	**Median**	**Mean**	**Lower**	**Upper**	**SD**
Angiogenin Serum	ANG_Ser	1467.10	1454.86	1389.09	1520.62	221.46	1459.05	1457.15	1368.65	1545.65	298.02
BDNF Serum	BDNF_Ser	280.25	719.56	378.08	1061.04	1149.92	286.35	1121.62	544.88	1698.35	1942.12
CXCL16 Serum	CXCL16_Ser	3726.70	3741.37	3550.00	3932.73	644.40	3827.50	3988.57	3687.27	4289.87	1014.61
ENA-78 Serum	ENA-78_Ser	348.70	664.23	453.24	875.21	710.48	276.40	593.05	394.98	791.11	666.97
MMP3 Serum	MMP3_Ser	2358.25	2373.10	2073.33	2672.87	1009.45	2305.20	2367.03	2091.83	2642.24	926.72
MMP7 Serum	MMP7_Ser	496.55	527.66	444.90	610.42	278.69	453.75	554.15	419.32	688.98	454.02
OPG Serum	OPG_Ser	2539.15	3010.92	2165.32	3856.52	2847.49	2428.10	3116.79	2415.06	3818.51	2363.01
PAI-1 Serum	PAI-1_Ser	6505.60	7930.35	6486.74	9373.96	4861.24	6693.65	7237.11	5904.80	8569.41	4486.42
TGF-β1 Serum	TGF-β1_Ser	91.20	140.68	98.90	182.47	140.70	99.15	177.84	103.81	251.87	249.29
TIMP-1 Serum	TIMP-1_Ser	7382.15	7280.32	7020.93	7539.71	873.47	7351.65	7382.74	7099.45	7666.03	953.95
TRANCE Serum	TRANCE_Ser	2078.70	2200.67	1885.39	2515.95	1061.69	2507.15	2560.51	2231.90	2889.12	1106.56
VE-cadherin Serum	VE-cad_Ser	6259.20	6527.08	5140.64	7913.53	4668.73	5308.05	6154.80	4988.12	7321.48	3928.70
VEGF Serum	VEGF_Ser	93.90	115.32	76.18	154.46	131.80	87.30	117.40	85.32	149.47	108.01
Angiogenin Saliva	ANG_Sal	721.85	720.83	652.98	788.69	228.48	754.05	758.02	702.29	813.74	187.65
BDNF Saliva	BDNF_ Sal	5.20	7.60	5.13	10.08	8.34	3.95	8.32	4.03	12.62	14.47
CXCL16 Saliva	CXCL16_Sal	109.40	183.94	121.59	246.29	209.95	100.60	207.09	130.24	283.95	258.80
ENA-78 Saliva	ENA-78_Sal	2424.60	2218.02	1925.14	2510.90	986.25	2482.60	2410.40	2087.41	2733.39	1087.63
MMP7 Saliva	MMP7_Sal	3290.90	3615.28	2949.23	4281.33	2242.87	3594.20	3666.79	3040.77	4292.82	2108.08
OPG Saliva	OPG_Sal	555.75	855.69	560.07	1151.32	995.49	732.30	1329.53	754.68	1904.38	1935.77
PAI-1 Saliva	PAI-1_Sal	24.40	85.02	45.07	124.96	134.51	40.40	93.14	32.77	153.52	203.32
TGF-β1 Saliva	TGF-β1_Sal	40.70	64.66	41.86	87.46	76.78	54.45	69.20	46.64	91.76	75.97
TIMP-1 Saliva	TIMP-1_Sal	4070.90	3963.81	3663.14	4264.48	1012.49	3889.80	3880.69	3664.71	4096.67	727.30
TRANCE Saliva	TRANCE_Sal	627.60	794.52	533.49	1055.56	879.02	698.75	1041.55	622.45	1460.64	1411.27
VE-cadherin Saliva	VE-cad_Sal	643.10	1008.24	657.65	1358.84	1180.60	666.70	1313.82	585.33	2042.30	2453.11
VEGF Saliva	VEGF_Sal	1181.35	1342.62	1125.23	1560.02	732.07	1441.65	1419.39	1281.99	1556.79	462.68

CI: Confidence Interval; SD: Standard Deviation.

Clinical features differentiate control subjects and TMJ OA patients. We present the Mann-Whitney U test in Supplementary Fig. 1 – c for comparison of both groups with respect to the following clinical variables: RangeAssMax, MusSor, RangeWOpain, Headaches and RangeUnaMax, defined in Table 1. We chose these features because they were measured in both groups and are part of the "*Diagnostic Criteria for Temporomandibular Disorders (DC/TMD) for Clinical and Research Applications: Recommendations of the International RDC/TMD Consortium Network and Orofacial Pain Special Interest Group*"[15]. Our results show that only RangeAssMax and RangeUnaMax were not statistically significantly different between the TMJ OA and control groups. The clinical features that presented statistically significant differences were correlated with pain or limited by pain. For example, for the maximum opening withodut pain (RangeWOpain), patients were instructed to open their mouths until they start to feel pain within their TMJs. This approach reduces the amount of opening for the TMJ OA patients that often present pain during opening; however, when the patients were asked to open the mouth as much as they could even with pain (i.e RangeUnaMAx) the values were not statistically significant between the groups. In Fig. 2 - C we display only the variables that were included in our diagnostic models, described in the following sections.

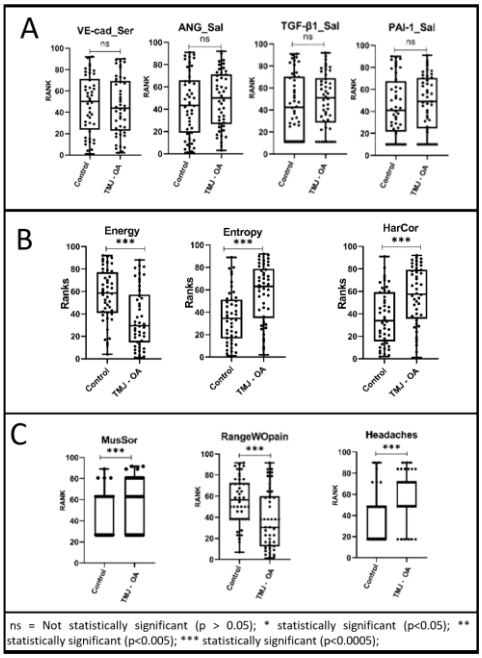

Fig. 2 – Mann-Whitney U test Comparison between the TMJ OA and control groups showing the variables included in our diagnosis prediction models; A- Biomolecular features; B- Radiomic features; C- Clinical features.

Diagnostic performance to predict TMJ OA status. In Fig. 3 – A, we show the values for the Area Under the curve (AUC) (outer circle), p-value (medium circle) and q-value (inner circle) for each of the 52 features. 10 features were identified as significantly associated with the OA status, including Headaches, Entropy, RangeWOpain, Energy, MusSor, ShortRHighGLE, HarCor, InvDifMom, RunLNU, and Inertia. Fig. 3 - B shows the AUC (upper), p-value (medium) and q-value (lower) for each category of features (biological, clinical and radiomics). Most of the features with significant AUC values are clinical or radiomic features; no biomolecular feature is detected with AUC>0.65; nevertheless, it is shown that the interaction of biomolecular features can attain an AUC of 0.74 (Figure 3 – C, 3 - D) and have a large contribution in prediction of TMJ OA status(Fig. 3 – B).

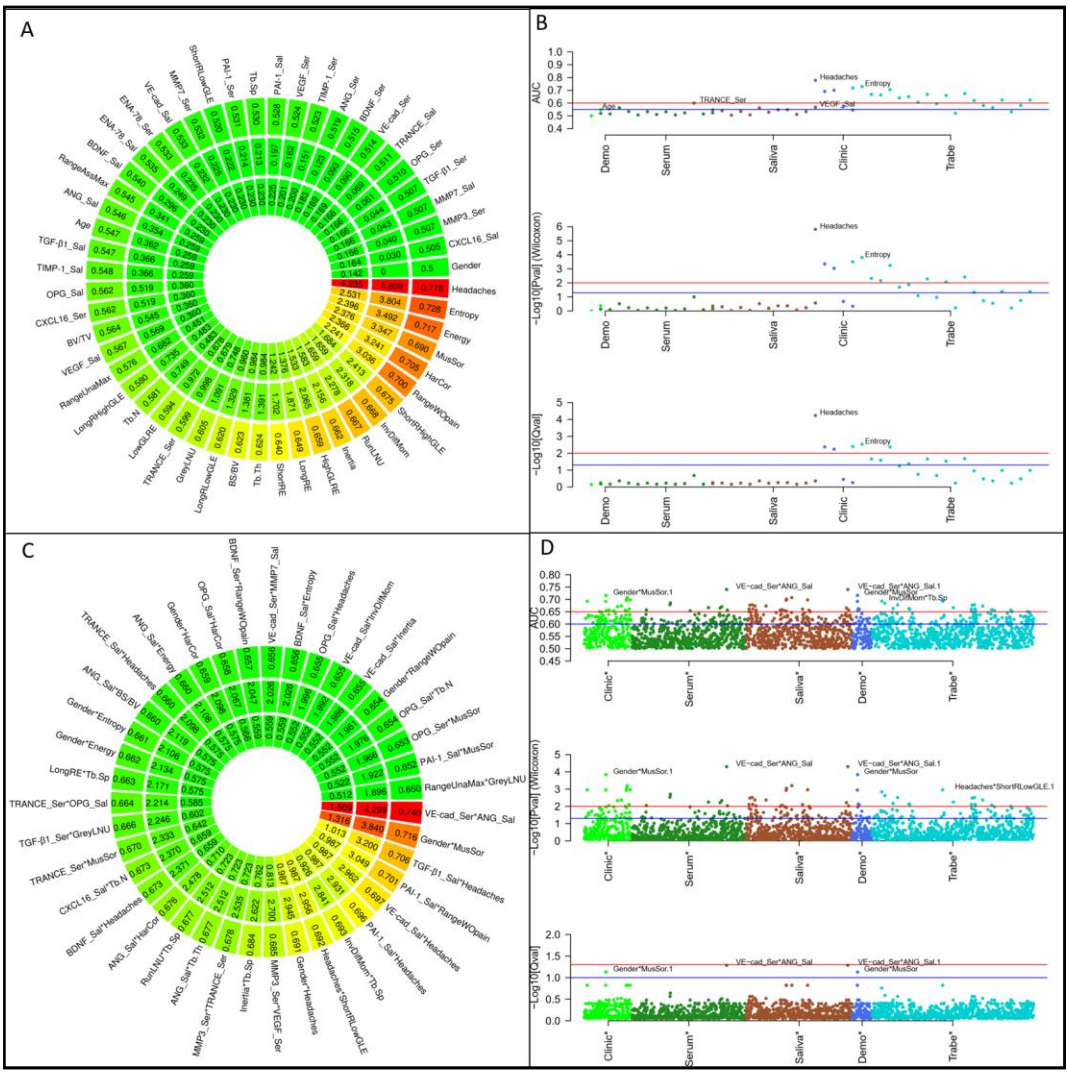

Fig. 3 - General association analysis of risk factors. Outer circle shows the AUC, middle circle shows the p-values, and inner circle shows the q-values for each single feature. **A** and **C**, for 52 features, and 39 interactions (with AUC>0.65), respectively. **B** and **D**, for 52 features and 1326 interactions, respectively. Upper graphic shows the AUC, middle graphic shows the p-values, and lower category shows the q-values for each category of features.

Contributions assessment of top features and interactions. Top features were filtered with {AUC>0.70} calculated from the training subjects and then fed into an XGBoost/LightGBM model to make diagnostic predictions. More details can be found in Method section. We demonstrate (Fig.) the contributions of the top (>95% contribution in sum) features selected from the 52 features with mutual interactions, according to feature importance[354,65] of n XGBoost (Fig. 4 – A) and LightGBM (Fig. 4 – B) prediction models, where each model is trained by using a training subset from the leave-one-out cross-validation. We find that 9 features using XGBoost model have a mean contribution larger than 95%, while for LightGBM a subset including 6 features contributes >95% information.

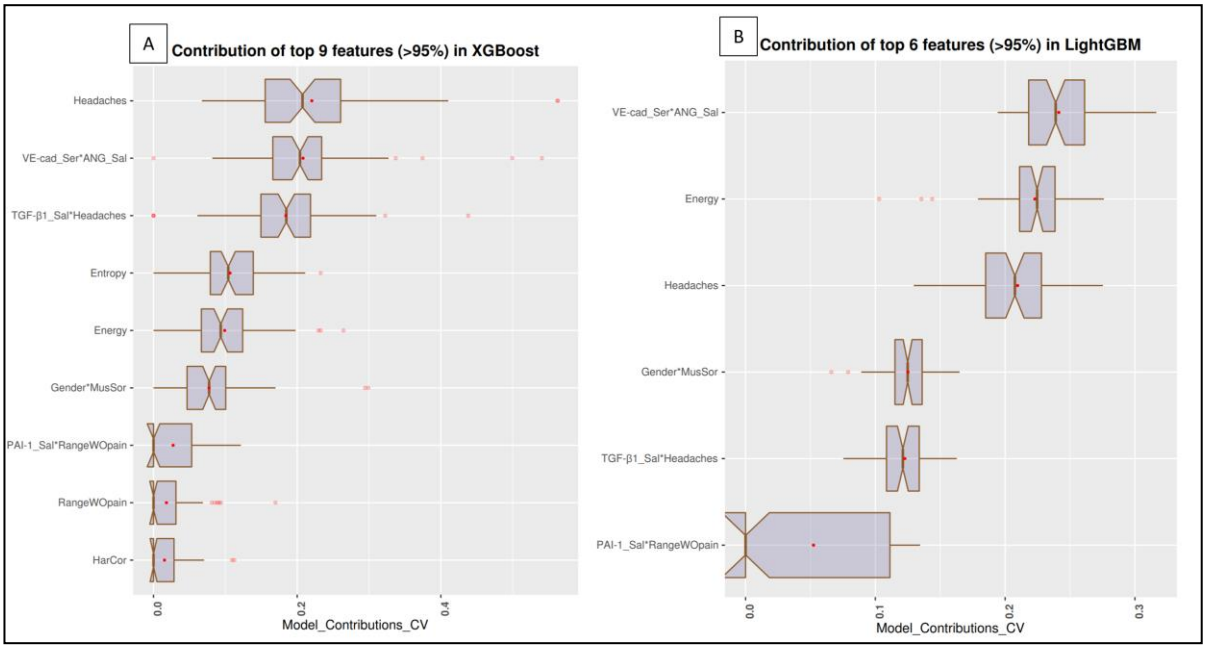

Fig. 4 - Top features with mean contribution greater than 95% according to feature importance. **A,** 9 features in the XGBoost prediction model; **B**, 9 features in the LightGBM prediction model.

Diagnosis of TMJ OA status based on the top features and interactions. After selection of the best features and interactions (Fig. 4), Fig. 5 - A displays the boxplots for comparison between OA and control groups. Fig. 5 – B shows the diagnostic performance based on the ROC curves of the top features to diagnose TMJ OA disease status and the XGBoost[35] and LightGBM[36] prediction models. The accuracy, precision, recall, AUROC and F1-score of four described methods (F_1, P_1), (F_2, P_1), (F_2, P_2) and (F_2, P_3) (see method section) are shown in Table 4. We found that the

LightGBM method with the interaction features included achieves an accuracy of 0.837, the AUC 0.862, and the F1-score 0.823. By using the one-sided paired DeLong test, we found that the AUC of the (F_2, P_3) is significantly larger than the logistic models (F_1, P_1) and (F_2, P_1) but not significant when comparing with (F_2, P_2). The p-values are 0.001, 0.014, and 0.129 respectively. Even though the main effect of bimolecular features are low, their interaction effects with clinical and radiomic features are important in diagnosis.

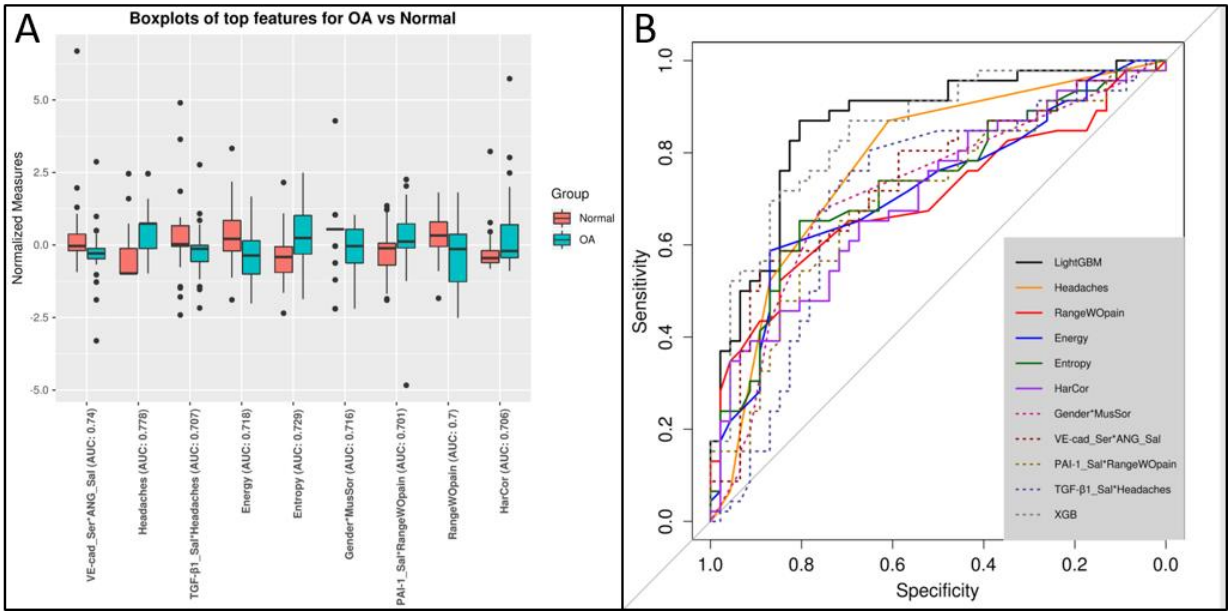

Fig. 5 - Top features to diagnose disease status. A- Boxplots of normalized features. B- ROC curves of diagnostic sensitivity and specificity.

Cross validation to control for overfitting. In order to select risk factors from the high-dimensional 52 features plus 1326 interactions, the control of overfitting is necessary. To take advantage of a larger training sample size to fulfil this aim, instead of using an independent test set, we use the leave-one-out cross validation and give evaluation and comparison using the average performance of different approaches on validation subjects. Each time in the leave-one-out CV, we select hyperparameters, i.e., the iteration steps, by further splitting the training subjects for 10-fold cross validation.

Table 4. Accuracy, precision, recall, AUROC and F1-score for the methods tested with different hyperparameters.

	(η,W,C,S)	Accuracy	Precision.OA	Precision.Control
(ℱ1, 𝒫1)	---	0.685 ([0.587,0.772])	0.718 ([0.600,0.833])	0.660 ([0.574,0.745])
(ℱ2, 𝒫1)	---	0.772 ([0.685,0.859])	0.778 ([0.686,0.892])	0.766 ([0.679,0.870])
(ℱ2, 𝒫2)	**(0.001,2,0.7,0.5)**	0.794 ([0.717,0.870])	0.829 ([0.738,0.923])	0.765 ([0.685,0.857])
(ℱ2, 𝒫2)	(0.001,1,0.7,0.5)	0.772 ([0.685,0.859])	0.820 ([0.725,0.919])	0.736 ([0.649,0.837])
(ℱ2, 𝒫2)	(0.01, 2, 0.7,0.5)	0.761 ([0.674,0.848])	0.786 ([0.684,0.889])	0.740 ([0.650,0.837])
(ℱ2, 𝒫2)	(0.001, 2, 0.5,0.5)	0.750 ([0.663,0.837])	0.780 ([0.682,0.881])	0.726 ([0.646,0.825])
(ℱ2, 𝒫3)	(0.01,1,0.5,0.5)	0.826 ([0.750,0.891])	0.812 ([0.727,0.900])	0.841 ([0.755,0.931])
(ℱ2, 𝒫3)	(0.01,1,0.7,0.5)	0.837 ([0.750,0.913])	0.816 ([0.729,0.911])	0.860 ([0.766,0.951])
(ℱ2, 𝒫3)	(0.001,1,0.7,0.5)	0.826 ([0.750,0.891])	0.800 ([0.714,0.884])	0.857([0.773,0.947])
(ℱ2, 𝒫3)	**(0.01,1,0.7,0.7)**	0.837 ([0.761,0.902])	0.816 ([0.736,0.911])	0.860 ([0.767,0.951])
(ℱ2, 𝒫3)	(0.01,2,0.7,0.5)	0.837 ([0.750,0.913])	0.816 ([0.727,0.913])	0.860 ([0.774,0.950])

	Recall.OA	Recall.Control	AUC	Mean.F1.Score
(ℱ1, 𝒫1)	0.609 ([0.457,0.739])	0.761 ([0.630,0.870])	0.725 ([0.613,0.829])	0.683 ([0.582,0.771])
(ℱ2, 𝒫1)	0.761 ([0.630,0.870])	0.783 ([0.674,0.913])	0.789 ([0.694,0.883])	0.772 ([0.685,0.859])
(ℱ2, 𝒫2)	0.739 ([0.609,0.870])	0.848 ([0.739,0.935])	0.835 ([0.752,0.911])	0.793 ([0.714,0.870])
(ℱ2, 𝒫2)	0.696 ([0.543,0.826])	0.848 ([0.739,0.935])	0.828 ([0.741,0.915])	0.770 ([0.678,0.858])
(ℱ2, 𝒫2)	0.717 ([0.565,0.848])	0.804 ([0.674,0.913])	0.831 ([0.742,0.906])	0.760 ([0.671,0.848])
(ℱ2, 𝒫2)	0.696 ([0.565,0.826])	0.804 ([0.696,0.913])	0.799 ([0.699,0.884])	0.749 ([0.662,0.836])
(ℱ2, 𝒫3)	0.848 ([0.739,0.935])	0.804 ([0.696,0.913])	0.859 ([0.782,0.927])	0.826 ([0.749,0.891])
(ℱ2, 𝒫3)	0.870 ([0.761,0.957])	0.804 ([0.674,0.913])	0.862 ([0.775,0.935])	0.837 ([0.750,0.913])
(ℱ2, 𝒫3)	0.870 ([0.783,0.957])	0.783 ([0.652,0.891])	0.860 ([0.78,00.927])	0.826 ([0.749,0.891])
(ℱ2, 𝒫3)	0.870 ([0.761,0.957])	0.804 ([0.696,0.913])	0.862 ([0.775,0.929])	0.837 ([0.761,0.902])
(ℱ2, 𝒫3)	0.870 ([0.761,0.957])	0.804 ([0.674,0.913])	0.862 ([0.777,0.937])	0.837 ([0.750,0.913])

Discussion

We report here, the diagnostic performance of machine learning approaches to predict TMJ osteoarthritis status. Through data acquisition, management and processing, we achieve one of the main challenges of healthcare delivery, that is to integrate the patient data information from multiple sources for accurate diagnosis and meaningful indicators of individual health[37]. To obtain patient-specific, precise diagnostic information, Data Science has become indispensable in medicine, with integration of data capture, management/processing and in-depth analysis with rigorous and standardized protocols[38,39].

In the carefully controlled data acquisition methods of our study, all subjects had the same imaging acquisition protocol, all clinical assessments were performed by the same pain specialist, and a single investigator collected the clinical, biological and imaging data. This study database was composed initially of 107 subjects, and 15 subjects were excluded due to incomplete or inadequate quality of data. As part of the data management and processing, we extracted radiomics information from each subject's HR-CBCT scan (Fig. 6) to obtain information that is hidden to the clinicians' naked eyes[40]. Our result in Supplementary Fig. 1 shows that most radiomic features were able to differentiate between control and TMJ OA patients. Advanced statistical learning approaches, shown in Fig. 4, demonstrate that Entropy, Energy and HarCor are included in our most accurate prediction models and corroborate our previous findings that found correlations between these features and the bone status[26], where a decreased energy was associated with bone sclerosis/loss, and the increased values for HarCor and Entropy was correlated to bone sclerosis/loss.

All clinical data were obtained using the DC/TMD[15] criteria. We have chosen features measured in both groups as described in Fig. 3, where headaches had the highest AUC among all the features. This marker is highly correlated to temporomandibular disorders in the literature[41], and now our study shows its improved diagnostic performance to predict OA status in conjunction with other features and machine learning approaches. Interestingly, the interaction of headaches with TGF-β1_Sal together was a top feature with >95% mean contribution to information gain in our statistical learning models. A possible clinical explanation is that patients with headaches had increased levels of this protein, as previous studies have indicated the expression and correlation of this cytokine with mandibular bone degradation in TMJ OA patients[42–45]. Other clinical markers included in our disease model were: RangeWOpain and its interaction with PAI-1_Sal. As TMJ OA patients present with pain in their TMJs, the decreased amount of mouth opening without pain was an important disease sign with an AUC of 0.70; and its interaction with PAI-1_Sal was an exciting finding, as this feature was increased in the OA patients (Fig. 4). PAI-1 is a serine protease inhibitor of tissue plasminogen activator and prevents the formation of plasmin; in OA, PAI-1 has a role in the cascade of enzymatic activities, compromising repair and increasing the cartilage degradation[19,46]. A recent study by our group, showed that PAI-1 is

correlated with areas of flattening in the lateral surface of mandibular condyles with OA[27], corroborating the results of this study. Finally, Gender and its interaction with MusSor was another significant feature included in our statistical prediction models. However, as TMJ OA prevalence is higher in women[47], a limitation of this study is the unequal number of male and female subjects; out of the 46 subjects in each group (sample size n=92), 39 were females and only 7 males. The role of MusSor in this interaction may be due to differences in pain sensitivity in women and men[48], and to the central sensitization caused by painful osteoarthritis as patients with temporomandibular disorders also presented higher prevalence of muscle related symptoms[49].

For the biomolecular markers, no differences between OA and control subjects (Supplementary Fig. 2 - A) were found, however, our prediction models show that the interaction between VE-cad_Ser*ANG_Sal, TGF-β1_Sal*Headaches and PAI-1_Sal*RangeWOpain are top features with an AUC higher than 0.70 and with mean >95% contribution to the information gain in the XGBoost and LightGBM predictive models. As markers of inflammation, VE-cad, ANG, TGF-β1 and PAI-1 have been previously shown[27] to be expressed in the TMJ synovial fluid and plasma and to be correlated with the condylar morphology in OA patients. It should be highlighted that in the present study, those markers were obtained from saliva and blood samples utilizing less invasive procedures for the patient, and circulating levels of pro-inflammatory proteins have been shown to contribute to the pathophysiology of disorders of the TMJ[50]. In addition, saliva has been described as a promising, accurate and non-invasive tool for a reliable diagnosis[34].

Complex, high-dimensional and biomedical data from multiple sources now benefit from data science, computational advances, and machine learning approaches to improve knowledge in terms of diagnosis, disease classification, clustering data and disease progression prediction[51–54]. For osteoarthritis, studies using mathematical algorithms for diagnosis and personalized treatment decisions are increasing[55]. We have previously shown the diagnostic performance to predict the disease status based on the condylar surface morphology and deep learning approaches[29,56] and now we show an integrative approach based on clinical, imaging radiomics and biomolecular patient specific data. Our in-depth statistical learning analysis was based on the integration of 52 features. We screened the diagnostic performance of each feature (Fig. 3 and 4) and built our machine

learning models based on the most relevant features. Our final prediction model had an accuracy of 0.837 with the confidence interval of ([0.750, 0.913]) to predict TMJ OA status using LightGBM with 52 features and 1326 interactions. Importantly, we show a comprehensive integration of new tools, data acquisition, management and approaches to improve articular joint health and predict patient-specific TMJ OA status.

Methods

We followed the *"Strengthening the Reporting of Observational studies in Epidemiology"* (STROBE) guidelines for observational studies[57].

Study design, setting and participants. After the Institutional Review Board approval (HUM00105204 and HUM00113199) from the University of Michigan, we enrolled patients and subjects from January 2016 to December 2018 that composed our TMJ OA and Control groups, respectively. This cross-sectional study sample was composed of 92 patients, 46 TMJ OA and 46 age and sex matched control subjects who were selected based on rigorous inclusion criteria. All patients were examined by a single temporomandibular disorders specialist at the Hospital of the University of Michigan (Medicine Oral Surgery Clinic) through the Diagnostic Criteria for Temporomandibular Disorders (DC/TMD)[15] for TMJ osteoarthritis diagnosis. The patients were diagnosed as TMJ OA when they presented pain in at least one TMJ for less than 10 years, TMJ noise during movement or function in the last 30 days and crepitus detected during mandibular excursive movements. The Control group subjects were recruited by advertisement and evaluated for the absence of TMJ OA. The diagnosis was confirmed utilizing the radiographic criteria[16], including the presence of subchondral cyst, erosion, generalized sclerosis and/or osteophytes. The joint side of choice used for analysis was the side with most severe clinical symptoms and radiographic signs in the TMJOA group and the matching control condyle.

Variables. Our study was composed by 3 main sub-groups of variables, which were: biomolecular features (composed by proteins of serum and saliva), imaging features (composed by trabecular bone radiomics and morphometry) and clinical features.

Biomolecular data: We evaluated 14 proteins in serum and saliva associated with arthritis initiation and progression, such as nociception, inflammation, angiogenesis and bone resorption, which were: 6ckine, Angiogenin, BDNF, CXCL16, ENA-78,

MMP-3, MMP-7, OPG, PAI-1, TGFb1, TIMP-1, TRANCE, VE-Cadherin and VEGF. However, the expression of 6ckine was not expressed in the serum and saliva samples in this study, and MMP-3 was not expressed in saliva. The raw data can be seen in the supplementary Fig. 2.

Blood and saliva acquisition protocol. The participants had 5 ml of venous blood collected by a trained nurse at the University of Michigan. The blood was centrifuged for 20 minutes at 1000 RPM to separate only the serum that was then aliquoted in 2 ml Eppendorf tubes and stored at -80C. For the saliva collection, the participants received a 14ml sterile test tube with a funnel inserted; they were instructed to tilt their head forward and drip the saliva off into the tube until 2ml was collected. They were informed to not spit, talk, or swallow during this process[58].

Custom Micro-Array. Custom human Quantibody® protein microarrays obtained from RayBiotech, Inc. Norcross, GA, were used to quantitatively assess the saliva and serum samples for the 14 specific biomarkers. Each participant had duplicates run for the saliva and serum samples (detailed description provided by Jiang et al.[59] and Huang et al.[60]). Supplementary Fig. 1 shows the raw values obtained for each participant and the supplementary Fig. 3 shows the standard curve for each protein analyzed.

Clinical Signs and Symptoms Acquisition Protocol. The same investigator collected and measured the clinical signs and symptoms of the participants based on the DC/TMD[15] criteria. The variables measured and selected for further statistical analysis were: Age pain began in years - TMJ OA Group only, Current Facial Pain - TMJ OA Group only, Worst Facial Pain in last 6 months -TMJ OA Group only, Average Pain -TMJ OA Group only, Last 6 Months Distressed by Headaches, Last 6 Months Distressed by Muscle Soreness, Vertical Range Unassisted Without Pain (mm), Vertical Range Unassisted Maximum (mm), Vertical Range Assisted Maximum (mm).

Imaging data acquisition. We acquired cone-beam computed tomography scans of each subject using the 3D Accuitomo (J. Morita MFG. CORP Tokyo, Japan) machine at the University of Michigan, School of Dentistry. The protocol for the temporomandibular joint high resolution CBCT was: field of view 40x40 mm; 90 kVp, 5 mAs, scanning time of 30.8 s and a voxel size of 0.08 mm^3. The images were exported in DICOM (.dcm) using the manufacture software: i-Dixel (J. Morita MFG.

CORP Tokyo, Japan) and optimization manufacture filter: G_103+H_009. Finally, the images were coded and de-identified to avoid investigator bias in the statistical analysis.

Imaging trabecular texture based features. We previously described the optimal parameters to extract radiomic features from the HR-CBCT scans in our study conditions and we followed these parameters to extract the information from our imaging data, using the BoneTexture module[26]. The region analyzed was the internal condylar lateral region (Fig. 6) due to our pilot results that showed this region to be the most significantly different between Control and TMJ OA patients. The textural information evaluated were: Energy, Entropy, Inverse Difference Moment, Inertia, Haralick Correlation, Short Run Emphasis, Long Run Emphasis, Grey Level Non Uniformity, Run Length Non Uniformity, Low Grey Level Run Emphasis, High Grey Level Run Emphasis, Short Run Low Grey Level Emphasis, Short Run High Grey Level Emphasis, Long Run Low Grey Level Emphasis, Long Run High Grey Level Emphasis, Bone Volume, Trabecular Thickness, Trabecular Separation, Trabecular Number and Bone Surface to Bone Volume Ratio.

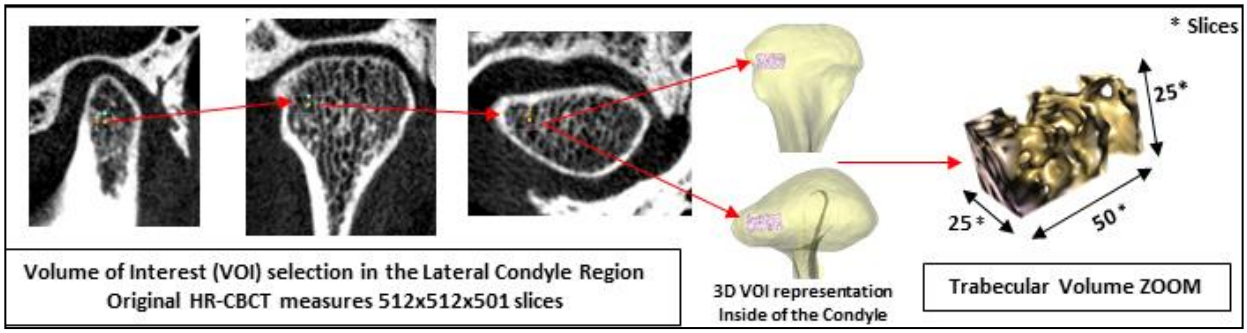

Fig. 6 - Image volume of interested selection to extract radiomics and bone morphometry features.

Exploratory tests. We first did a traditional statistical analysis to explore our data and to test the hypothesis that there is no difference between our groups. Our data does not show normality distribution and for this reason, we chose non-parametrical tests for our analysis. The descriptive analysis, Mann-Whitney U test was done using the software GraphPad Prisma V 8.11 (GraphPad Software, Inc., San Diego, CA). For the descriptive analysis, we showed the median in addition to the mean, the 95% confidence intervals and the standard deviation. The Mann-Whitney U test was used to test our hypothesis and we used a two tailed test with α of 5%.

Machine learning approaches. We diagnose the OA/control disease status based on the 52 features including five clinical variables, 20 radiomic features, 25 bimolecular features (13 from serum and 12 from saliva) and two demographic variables (age and gender). First, we normalized all features to have zero mean and one standard deviation. Next, we calculated the AUROC (Area under the Receiver Operating Characteristic curve), p-value and q-value[61] from a two-sample Mann-Whitney U test to evaluate the significance of each feature (Fig. 3). Afterwards, we compared four different prediction methods, each of which follows the four steps: (I) Cross validation to avoid overfitting (II) feature selection (III) risk prediction (IV) method evaluation. We used one-sided paired DeLong test[62,63] to validate the significance of AUC comparison between different approaches.

Cross validation (CV). We applied the leave-one-out CV by taking n-1=91 individuals as training and the remaining one subject as validation for n times. At each time, we normalized the original 52 features denoted as F1 based on the training subjects and then took the product between each pair of them to generate additional 1326 interactions and denoted the set of 1378 features as F2. We performed the following two-step procedures by using only the training dataset and feature pools F_1 and F_2, respectively, where F_1 represents the set of original 52 features, and we took the product between each pair of F_1 to generate an additional 1326 interactions and denoted the set of 1378 features as F_2.

Feature selection. We calculate the AUC for each single feature in F_2 and select top features according to $\{f \in F_1 | \text{AUC of } f > 0.7\}$ and $\{f \in F_2 | \text{AUC of } f > 0.7\}$ for feature pools met F_1 and F_2, respectively.

Evaluation and risk prediction. We trained the logistic regression model (method P1), Extreme Gradient Boosting (XGBoost; method P2)[35], Light Gradient Boosting Machine (LightGBM; method P3)[36] model by using the extracted features from the last step for risk prediction of the validation subject. For both XGBoost and LightGBM models, we we fix the depth D=1, and tune the iteration steps by further splitting the training subjects into training and validation subjects for 10-fold cross validation, where AUC is chosen as the evaluation criterion. We evaluate the prediction performance of four pairs of feature set and methods (F_1, P_1), (F_2, P_1), (F_2, P_2) and (F_2, P_3) by using the accuracy, precision, recall, AUROC and F1-score[64] on the leave-one-out CV validation subjects. We also compare the results with other

different hyperparameters. For example, we show in Table 2 the results for the results for min_child_weight $W \in \{1,2\}$, colsample_bytree $C \in \{0.5,0.7\}$, subsample $S \in \{0.5,0.7\}$ and the learning rate $\eta \in \{0.001,0.01\}$. Our results showed that the LightGBM (F_2, P_3) with W=1, C=0.7, S=0.5, η=0.01 has the best performance on the validation subjects; meanwhile, the results of LightGBM are robust to the variation of those hyperparameters, in comparison to XGBoost.

Data availability. The data analyzed are available from the corresponding author on reasonable request.

Code availability. Source code for the Computation and Integration web system (DSCI) is available at https://github.com/DCBIA-OrthoLab/shiny-tooth and for the Data Base interactor 3D-slicer Plugin: https://github.com/DCBIA-OrthoLab/DatabaseInteractorExtension.

REFERENCES

1. Vos, T. *et al.* Global, regional, and national incidence, prevalence, and years lived with disability for 328 diseases and injuries for 195 countries, 1990-2016: A systematic analysis for the Global Burden of Disease Study 2016. *Lancet* **390**, 1211–1259 (2017).
2. March, L. & Cross, M. Epidemiology and risk factors for osteoarthritis. Available at: https://www.uptodate.com/contents/epidemiology-and-risk-factors-for-osteoarthritis.
3. Herrero-Beaumont, G., Roman-Blas, J. A., Castañeda, S. & Jimenez, S. A. Primary Osteoarthritis No Longer Primary: Three Subsets with Distinct Etiological, Clinical, and Therapeutic Characteristics. *Semin. Arthritis Rheum.* **39**, 71–80 (2009).
4. Wang, X. D., Zhang, J. N., Gan, Y. H. & Zhou, Y. H. Current Understanding of Pathogenesis and Treatment of TMJ Osteoarthritis. *J. Dent. Res.* **94**, 666–673 (2015).
5. National Institute of Dental and Craniofacial Research. Facial Pain. Available at: https://www.nidcr.nih.gov/research/data-statistics/facial-pain.
6. Embree, M. *et al.* Role of Subchondral Bone during Early-stage Experimental TMJ Osteoarthritis. *J. Dent. Res.* **90**, 1331–1338 (2011).
7. Wang, X. D., Zhang, J. N., Gan, Y. H. & Zhou, Y. H. Current understanding of pathogenesis and treatment of TMJ osteoarthritis. *J. Dent. Res.* **94**, 666–73 (2015).
8. Jiao, K. *et al.* Subchondral bone loss following orthodontically induced cartilage degradation in the mandibular condyles of rats. *Bone* **48**, 362–371 (2011).

9. Nieminen, M. T., Casula, V., Nevalainen, M. T. & Saarakkala, S. Osteoarthritis year in review 2018: imaging. *Osteoarthr. Cartil.* **27**, 401–411 (2019).
10. Ebrahim, F. H. *et al.* Accuracy of biomarkers obtained from cone beam computed tomography in assessing the internal trabecular structure of the mandibular condyle. *Oral Surg. Oral Med. Oral Pathol. Oral Radiol.* **124**, 588–599 (2017).
11. Pauwels, R., Araki, K., Siewerdsen, J. H. & Thongvigitmanee, S. S. Technical aspects of dental CBCT: State of the art. *Dentomaxillofacial Radiol.* **44**, 1–20 (2015).
12. Paniagua, B. *et al.* Validation of CBCT for the computation of textural biomarkers. *SPIE Med. Imaging* **9417**, 1–15 (2015).
13. Panmekiate, S., Ngonphloy, N., Charoenkarn, T., Faruangsaeng, T. & Pauwels, R. Comparison of mandibular bone microarchitecture between micro-CT and CBCT images. *Dentomaxillofacial Radiol.* **44**, (2015).
14. Buch, K. *et al.* Quantitative assessment of variation in CT parameters on texture features: Pilot study using a nonanatomic phantom. *Am. J. Neuroradiol.* **38**, 981–985 (2017).
15. Schiffman, E. *et al. Diagnostic Criteria for Temporomandibular Disorders (DC/TMD) for Clinical and Research Applications: Recommendations of the International RDC/TMD Consortium Network* and Orofacial Pain Special Interest Group†*. *Journal of Oral & Facial Pain and Headache* **28**, 6–27 (2014).
16. Ahmad, M. *et al.* Research diagnostic criteria for temporomandibular disorders (RDC/TMD): development of image analysis criteria and examiner reliability for image analysis. *Oral Surgery, Oral Med. Oral Pathol. Oral Radiol. Endodontology* **107**, 844–860 (2009).
17. Li, G. *et al.* Subchondral bone in osteoarthritis: insight into risk factors and microstructural changes. *Arthritis Res. Ther.* **15**, 223 (2013).
18. Chen, J. *et al.* Altered functional loading causes differential effects in the subchondral bone and condylar cartilage in the temporomandibular joint from young mice. *Osteoarthr. Cartil.* **17**, 354–61 (2009).
19. Brandt, K. D., Radin, E. L. & Dieppe, P. a. Not a Cartilage Disease. *Ann. Rheum. Dis.* **65**, 1261–1265 (2006).
20. Hunter, D. J. & Bierma-Zeinstra, S. Osteoarthritis. *Lancet* **393**, 1745–1759 (2019).
21. Ghahramani, Z. Probabilistic machine learning and artificial intelligence. *Nature* **521**, 452–459 (2015).
22. Raghupathi, W. & Raghupathi, V. Big data analytics in healthcare: promise and potential. *Heal. Inf. Sci. Syst.* **2**, 3 (2014).
23. Jamshidi, A., Pelletier, J. P. & Martel-Pelletier, J. Machine-learning-based patient-specific prediction models for knee osteoarthritis. *Nat. Rev. Rheumatol.* **15**, 49–60 (2019).
24. O'Connor, J. P. B. *et al.* Imaging biomarker roadmap for cancer studies. *Nat. Rev. Clin. Oncol.* **14**, 169–186 (2017).
25. Johnson, V. L., Giuffre, B. M. & Hunter, D. J. Osteoarthritis: What does imaging tell us about its etiology? *Semin. Musculoskelet. Radiol.* **16**, 410–418 (2012).

26. Bianchi, J. *et al.* Software comparison to analyze bone radiomics from high resolution CBCT scans of mandibular condyles. *Dentomaxillofac. Radiol.* 20190049 (2019). doi:10.1259/dmfr.20190049
27. Cevidanes, L. H. S. *et al.* 3D osteoarthritic changes in TMJ condylar morphology correlates with specific systemic and local biomarkers of disease. *Osteoarthr. Cartil.* **22**, 1657–67 (2014).
28. Nelson, A. E. *et al.* A machine learning approach to knee osteoarthritis phenotyping: data from the FNIH Biomarkers Consortium. *Osteoarthr. Cartil.* **27**, 994–1001 (2019).
29. Michoud, L. *et al.* A web-based system for statistical shape analysis in temporomandibular joint osteoarthritis. *Proc. SPIE--the Int. Soc. Opt. Eng.* **10953**, (2019).
30. Pieper, S., Halle, M. & Kikinis, R. 3D Slicer. in *2004 2nd IEEE international symposium on biomedical imaging: nano to macro (IEEE Cat No. 04EX821)* 632–635 (IEEE, 2004).
31. Mirabel, C. DatabaseInteractor. Available at: https://www.slicer.org/wiki/Documentation/Nightly/Modules/DatabaseInteractor.
32. Paniagua, B. *et al.* Validation of CBCT for the computation of textural biomarkers. *Proc. SPIE--the Int. Soc. Opt. Eng.* **9417**, 94171B (2015).
33. Goldring, M. B. & Goldring, S. R. Articular cartilage and subchondral bone in the pathogenesis of osteoarthritis. *Ann. N. Y. Acad. Sci.* **1192**, 230–7 (2010).
34. Pfaffe, T., Cooper-White, J., Beyerlein, P., Kostner, K. & Punyadeera, C. Diagnostic potential of saliva: Current state and future applications. *Clin. Chem.* **57**, 675–687 (2011).
35. Chen, T. & Guestrin, C. Xgboost: A scalable tree boosting system. in *Proceedings of the 22nd acm sigkdd international conference on knowledge discovery and data mining* 785–794 (ACM, 2016).
36. Ke, G. *et al.* Lightgbm: A highly efficient gradient boosting decision tree. in *Advances in Neural Information Processing Systems* 3146–3154 (2017).
37. Alyass, A., Turcotte, M. & Meyre, D. From big data analysis to personalized medicine for all : challenges and opportunities. 1–12 (2015). doi:10.1186/s12920-015-0108-y
38. Marx, V. Biology: The big challenges of big data. *Nature* **498**, 255–60 (2013).
39. Sejdić, E. Medicine: Adapt current tools for handling big data. *Nature* **507**, 306 (2014).
40. Gillies, R. J., Kinahan, P. E. & Hricak, H. Radiomics: Images Are More than Pictures, They Are Data. *Radiology* (2016). doi:10.1148/radiol.2015151169
41. Ciancaglini, R. & Radaelli, G. The relationship between headache and symptoms of temporomandibular disorder in the general population. **29**, (2001).
42. Güzel, I., Taşdemir, N., Celik, Y. & Çelik, Y. Evaluation of serum transforming growth factor β1 and C-reactive protein levels in migraine patients. *Neurol. Neurochir. Pol.* **47**, 357–362 (2013).
43. Bruno, P. P., Carpino, F., Carpino, G. & Zicari, A. An overview on immune system and migraine. *Eur. Rev. Med. Pharmacol. Sci.* **11**, 245 (2007).

44. Jiao, K. *et al.* Overexpressed TGF-β in subchondral bone leads to mandibular condyle degradation. *J. Dent. Res.* **93**, 140–147 (2014).
45. Ishizaki, K. *et al.* Increased Plasma Transforming Growth Factor-β1 in Migraine. *Headache J. Head Face Pain* **45**, 1224–1228 (2005).
46. Ghosh, P. & Cheras, P. A. Vascular mechanisms in osteoarthritis. *Best Pract. Res. Clin. Rheumatol.* **15**, 693–709 (2001).
47. Rando, C. & Waldron, T. TMJ osteoarthritis: A new approach to diagnosis. *Am. J. Phys. Anthropol.* **148**, 45–53 (2012).
48. Sarlani, E., Garrett, P. H., Grace, E. G. & Greenspan, J. D. Temporal summation of pain characterizes women but not men with temporomandibular disorders. *J. Orofac. Pain* **21**, 309–17 (2007).
49. Bajaj, P. P. *et al.* Osteoarthritis and its association with muscle hyperalgesia: an experimental controlled study. *Pain* **93**, 107–114 (2001).
50. Slade, G. D. *et al.* Cytokine biomarkers and chronic pain: association of genes, transcription, and circulating proteins with temporomandibular disorders and widespread palpation tenderness. *Pain* **152**, 2802–12 (2011).
51. Swan, A. L., Mobasheri, A., Allaway, D. & Liddell, S. Application of Machine Learning to Proteomics Data : Classification and Biomarker Identification in Postgenomics Biology. **17**, (2013).
52. Deng, L. *et al.* PDRLGB: Precise DNA-binding residue prediction using a light gradient boosting machine. *BMC Bioinformatics* **19**, (2018).
53. Miotto, R., Wang, F., Wang, S., Jiang, X. & Dudley, J. T. Deep learning for healthcare: Review, opportunities and challenges. *Brief. Bioinform.* **19**, 1236–1246 (2017).
54. Vanneste, S., Song, J. J. & De Ridder, D. Thalamocortical dysrhythmia detected by machine learning. *Nat. Commun.* **9**, (2018).
55. Ashinsky, B. G. *et al.* Machine learning classification of OARSI-scored human articular cartilage using magnetic resonance imaging. *Osteoarthr. Cartil.* **23**, 1704–12 (2015).
56. Shoukri, B. *et al.* (in press) Minimally Invasive Approach for Diagnosing TMJ Osteoarthritis. *J. Dent. Res.* (2019).
57. Vandenbroucke, J. P. *et al.* Strengthening the Reporting of Observational Studies in Epidemiology (STROBE). *Epidemiology* **18**, 805–835 (2009).
58. Kaczor-Urbanowicz, K. E. *et al.* Salivary exRNA biomarkers to detect gingivitis and monitor disease regression. *J. Clin. Periodontol.* **45**, 806–817 (2018).
59. Jiang, W. *et al.* Protein expression profiling by antibody array analysis with use of dried blood spot samples on filter paper. *J. Immunol. Methods* **403**, 79–86 (2014).
60. Huang, R. *et al.* A biotin label-based antibody array for high-content profiling of protein expression. *Cancer Genomics and Proteomics* **7**, 129–141 (2010).
61. Storey, J. D. The positive false discovery rate: a Bayesian interpretation and the q-value. *Ann. Stat.* **31**, 2013–2035 (2003).
62. Robin, X. *et al.* pROC: an open-source package for R and S+ to analyze and compare ROC curves. *BMC Bioinformatics* **12**, 77 (2011).

63. DeLong, E. R., DeLong, D. M. & Clarke-Pearson, D. L. Comparing the areas under two or more correlated receiver operating characteristic curves: a nonparametric approach. *Biometrics* **44**, 837–845 (1988).

64. Lipton, Z. C., Elkan, C. & Naryanaswamy, B. Optimal thresholding of classifiers to maximize F1 measure. in *Joint European Conference on Machine Learning and Knowledge Discovery in Databases* 225–239 (Springer, 2011)

Acknowledgements

This study was supported by NIH grants R01DE024450, R01MH116527, R21DE025306 and funded in part by the *Coordenação de Aperfeiçoamento Pessoal de Nível Superior – Brasil* (CAPES) - Finance Code 001.

SUPPLEMENTARY FIGURES

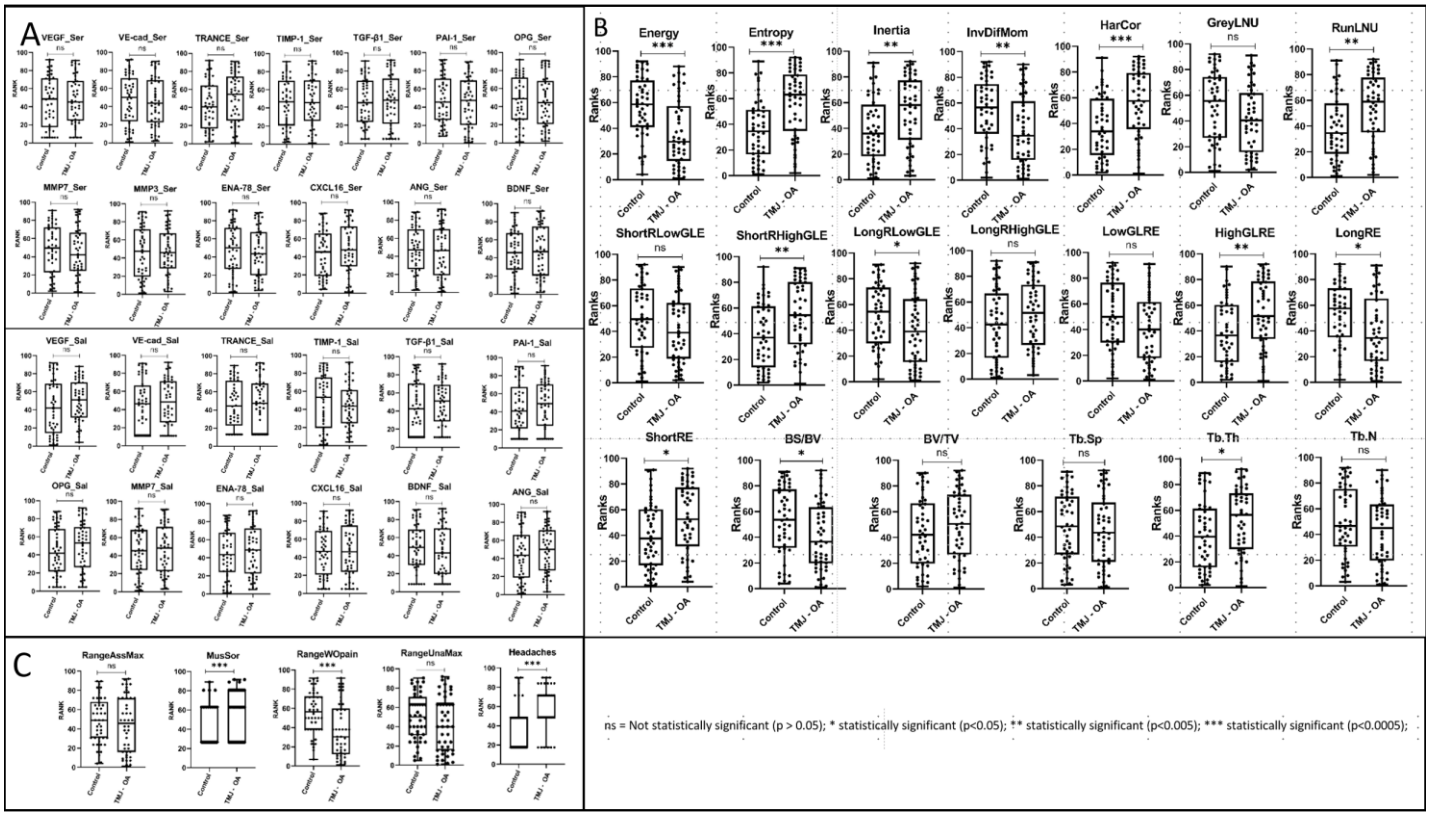

Supplementary Figure 1 - Descriptive values for each variable used in this study and their abbreviation.

A

Target	LOD (pg/ml)	Best Confident Range	Maximum Value	Highest Reported Value	Lowest Reported Value	% Below LOD	% Above LOD but <3xLOD	% in Best Confidence	% Above Maximum
6ckine	4716.2	14,148.7 - 13,333	40,000	16,426.4	0.0	98.8	1.0	0.3	0.0
Angiogenin	1.6	4.9 - 667	2,000	1,310.9	0.2	0.3	0.0	99.8	0.0
BDNF	14.2	42.6 - 3,333	10,000	4,638.9	0.0	42.0	15.8	42.3	0.0
CXCL16	12.6	37.9 - 3,333	10,000	4,497.6	0.0	13.8	4.5	81.8	0.0
ENA-78	19.6	58.7 - 3,333	10,000	5,139.9	0.0	3.3	8.5	88.3	0.0
MMP-3	16.9	50.8 - 10,000	30,000	3,081.2	0.0	37.5	7.0	55.5	0.0
MMP-7	9.9	29.7 - 6,667	20,000	12,776.4	0.0	2.3	0.8	97.0	0.0
OPG	124.2	372.5 - 6,667	20,000	10,509.1	0.0	11.5	7.5	81.0	0.0
PAI-1	75.0	225.1 - 13,333	40,000	13,013.2	0.0	34.0	10.8	55.3	0.0
TGFb1	125.3	375.8 - 6,667	20,000	801.5	0.0	79.8	19.0	1.3	0.0
TIMP-1	17.6	52.9 - 6,667	20,000	6,263.3	21.8	0.0	0.3	99.8	0.0
TRANCE	219.1	657.3 - 33,333	100,000	7,032.7	0.0	22.5	13.3	64.3	0.0
VE-Cadherin	2297.8	6,893.4 - 66,667	200,000	18,249.7	0.0	62.8	33.8	3.5	0.0
VEGF	43.6	130.9 - 3,333	10,000	3,137.1	0.0	25.3	21.5	53.3	0.0

B

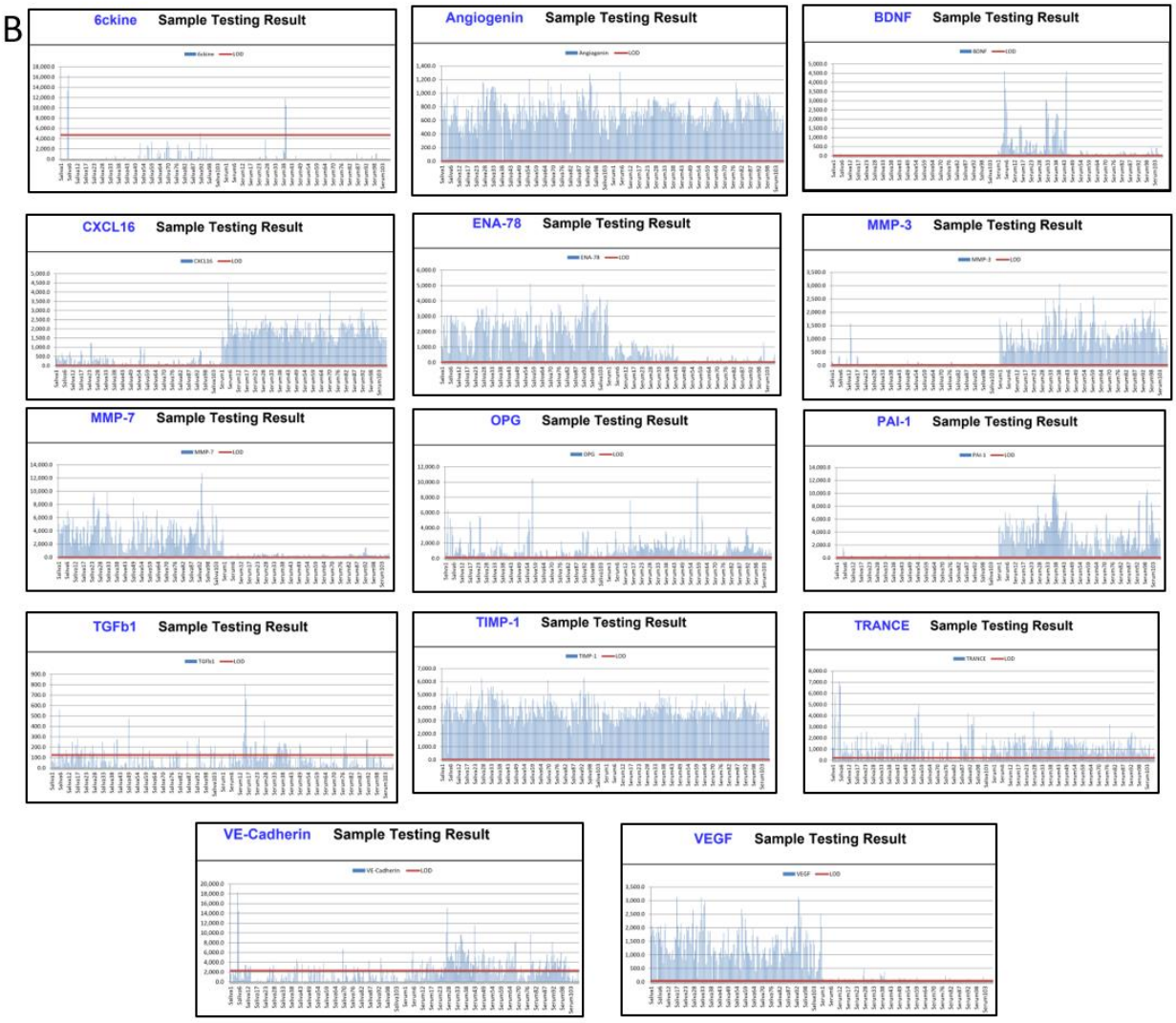

Supplementary Figure 2 - A. Summary report for each protein, saliva and serum values are together. LOD: limit of detection; B. Values for each subject, saliva and serum separately.

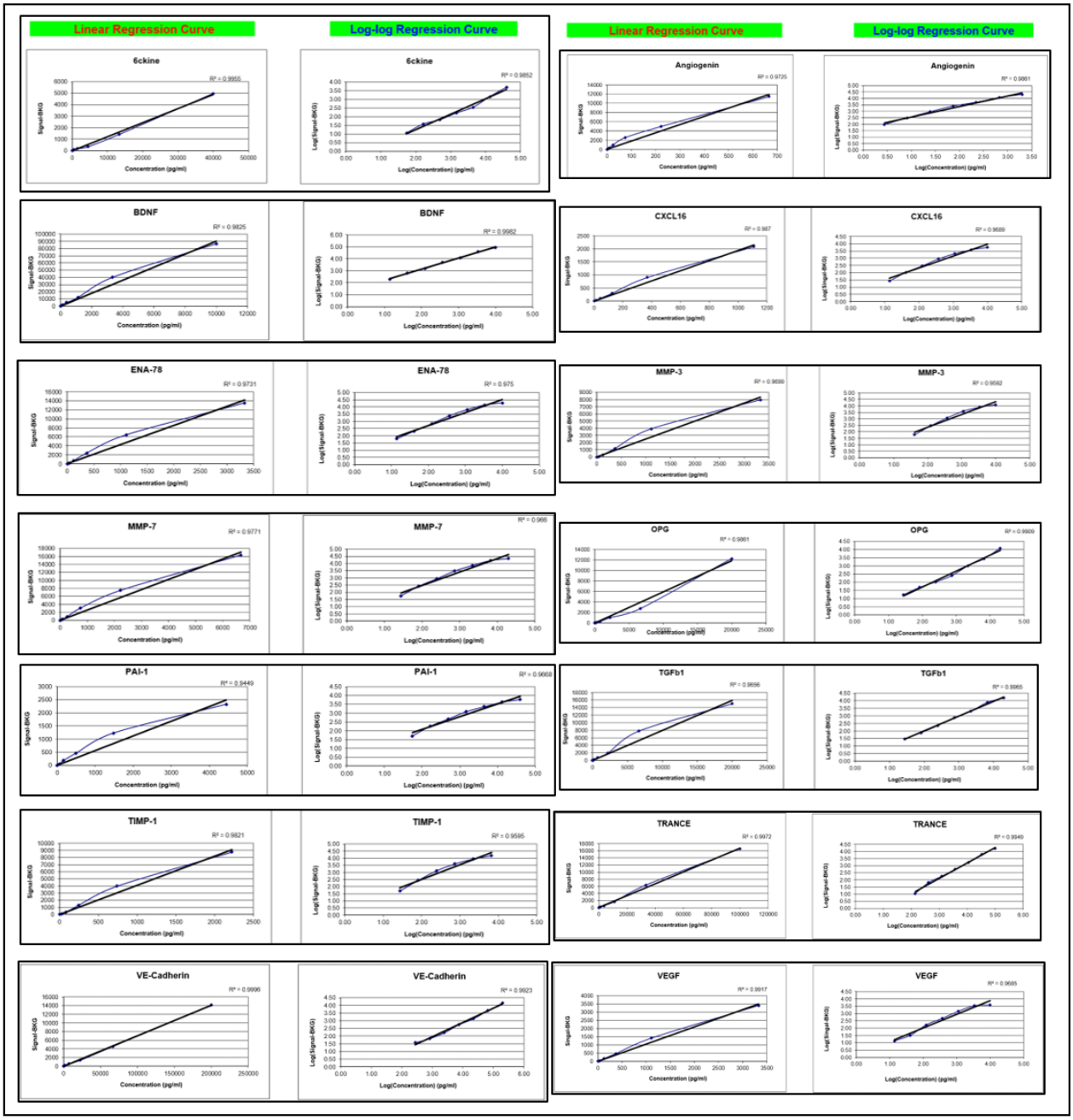

Supplementary Figure 3 - Micro-array standard curves for each protein

4 CONCLUSÃO

Essa tese demonstrou por meio de 3 artigos científicos a viabilidade do uso de imagens de alta resolução de TCFC, marcadores moleculares, dados clínicos e inteligência artificial para diagnóstico da osteoartrite nas ATMs. Nosso primeiro trabalho demonstrou que o modulo Bonetexture do software 3D-Slicer pode ser utilizado para avaliar e extrair marcadores por imagem de TCFC de alta resolução. Já o segundo artigo, atualmente em revisão demonstrou que os marcadores de imagem, também conhecidos como *radiomics* são capazes de diferenciar com significância estatística pacientes controle e com OA nas ATMs. Por fim, nosso terceiro artigo demonstrou que uma análise integrativa com machine learning e marcadores moleculares, dados clínicos e por imagem é capaz de geral um modelo com alta acurácia para diagnosticar a presença ou ausência de osteoartrite nas ATMs em nossa amostra.

REFERÊNCIAS*

1. Felson DT, Lawrence RC, Dieppe PA, Hirsch R, Helmick CG, Jordan JM et al. Osteoarthritis : new insights Part 1: the disease and Its risk factors. Ann Intern Med. 2000; 133(8): 637–9.

2. Wieland HA, Michaelis M, Kirschbaum BJ, Rudolphi KA. Osteoarthritis: an untreatable disease? Nat Rev Drug Discov. 2005; 4(4): 331–44.

3. Fan Z, Wang J, Ahn M, Shiloh-Malawsky Y, Chahin N, Elmore S et al. Characteristics of magnetic resonance imaging biomarkers in a natural history study of golden retriever muscular dystrophy. Neuromuscul Disord. 2014; 24(2): 178–91.

4. Abramson SB, Attur M. Developments in the scientific understanding of osteoarthritis. Arthritis Res Ther. 2009; 11(3): 227.

5. Wang XD, Zhang JN, Gan YH, Zhou YH. Current understanding of pathogenesis and treatment of tmj osteoarthritis. J Dent Res. 2015; 94(5): 666–73.

6. Arnett GW, Milam SB, Gottesman L. Progressive mandibular retrusion-idiopathic condylar resorption. Part I. Am J Orthod Dentofacial Orthop. 1996; 110(2): 117–27.

7. Tanaka E, Detamore MS, Mercuri LG. Degenerative disorders of the temporomandibular joint: etiology, diagnosis, and treatment. J Dent Res. 2008; 87(4): 296–307.

8. Wolford LM. Clinical indications for simultaneous TMJ and orthognathic surgery. Cranio. 2007; 25(4): 273–82.

9. Wolford LM, Gonçalves JR. Condylar resorption of the temporomandibular joint: how do we treat it? Oral Maxillofac Surg Clin North Am. 2015; 27(1): 47–67.

10. Johnson VL, Giuffre BM, Hunter DJ. Osteoarthritis: what does imaging tell us about its etiology? Semin Musculoskelet Radiol. 2012; 16(5): 410–8.

11. Scarfe WC, Li Z, Aboelmaaty W, Scott SA, Farman AG. Maxillofacial cone beam computed tomography: essence, elements and steps to interpretation. Aust Dent J. 2012; 57 Suppl 1: 46–60.

12. Larheim TA, Abrahamsson AK, Kristensen MLZA. Temporomandibular joint imaging using CBCT. Dentomaxillofacial Radiol. 2015; 44(1): 20140235.

* De acordo com o Guia de Trabalhos Acadêmicos da FOAr, adaptado das Normas Vancouver. Disponível no site da Biblioteca: http://www.foar.unesp.br/Home/Biblioteca/guia-de-normalizacao-atualizado.pdf

13. Paniagua B, Bompard L, Cates J, Whitaker R, Datar M, Vachet C et al. Combined SPHARM-PDM and entropy-based particle systems shape analysis framework. Proc SPIE. 2012; 8317(919): 83170L.

14. Cevidanes LHS, Walker D, Schilling J, Sugai J, Giannobile W, Paniagua B et al. 3D osteoarthritic changes in TMJ condylar morphology correlates with specific systemic and local biomarkers of disease. Osteoarthr Cartil. 2014; 22(10): 1657–67.

15. Bauer DC, Hunter DJ, Abramson SB, Attur M, Corr M, Felson D et al. Classification of osteoarthritis biomarkers: a proposed approach. Osteoarthritis Cartilage. 2006; 14(8): 723–7.

16. Li G, Yin J, Gao J, Cheng TS, Pavlos NJ, Zhang C et al. Subchondral bone in osteoarthritis: insight into risk factors and microstructural changes. Arthritis Res Ther. 2013; 15(6): 223.

17. Walker WT, Kawcak CE, Hill AE. Medial femoral condyle morphometrics and subchondral bone density patterns in thoroughbred racehorses. Am J Vet Res. 2013; 74(5): 691–9.

18. Goldring SR. Alterations in periarticular bone and cross talk between subchondral bone and articular cartilage in osteoarthritis. Ther Adv Musculoskelet Dis. 2012; 4(4): 249–58.

19. Bousson V, Lowitz T, Laouisset L, Engelke K, Laredo JD. CT imaging for the investigation of subchondral bone in knee osteoarthritis. Osteoporos Int. 2012; 23(8 SUPPL): 861–5.

20. Urish KL, Keffalas MG, Durkin JR, Miller DJ, Chu CR, Timothy J Mosher M. T2 Texture index of cartilage can predict early symptomatic oa progression: data from the osteoarthritis initiative. Osteoarthr Cartil. 2014; 21(10):1550–7.

21. Marx V. Biology: the big challenges of big data. Nature. 2013; 498(7453): 255–60.

22. Ghahramani Z. Probabilistic machine learning and artificial intelligence. Nature. 2015; 521(7553): 452–9.

23. Madabhushi A, Lee G. Image analysis and machine learning in digital pathology: challenges and opportunities. Med Image Anal. 2016; 33: 170–5.

24. Alyass A, Turcotte M, Meyre D. From big data analysis to personalized medicine for all : challenges and opportunities. BMC Med Genomics. 2015; 33(8): 1–12.

25. Schiffman E, Ohrbach R, Truelove E, Look J, Anderson G, Goulet J-P et al. Diagnostic criteria for temporomandibular disorders (DC/TMD) for clinical and research applications: recommendations of the international RDC/TMD consortium network* and orofacial pain special interest group. J Oral Facial Pain Headache. 2014; 28(1): 6-27.

26. Paniagua B, Ruellas AC, Benavides E, Marron S, Wolford L, Cevidanes L. Validation of CBCT for the computation of textural biomarkers. SPIE Med Imaging. 2015; 9417: 1–15.

ANEXO A – Aprovação do Comitê de Ética

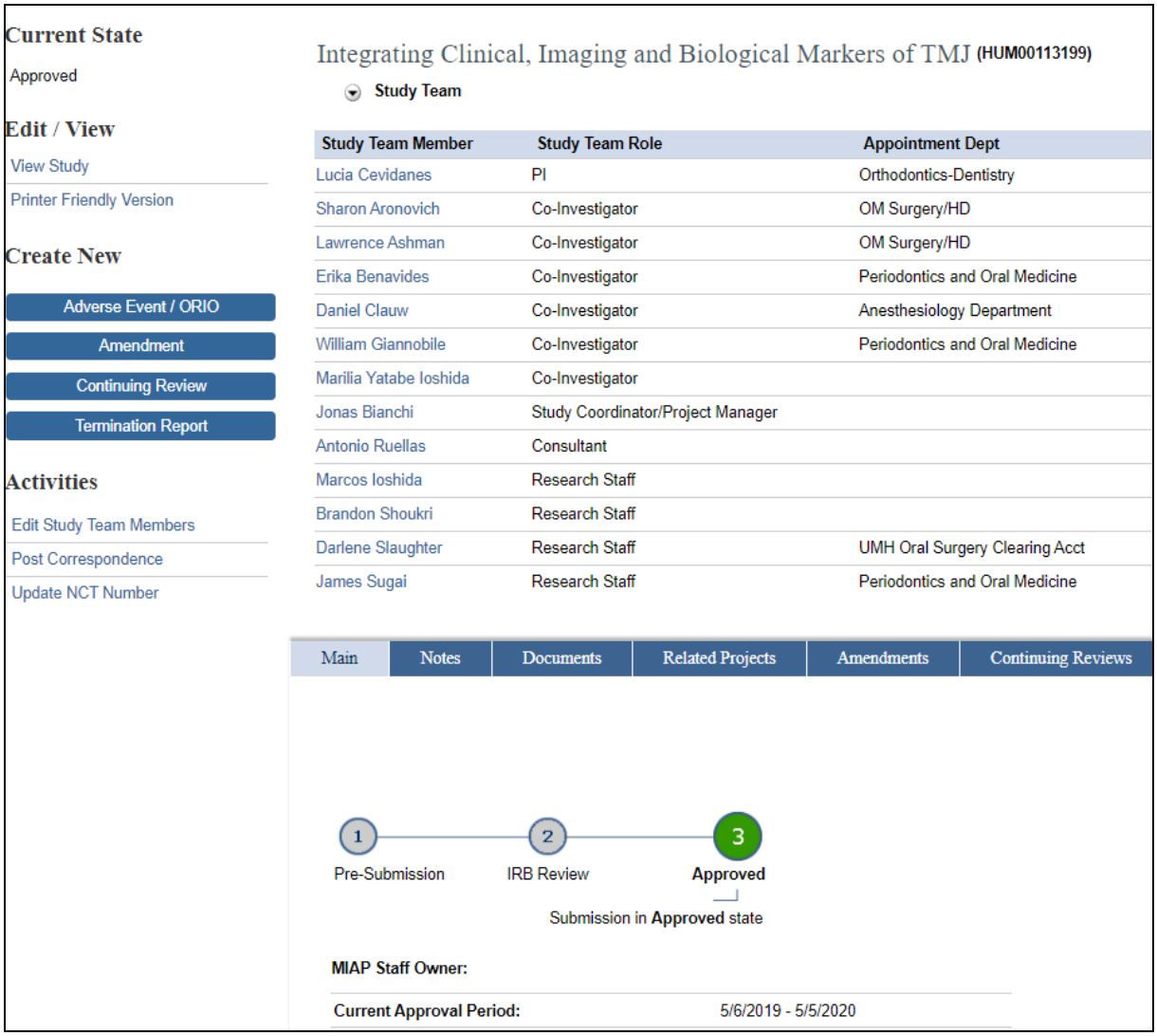

Current State

Approved

Edit / View

View Study

Printer Friendly Version

Create New

Adverse Event / ORIO

Amendment

Continuing Review

Termination Report

Activities

Edit Study Team Members

Post Correspondence

Update NCT Number

Integrating Clinical, Imaging and Biological Markers of TMJ **(HUM00113199)**

Study Team

Study Team Member	Study Team Role	Appointment Dept
Lucia Cevidanes	PI	Orthodontics-Dentistry
Sharon Aronovich	Co-Investigator	OM Surgery/HD
Lawrence Ashman	Co-Investigator	OM Surgery/HD
Erika Benavides	Co-Investigator	Periodontics and Oral Medicine
Daniel Clauw	Co-Investigator	Anesthesiology Department
William Giannobile	Co-Investigator	Periodontics and Oral Medicine
Marilia Yatabe Ioshida	Co-Investigator	
Jonas Bianchi	Study Coordinator/Project Manager	
Antonio Ruellas	Consultant	
Marcos Ioshida	Research Staff	
Brandon Shoukri	Research Staff	
Darlene Slaughter	Research Staff	UMH Oral Surgery Clearing Acct
James Sugai	Research Staff	Periodontics and Oral Medicine

Main | Notes | Documents | Related Projects | Amendments | Continuing Reviews

1 Pre-Submission — 2 IRB Review — 3 Approved

Submission in **Approved** state

MIAP Staff Owner:

Current Approval Period: 5/6/2019 - 5/5/2020

ANEXO B – Carta de Permissão da Editora

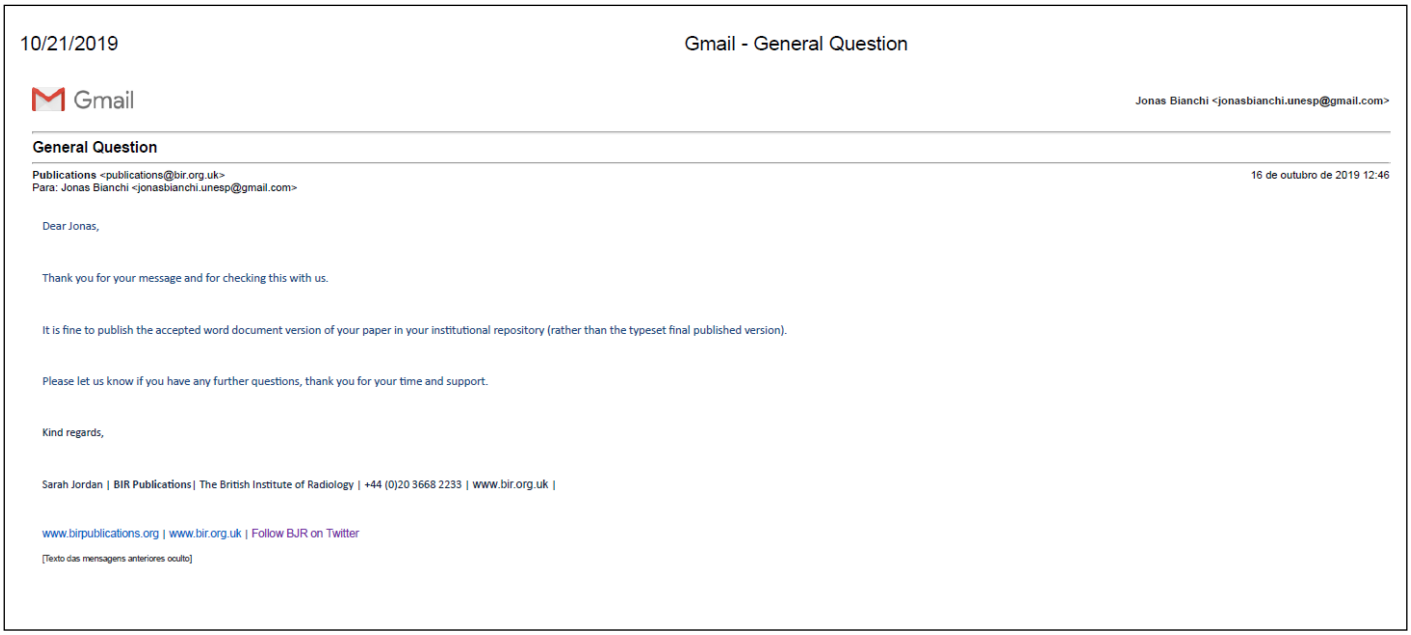

10/21/2019 Gmail - General Question

Gmail Jonas Bianchi <jonasbianchi.unesp@gmail.com>

General Question

Publications <publications@bir.org.uk>
Para: Jonas Bianchi <jonasbianchi.unesp@gmail.com>
16 de outubro de 2019 12:46

Dear Jonas,

Thank you for your message and for checking this with us.

It is fine to publish the accepted word document version of your paper in your institutional repository (rather than the typeset final published version).

Please let us know if you have any further questions, thank you for your time and support.

Kind regards,

Sarah Jordan | **BIR Publications** | The British Institute of Radiology | +44 (0)20 3668 2233 | www.bir.org.uk |

www.birpublications.org | www.bir.org.uk | Follow BJR on Twitter

[Texto das mensagens anteriores oculto]

Não autorizo a publicação deste trabalho pelo prazo de 02 anos

(Direitos de publicação reservado ao autor)

Araraquara, 06 de Dezembro de 2019.

Jonas Bianchi